Proof of Concept and Evaluation of a Novel Implant Device for Plantar Plate Repair

Logan N. Dickinson

Thesis submitted to the faculty of the Virginia Polytechnic Institute and State University
in partial fulfillment of the requirements for the degree of

Master of Science
In
Biomedical Engineering

Vincent M. Wang, Chair
Jennifer S. Wayne
John R. Clements

April 27, 2023
Blacksburg, Virginia

Keywords: Plantar Plate, Biomechanics, Implant, Mechanical Testing

Copyright © 2023 by Logan N. Dickinson

Proof of Concept and Evaluation of a Novel Implant Device for Plantar Plate Repair

Logan N. Dickinson

ABSTRACT

The plantar plate is a fibrocartilaginous tissue beneath the metatarsophalangeal joint (MTPJ). Plantar plate function centers around maintaining the static stability of the MTPJ, and its integrity facilitates the dynamic stabilizing functions of surrounding soft tissue structures. Injury to the plantar plate can cause significant forefoot discomfort focused around the MTPJ, swelling, and altered forefoot biomechanics from toe instability. Significant injury like either partial or complete tear of the plantar plate commonly requires surgical intervention to repair the tissue. As fibrocartilage, the plantar plate lacks an intrinsic capacity for robust healing, thus requiring a surgical repair aiming to restore proper function. Existing plantar plate repair techniques afford different perspectives for restoring plantar plate biomechanical function, though room for improvement exists for an enhanced repair. Our senior design team developed a novel approach for plantar plate repair using a two-piece snap fitting permanent implant. This novel technique was reduced to practice and required further experimental analysis of its functional capacity to inform future development.

Two methodologies were used to evaluate the novel implant device designed for plantar plate repair. An implant isolated mechanical testing protocol was developed to evaluate the implant and suture construct of the repair in anatomically relevant orientations. A human cadaver tissue model protocol was employed to evaluate the integrity of the native plantar plate tissue, a simulated conventional repair, and our novel implant fixation

repair. These methodologies used uniaxial tensile testing with custom test configurations to evaluate the structural integrity and properties of the implant-suture construct and simulated tissue only or tissue-repair constructs, respectively. Our results provided encouraging support for the use of mechanical testing and the continued development of this novel implant device for plantar plate repair. Additionally, qualitative outcomes from this testing revealed additional avenues to improve the novel implant device in support of further advancing the product for future use in the field of podiatric medicine.

Proof of Concept and Evaluation of a Novel Implant Device for Plantar Plate Repair

Logan N. Dickinson

GENERAL AUDIENCE ABSTRACT

The plantar plate is a soft, biological tissue that lies beneath the metatarsophalangeal joint (MTPJ), which comprises the ball of the foot. When injured, the plantar plate lacks capacity to fully heal the tissue, as its structural properties more closely resemble that of cartilage and ligaments, which also commonly fail to fully heal after injury. Due to the difficulties in facilitating healing and restoring its function, a plantar plate tear or rupture is commonly repaired surgically. Current methods for repairing a plantar plate tear vary, though room to enhance the overall surgical repair technique exists. Our senior design team developed a novel implant device for use in a modified surgical repair of the plantar plate, which aimed to improve upon the existing methods. This work focused on developing experimental methods to analyze and evaluate the function of this novel implant device that is relevant to the clinical application of plantar plate repairs.

Two experimental setups were developed and used to analyze the function of our novel implant device. A simulated repair setup, relevant to the natural function of the plantar plate, was employed to evaluate the function of the implant and suture used in the repair. A human cadaver model experimental setup aimed to evaluate the plantar plate naturally, a conventional or existing repair, and our novel repair of a simulated torn plantar plate. The outcomes from these experiments encourage further exploration of implant product development as well as continued testing of this device in the future. Ultimately, this work has provided a foundation for the continued development of our novel implant

device for plantar plate repair with the aim to bring this product to market and enhance the field of podiatric medicine.

Acknowledgements

I would like to acknowledge and thank all those who have supported me in my efforts throughout my time at Virginia Tech. Firstly, I would like to thank my advisor, Dr. Vincent Wang, for his unending support and guidance throughout my time working in the Orthopedic Mechanobiology Lab as both an undergraduate and graduate student. Additionally, I want to thank Dr. Jennifer Wayne and Dr. John Clements for their constant support and encouragement for me and this work. Their expertise and guidance have been beyond measure in propelling this project to where it is today. I would like to acknowledge my lab mates and peers for all their support and friendship through all the time spent mentoring and assisting me with many tasks.

To my family and friends, I am most sincerely grateful for all the love and support. Alyssa, your constant reassurance, steadiness, and unwavering support of me in this pursuit have meant the world. I look forward to being on the flip side of that and returning my constant support of you in your coming pursuits. Mom and Dad, it is too much to sum up in a few sentences but thank you for always giving me the subtle push of encouragement to pursue my goals. Your consistency and parenting have always been a constant reminder of your love and support for me in whatever I choose to do, and I will always be grateful for that. Colby, having an amazing older sibling to always look up to and now to share experiences with is something that I will never forget. Your persistence, kindness, and aspirations in your life inspire me beyond measure and I cannot wait to boast about all the great things you will do.

For those not mentioned directly and those no longer present, I am most thankful for all the ways in which you have impacted my life. I aspire to continue my journey as an engineer, student, and most importantly a kind human being to make a positive mark in this world however I can because of you all. Thank you so much.

Table of Contents

ABSTRACT ii
GENERAL AUDIENCE ABSTRACT iv
Acknowledgements vi
Table of Contents vii
List of Figures ix
List of Tables xii
List of Abbreviations xiii
Chapter 1: Introduction 1
1.1 Anatomy 1
1.2 Microstructure 3
1.3 Biomechanics 8
1.4 Plantar Plate Injuries and Treatment 11
1.5 Existing Surgical Solutions 16
1.5.1 Wright Medical Group GRAVITY Plantar Plate Repair System 16
1.5.2 CrossRoads Extremity Systems STRoPP System 18
1.6 Room for Improvement 20
1.7 A Novel Approach for Plantar Plate Repair 23
1.8 Objective 26
Chapter 2: Methods 28
2.1 Novel Implant Design 28
2.1.1 Two-Piece Snap-Fit Connection Features 29
2.1.2 Crossbar Feature for Suture Weightbearing and Cortical Bone Insulation 31
2.1.3 Proposed Surgical Technique Modifications 32
2.2 Implant Mechanical Testing and Validation 33
2.2.1 Isolated Implant Mechanical Testing Apparatus 33
2.2.2 MTS Test Setup 35
2.2.3 Load to Failure Mechanical Testing 39
2.2.4 Load to Failure Statistical Analysis 42
2.2.5 Cyclic Loading Mechanical Testing 42
2.2.6 Cyclic Loading Statistical Analysis 48
2.2.7 Comparative Load to Failure Analysis 48
2.3 Cadaver Tissue Sample Harvesting 49
2.3.1 Specimen Storage 50
2.3.2 Post-Harvest Storage 50

2.3.3 Tissue Harvesting 51
2.3.4 Simulated Repair Fixations 53
2.4 Cadaver Tissue Mechanical Testing Setup 55
2.4.1 Sample Preparation 57
2.4.2 Dental Cement Potting 58
2.4.3 Plantar Plate Dissection and Isolation 59
2.5 Cadaver Model Mechanical Testing Protocol 60
2.6 Cadaver Model Data Analysis 63
Chapter 3: Results 65
3.1 Isolated Implant Construct Analysis 65
3.1.1 Load to Failure Analysis 65
3.1.2 Cyclic Loading Analysis 71
3.1.3 Follow-up Load to Failure Analysis and Comparison 73
3.2 Cadaver Tissue Model Analysis 81
3.2.1 Sample Exclusion Determination 83
3.2.2 Statistical Analysis 84
3.2.3 Failure Modes 87
Chapter 4: Discussion 91
4.1 Summary and Assessment 91
4.2 Limitations 95
4.3 Future Directions 97
4.4 Conclusion 100
References 101
Appendix A: MATLAB Codes 107
Appendix B: Mechanical Testing Protocols 113
Appendix C: Supplemental Materials 127

List of Figures

Figure 1.1: Descriptive 3D schematic of the MTPJ and plantar plate....2
Figure 1.2: Hierarchical structure of collagen within a tendon or other primarily collagenous tissue....4
Figure 1.3: Illustration of ECM components of cartilage....7
Figure 1.4: Illustration of nonlinear tissue mechanical response for a paired:....9
Figure 1.5: Illustration of a proximal phalanx drawer test to evaluate plantar plate integrity....13
Figure 1.6: Illustration of joint subluxation for relevant plantar plate injury grades....15
Figure 1.7: Illustration of common plantar plate injury grades and relative tear patterns from dorsal perspective....15
Figure 1.8: Schematic of two-piece snap fitting implant with female and male components....24
Figure 2.1: Labeled illustration of assembled novel implant construct and interior snap-fit mechanism....29
Figure 2.2: Labeled feature illustration of female component....30
Figure 2.3: Labeled feature illustration of the male component....31
Figure 2.4: Labeled and annotated front perspective of the mechanical testing apparatus for novel implant-suture construct....34
Figure 2.5: Simulated anatomical overlay on testing apparatus in 80° dorsiflexion orientation....35
Figure 2.6: Female component preloaded with suture passing device inserted in centerpiece of rigid test apparatus....36
Figure 2.7: Male component snapped within female component in centerpiece of test apparatus 36
Figure 2.8: Image of suture thread wrapped around ring loop and inserted through suture passing loops for shuttling through implant....38
Figure 2.9: Illustration of suture knot fixation....39
Figure 2.10: Side perspective of centerpiece simulated dorsiflexion orientations....43
Figure 2.11: Schematic of load controlled cyclic loading immediately followed by load to failure at a constant crosshead speed (1 mm/s)....45
Figure 2.12: Schematic of individual elongation amplitude calculations from first and last cycles....46
Figure 2.13: Schematic of 1st and 5th cycle secant stiffness calculations....47
Figure 2.14: Labeled image of dissected sample before resecting surrounding soft tissue....52
Figure 2.15: Labeled image of dissected sample after resecting surrounding soft tissue....52
Figure 2.16: Simulated plantar aspect perspective of a novel repair sample fixed for mechanical testing....54
Figure 2.17: Annotated image of cadaver tissue mechanical testing setup....56
Figure 2.18: Angled perspective of sample vertical alignment for:....61

Figure 3.1: Example of 0° dorsiflexion load to failure experimental data and analysis in MATLAB 65
Figure 3.2: Example of 40° dorsiflexion load to failure experimental data and analysis in MATLAB 66
Figure 3.3: Example of 80° dorsiflexion load to failure experimental data and analysis in MATLAB 66
Figure 3.4: Scatterplot of the maximum load (N) data for each dorsiflexion condition 68
Figure 3.5: Scatterplot of the tangent stiffness (N/mm) data for each dorsiflexion condition 68
Figure 3.6: Scatterplot of the secant stiffness (N/mm) data for each dorsiflexion condition 69
Figure 3.7: Example of cyclic loading experimental data 72
Figure 3.8: Example of 0° dorsiflexion post-cyclic load to failure experimental data and analysis in MATLAB 74
Figure 3.9: Example of 80° dorsiflexion post-cyclic load to failure experimental data and analysis in MATLAB 74
Figure 3.10: Scatterplot of the maximum load (N) data during load to failure testing after cyclic loading 75
Figure 3.11: Scatterplot of the tangent stiffness (N/mm) data during load to failure testing after cyclic loading 75
Figure 3.12: Scatterplot of the secant stiffness (N/mm) data during load to failure testing after cyclic loading 76
Figure 3.13: Scatterplot data for maximum load (N) comparing the load to failure conditions for 0° dorsiflexion 77
Figure 3.14: Scatterplot data of tangent stiffness (N/mm) comparing the load to failure conditions for 0° dorsiflexion 78
Figure 3.15: Scatterplot data of secant stiffness (N/mm) comparing the load to failure conditions for 0° dorsiflexion 78
Figure 3.16: Scatterplot data of maximum load (N) comparing the load to failure conditions for 80° dorsiflexion 80
Figure 3.17: Scatterplot data of tangent stiffness (N/mm) comparing load to failure conditions for 80° dorsiflexion 80
Figure 3.18: Scatterplot data of secant stiffness (N/mm) comparing load to failure conditions for 80° dorsiflexion 81
Figure 3.19: Native plantar plate sample experimental data and analysis in MATLAB 82
Figure 3.20: Conventional repair sample experimental data and analysis in MATLAB 82
Figure 3.21: Novel repair sample experimental data and analysis in MATLAB 83
Figure 3.22: Scatterplot data of maximum load (N) for cadaver mechanical testing groups 85
Figure 3.23: Scatterplot data of tangent stiffness (N/mm) for cadaver mechanical testing groups 86
Figure 3.24: Scatterplot data of secant stiffness (N/mm) for cadaver mechanical testing groups .86

Figure 3.25: Example of distal, transverse tear of plantar plate in native plantar plate test group sample.....87
Figure 3.26: Example of avulsion tear at plantar plate insertion in proximal phalanx for native plantar plate test group sample.....88
Figure 3.27: Example of transverse tear, adjacent to the location of suture placement within plantar plate for conventional repair sample.....89
Figure 3.28: Example of male component fracture (red circle) and distal suture pullout (green circle) for a novel repair test group sample.....90

List of Tables

Table 1.1: Clinical Grading System for Plantar Plate Injury.....14
Table 3.1: Normal Distribution Goodness-of-Fit p-values for Load to Failure Only Testing.....67
Table 3.2: Summary Statistics from Load to Failure Only Testing.....70
Table 3.3: Normal Distribution Goodness-of-Fit Test p-values for Cyclic Loading Data.....72
Table 3.4: Unequal Variance Test p-values for Cyclic Loading Data.....72
Table 3.5: Summary Statistics from Cyclic Loading Testing.....73
Table 3.6: Summary Statistics for Cadaver Tissue Mechanical Testing.....84

List of Abbreviations (in alphabetical order)

MTPJ	Metatarsophalangeal joint
ACL	Accessory collateral ligament
DTML	Deep transverse metatarsal ligament
PCL	Proper collateral ligament
ECM	Extracellular matrix
ROM	Range-of-motion
STRoPP	Single Tunnel Repair of Plantar Plate
AVN	Avascular necrosis
PEEK	Polyether ether ketone
ESM	Engineering Science and Mechanics
ANOVA	Analysis of variance
FOS	Factor of safety
K-wire	Kirschner wire

Chapter 1: Introduction

1.1 Anatomy

The plantar plate is a soft biological tissue positioned beneath the metatarsophalangeal join (MTPJ), an ellipsoid synovial joint comprising the metatarsal and proximal phalanx [1-3]. On the plantar aspect of the MTPJ, the plantar plate is a centrally located tissue that permits anchoring of the surrounding ligaments. The accessory collateral ligament (ACL) and deep transverse metatarsal ligament (DTML) run congruent with the plantar plate (Figure 1.1). Each of these ligaments provide passive structural support of the MTPJ and specifically depend on the plantar plate as an attachment site. The proper collateral ligament (PCL) runs adjacent to the plantar plate, spanning the MTPJ on its medial and lateral sides (Figure 1.1). The PCL provides additional medial and lateral support of the MTPJ, though without direct attachment to the plantar plate [2-7].

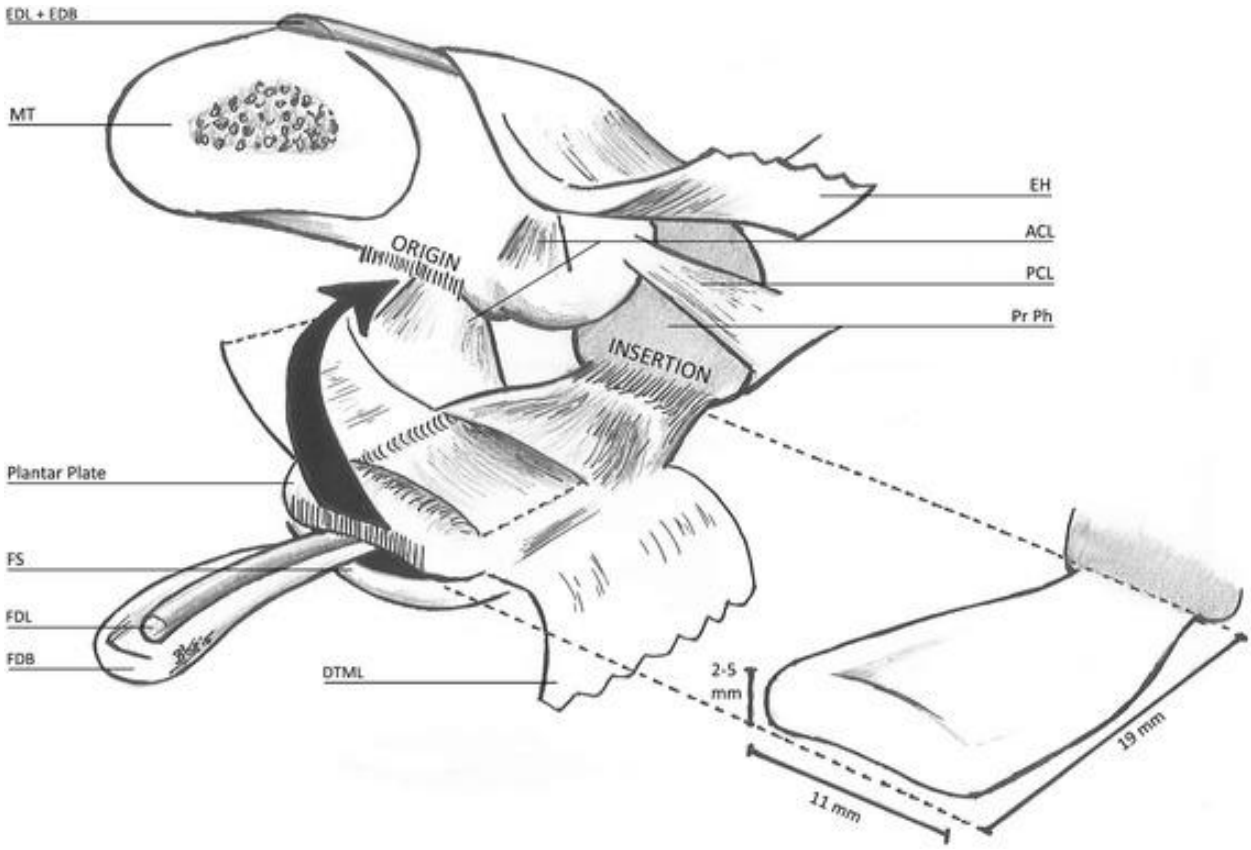

Figure 1.1: Descriptive 3D schematic of the MTPJ and plantar plate. Legend: EDL+EDB, extensor digitorum longus/brevis; MT, metatarsal; EH, extensor hood; ACL, accessory collateral ligament; PCL, proper collateral ligament; Pr Ph, proximal phalanx; FS, flexor sheath; FDL+FDB, flexor digitorum longus/brevis; DTML, deep transverse metatarsal ligament [4] Maas, et al.

The plantar surface of the plantar plate has a grooved contour facilitating passage of the flexor tendons on the plantar side of each toe [2, 3]. Tendons passing the length of the MTPJ provide dynamic stability and control the joint motion, particularly through dorsiflexion and plantarflexion. Extensor tendons pass dorsally, primarily controlling the dorsiflexion or upward rotation of the toe (Figure 1.1) [4]. Flexor tendons pass plantarly directly beneath the plantar plate, controlling the plantarflexion or downward rotation of the toe (Figure 1.1) [3,6,7].

The origin of the plantar plate is at the distal end of the metatarsal neck, just proximal to the metatarsal head [2,4]. A thin synovial membrane attachment connects the plantar plate to the metatarsal [3]. Distally, the plantar plate inserts into the base of the proximal phalanx, with distinct, thick attachment points medially and laterally [2-4,6,8]. While the plantar plate originates and inserts into two separate bones like a ligament, the tissue is not classified as a ligament. The plantar plate is a fibrocartilaginous tissue, which allows for adaptability and varying functions throughout its length [3,4,7-11]. Microscopically the plantar plate has distinctions characterizing its morphology as fibrocartilaginous as opposed to ligamentous. Functionally, the plantar plate serves as an anchor for ligamentous attachments and provides structural attributes that are essential to maintaining proper MTPJ alignment and function biomechanically [2,4,6,8,12-14].

1.2 Microstructure

The morphology of the plantar plate informs its classification as fibrocartilage [3,4,7-11]. Fibrocartilage is a tissue that possesses features of both cartilage and ligament, though with some distinctions molecularly. It is found throughout the musculoskeletal system including the meniscus in the knee and intervertebral discs in the spine [7,16-18]. At the molecular level, fibrocartilage is made up of an extracellular matrix (ECM) of mostly water and other proteins and cells [11,15,19,20]. The dry weight of fibrocartilage is dominated by collagen [9,10,20,21].

With 28 different types, collagen is the most abundant protein in mammals or vertebrates, providing much of the cellular structure for many tissues beyond those in the musculoskeletal system [20,22,23]. Fibrillar collagen (Types I-III, V, XI, XXIV, XXVII) provides mechanical stability, elasticity, and strength, which are necessary for supporting tissue functions in the musculoskeletal system [24, 25]. Collagen types I and II are the most abundant types within connective tissues like tendons, ligaments, and cartilage [9,11,15,18,19,20,23,26-31]. Collagen types I-III are considered fibrillar collagens and generally have a crimped structure that reduces the packing density when organized into fibrils [9,13,20,24,28-30]. The hierarchical structure of collagen and collagenous tissues flow from individual collagen molecules, grouped together as fibrils, which are bundled together as fibers and further bundled as fascicles that ultimately provide structure of the tissue [20,24]. Composition of collagen types and its organization in tissues are indicators of overall tissue function and response to mechanical loading.

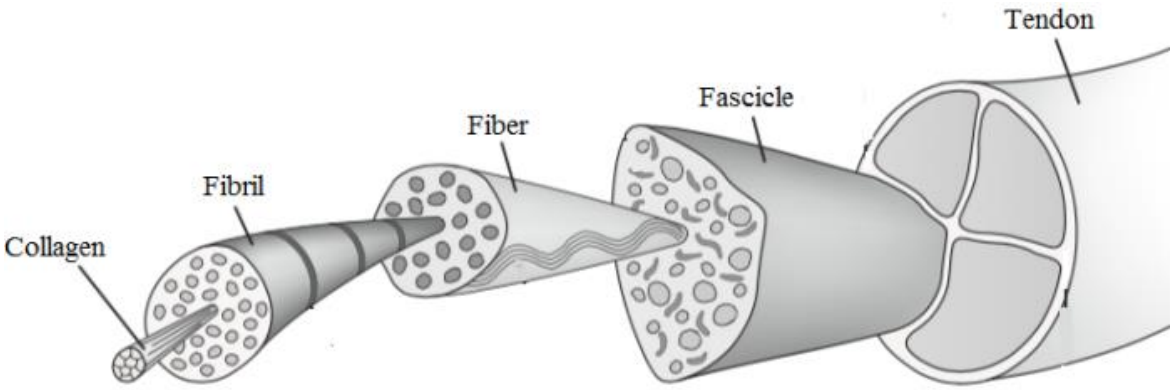

Figure 1.2: Hierarchical structure of collagen within a tendon or other primarily collagenous tissue. (Reproduced from [60] Hydrolyzed Collagen: Questions and Answers.")

Tendons and ligaments are mostly made up of type I collagen [20]. Their collagen fibers tend to be oriented parallel to the loading axis, primarily oriented in a singular direction [9,10,20,26-28]. Tissue function impacts the directionality of these fibers, since most tendons transfer muscle contractile loads to bones and ligaments restrict bone or joint movement within an acceptable range-of-motion (ROM). Therefore, the orientation of the collagen fibers provides considerable tensile strength along the length of the collagen fibers in ligaments and tendons, coinciding with their intended loading axes. Under normal physiological conditions, these tissues are not overloaded and maintain their intrinsic tissue properties. When tissues are overloaded past their linear regions, permanent deformation results. Microtears in the collagen fibers can induce a loss in the gross tissue strength and function, requiring either intrinsic or extrinsic tissue repair [11,13,26,28,31].

For fibrocartilage in the plantar plate specifically, the gross tissue function varies along its length. The volume of collagen in the plantar plate is mostly composed of type I collagen, approximately 75%, and type II collagen, approximately 21% [2,4,7]. Type I collagen is a fibrillar molecule that presents as wavy or crimped and is most abundant in ligaments and tendons where tensile strength is imperative [9,15,23,29,30]. Type II collagen has thinner fibrils surrounded by proteoglycans and chondrocytes and is typically more abundant in cartilage [9,11]. The composition of type I and II collagen in the plantar plate distinguishes it from a ligament in favor of fibrocartilage. Biomechanically, the plantar plate connects bone to bone rather than muscle to bone, distinguishing it from classification as a tendon.

Collagen orientation and composition is less uniform in the plantar plate as compared to common tendons or ligaments. The overall tissue structure of the plantar plate differs from the single axis fiber orientation, common for both tendons and ligaments in the direction of loading. Instead, fibrocartilage typically has bundles of collagenous fibers organized in layers running in multiple directions [3,8,10]. This multidirectional organization of collagen fibers affords strength and function throughout the tissue in different directions. Collagen fibers in the plantar plate are key to understanding the function and strength of various portions or sections of the tissue within the greater MTPJ space. Proximally and dorsally, the plantar plate appears as an articular cartilage, with a smooth dorsal surface beneath the metatarsal head [3,6,13]. The composition of the proximal plantar plate is mostly type II collagen with a higher concentration of chondrocytes, which closely resembles the composition of articular cartilage [8,21]. Shorter collagen fibrils with proteoglycans and chondrocytes dispersed throughout the ECM allow this section of the plantar plate to better resist compressive loads (Figure 1.3) [11,19].

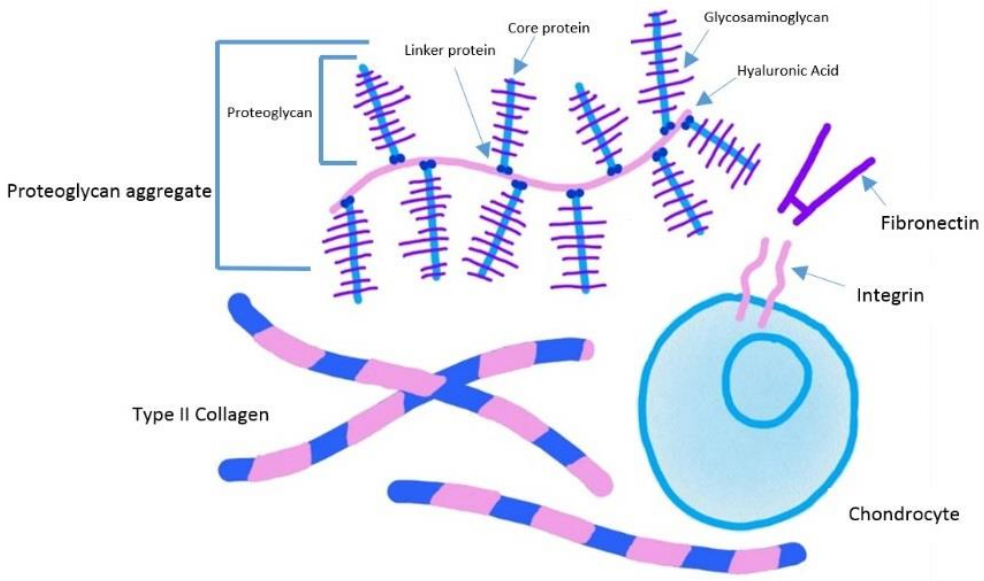

Figure 1.3: Illustration of ECM components of cartilage. (Reproduced from [61] "Proteoglycans.")

Distally, the plantar plate predominantly has bundles of type I collagen and an abundance of fibroblasts towards its insertion into the proximal phalanx [8,13]. These fibers are longitudinally oriented bundles, along the length and loading axis of the MTPJ and make up the dorsal two-thirds of the plantar plate thickness. The plantar one-third of the plantar plate has transversely oriented fiber bundles that coincide with the surrounding anatomy, where the plantar plate attaches and runs congruent with the ACL and DTML [3]. Fibroblast concentration at the distal portion of the plantar plate and fiber bundle organization along its loading axis are similar to ligamentous tissue structure and indicate enhanced tensile strength [28]. Overall, the composition and cellular structure of the plantar plate throughout its length are essential when considering its overall biomechanical functions.

As a connective tissue, the plantar plate affords stability and structural integrity to the MTPJ. While the plantar plate connects the metatarsal and proximal phalanx directly, it is not exactly a ligament in its composition. The importance of its biomechanical function is directly related to its microstructure or composition as fibrocartilage. Proximally, the plantar plate mainly supports compressive loads beneath the metatarsal head. Distally, the plantar plate primarily withstands tensile loads along its length when the toe rotates in dorsiflexion. These loading patterns and the plantar plate microstructure relate closely such that its composition equips the overall tissue to withstand the biomechanical demands imposed by the surrounding gross anatomy of the MTPJ.

1.3 Biomechanics

Biomechanics of the forefoot are essential to maintain the stability and flexibility to the foot. Naturally, most of the forefoot ROM occurs in the sagittal plane, through dorsiflexion and plantarflexion. As such, the plantar plate is an important static stabilizer for the forefoot, particularly influential in the lesser toes [4]. Located beneath the MTPJ, the plantar plate spans the distal metatarsal head and proximal phalanx. This location is crucial for individual joint function and as a contributor in whole foot function. Many soft tissues within the forefoot and near the MTPJs run congruent or adjacent to the plantar plate, relying on its stability and integrity to maintain proper foot biomechanics [7,8,13,31].

In a relaxed state, the collagen molecules are crimped in the ECM and tightly packed within each fiber. Under load, each collagen molecule readily deforms along its length,

uncrimping before becoming taut and exhibiting stiffer mechanical behavior. This phenomenon is commonly reflected in a nonlinear response of a material under load (Figure 1.4 (a)) [9,19,23,24,33]. For collagenous tissues, low loads are met with considerable compliance as the fibers and molecules align in the direction of loading, seen as the "toe" region of the load vs. displacement curve (Figure 1.4 (b)). Once the fibers are mostly aligned and the crimp is removed, the tissue fibers stiffen in response to load and provide a linear response in the load vs. displacement curve. After significant deformation, the tissue will yield, and stiffness decreases as fibers are damaged under the load until an ultimate failure strength is reached as the tissue gives out. This pattern of the mechanical loading response is common for many soft tissues, especially those predominantly collagenous [23,24,34].

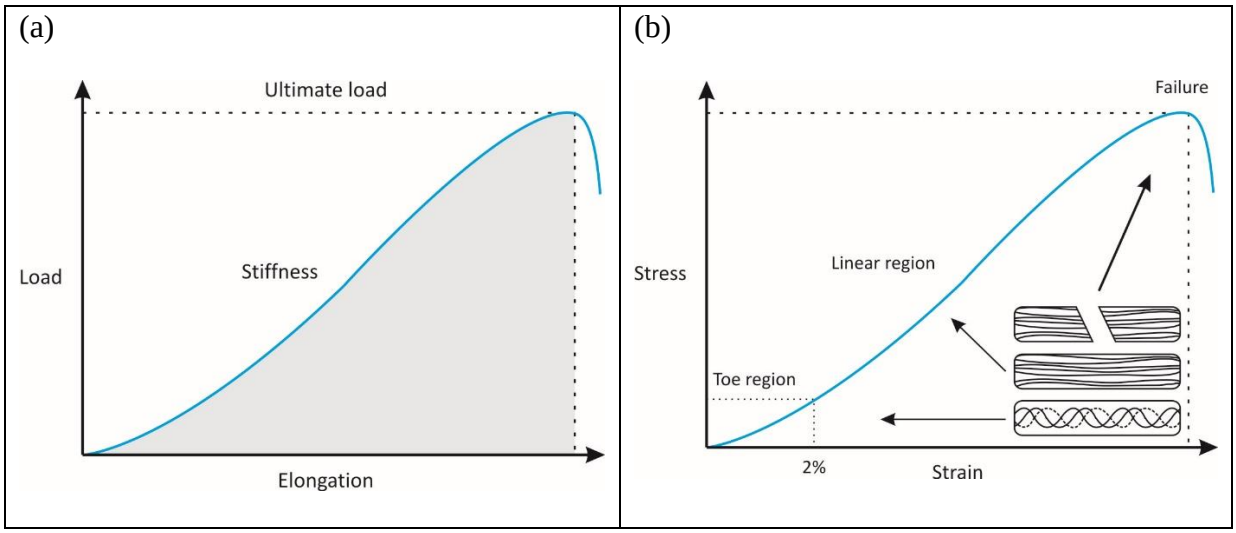

Figure 1.4: Illustration of nonlinear tissue mechanical response for a paired: (a) Load vs. displacement curve, and (b) Stress vs. strain response with annotated regions and representative collagen fiber response. (Adapted from [62] K. Robi, et al.)

Given that the plantar plate runs on the plantar aspect of the joints, its biomechanical function is particularly relevant when the toes are in dorsiflexion or raised upward relative to the midfoot. In this position and motion, plantar soft tissue structures are loaded primarily in tension. The proximal portion of the plantar plate lies directly below the distal metatarsal head, a compression load bearing site in the forefoot [3,6,8]. Direct ground contact during ambulation induces compressive forces at the base of the metatarsal head where the plantar plate supports the plantar bony surfaces. The 2nd and 3rd toes are of higher risk for plantar plate injury and MTPJ malalignment due to their position adjacent to the great toe [4,6,7,13,32]. As such, these toes bear a significant fraction of overall ground reaction forces and tensile loads in normal foot ROM than the 4th or 5th toes. The plantar plate beneath each of the 2nd and 3rd toes provides a localized anchor point for surrounding ligaments while needing to withstand a variety of loads.

Proximally, beneath the metatarsal head, the plantar plate closely resembles articular cartilage in histological assessment [8]. Biomechanically, this portion of the plantar plate primarily supports compressive loading from ground reaction forces distributed through the plantar side of the foot, mostly at the high pressure point of the ball of the foot [3,6,8]. The plantar plate insulates the plantar surface of the metatarsal head, distributing the compressive ground reaction forces over a greater area and volume of the metatarsal head, effectively reducing the stresses and risks of metatarsal fracture at the metatarsal head or neck. On its dorsal surface, the proximal plantar plate is smooth and contoured to

the plantar surface of the metatarsal head, visually consistent with its biomechanical function of supporting the metatarsal in compression [3,6,13].

The plantar plate spans the gap between the metatarsal and proximal phalanx. When dorsiflexed, the phalanx rotates upward relative to the metatarsal in the MTPJ, directly inducing a tensile load on the plantar plate [6]. The gap between the metatarsal and proximal phalanx increases on the plantar side and much of the tensile force is distributed through the longitudinally oriented fibers of the distal plantar plate and the cartilaginous proximal plantar plate. As a result, the plantar plate lengthens in this process. An intact, healthy plantar plate maintains the static stability of the MTPJ when in dorsiflexion [4,7,8,13,32]. Surrounding tendons induce plantarflexion and dorsiflexion in the MTPJ and primarily provide a dynamic stability function [8,13]. Surrounding congruent and adjacent tissues, particularly the PCLs and ACLs, provide limited support of the plantar plate when in dorsiflexion, though these tissues have different longitudinal axes of loading compared to the plantar plate. Without proper integrity of the plantar plate, static stability of the MTPJ is compromised and commonly results in joint misalignment among other symptoms [8,12,14].

1.4 Plantar Plate Injuries and Treatment

Plantar plate injuries can vary in severity, causes, and treatment, similar to other soft tissue orthopedic injuries. Physicians aim to limit initial intervention for a plantar plate injury, likely opting for conservative care for less severe injuries or symptoms [4,12,13]. Propagation of a plantar plate tear and subsequent increasing severity of the injury during

conservative treatment or normal activities can increase the difficulty and degree of intervention necessary to treat the plantar plate. Surgical intervention is most common for more severe partial or complete plantar plate tears. Surgical repair of the plantar plate can prove challenging, especially when timing the more aggressive treatment appropriately to mitigate further injury aggravation [13].

For most plantar plate injuries, common symptoms that present are metatarsalgia, or focused pain around the injured MTPJ, swelling or edema, and altered toe biomechanics or cosmetic appearance [4,8,12,33]. A drawer test of the injured MTPJ can provide an estimate for the severity of plantar plate injury. The drawer test evaluates the integrity of the plantar plate by shifting the proximal phalanx vertically relative to the metatarsal, which is held still (Figure 1.5) [4,6,34]. The MTPJ drawer test for plantar plate evaluation is similar to the anterior drawer or Lachman test to examine knee stability and anterior cruciate ligament integrity [35]. Laxity in the joint during the drawer test is a potential indicator for moderate to severe plantar plate injury. Depending on the results of an initial plantar plate examination, additional imaging may be necessary to assess the full extent of the injury.

Figure 1.5: Illustration of a proximal phalanx drawer test to evaluate plantar plate integrity. (Reproduced from [34] "Plantar Plate Tear of the Lesser Toes")

Natively, the plantar plate affords static stability in the sagittal plane, reducing the loads on surrounding tissues and integrating surrounding ligaments to maintain MTPJ alignment [4,7,8,13,32]. When torn, the compromised integrity of the plantar plate heavily impacts MTPJ alignment and surrounding soft tissue function. A plantar plate tear commonly occurs at the distal portion of the tissue, wherein the structure resembles a ligamentous tissue [6,8]. The distal plantar plate is subjected to primarily tensile loading when the MTPJ is in dorsiflexion. This load pattern is consistent with the inherent tissue structure and longitudinally oriented collagen fibers of the distal plantar plate equipped to withstand tensile stress.

Table 1.1: Clinical Grading System for Plantar Plate Injury (Reprinted from [5] Nery, et al., with permission from Elsevier)

Grade 0	Metatarsal phalangeal (MTP) joint alignment; pain with no deformity Plantar pain, thickening or swelling under MTP joint, reduced toe purchase, negative drawer test
Grade 1	Mild misalignment, widening of web space, medial toe deviation MTP joint pain and swelling, loss of toe purchase, mild positive drawer test (<50% subluxable)
Grade 2	Moderate misalignment; medial, lateral, dorsal, or dorsomedial deformity; hyperextension of toe MTP joint pain, reduced swelling, no toe purchase, moderate positive drawer test (>50% subluxable)
Grade 3	Severe misalignment, dorsal or dorsomedial deformity, crossover toe, or flexible hammertoe MTP joint and toe pain, little swelling, no toe purchase, very positive drawer test (dislocatable MTP joint), and flexible hammertoe
Grade 4	Dorsomedial or dorsal dislocation, severe deformity, fixed hammertoe MTP joint and toe pain, little or no swelling, no toe purchase, dislocated MTP joint, fixed hammertoe

Minor plantar plate injuries, typically categorized by a grade 1 tear, are most frequently approached with conservative treatments (Table 1.1) [5]. Conservative treatments of plantar plate injury include supportive strapping or taping of the joint in plantarflexion for stability, padded or supportive footwear, and other orthotics [4,12,13]. A conservative treatment of a minor plantar plate tear aims to afford joint stability and alignment while the tissue is compromised. These approaches have a limited capability to support tissue healing since the plantar plate has a limited intrinsic capacity for remodeling or healing [13]. Ultimately, conservative treatment of plantar plate injury persists with aims to prevent further injury and maintain proper forefoot function without invasive surgical intervention to directly repair and stabilize the plantar plate. When the injury becomes unmanageable with conservative treatment, further treatment is needed to restore tissue function and surrounding forefoot stability.

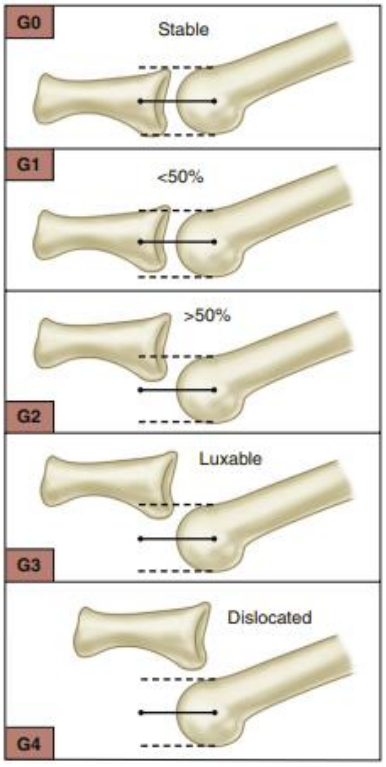

Figure 1.6: Illustration of joint subluxation for relevant plantar plate injury grades. (Reprinted from [5] Nery, et al., with permission from Elsevier)

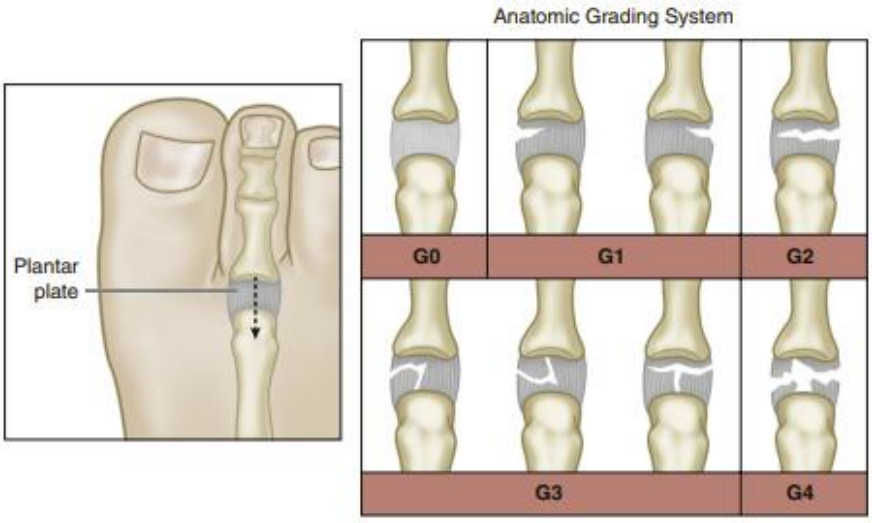

Figure 1.7: Illustration of common plantar plate injury grades and relative tear patterns from dorsal perspective. (Reprinted from [5] Nery, et al., with permission from Elsevier)

Severe plantar plate injuries, denoted grade 2 or greater, tend to require invasive interventions to restore full tissue function (Figures 1.6 and 1.7) [5]. Most commonly, surgical plantar plate repair is performed to reattach the healthy, proximal plantar plate to its distal attachment site at the base of the phalanx. Various surgical procedures and methods are used to achieve plantar plate reattachment [5,12-14,32,36-39]. Following the surgical repair, most recovery timelines include an extended period of joint immobilization as well as progressive physical therapy and rehabilitation [16,31,40]. Due to limited vasculature and intrinsic healing capacity of the plantar plate, the repair technique needs to be strong and robust to facilitate the rehabilitation process and restore tissue function.

1.5 Existing Surgical Solutions

Various devices and surgical techniques exist within podiatry to repair an injured plantar plate [5,12-14,32,36-39]. These fixation methods and repairs include techniques with and without an implant for support. Commonly, the primary intent of a surgical technique is to reattach or affix the remaining healthy plantar plate to the distal insertion site at the base of the proximal phalanx. Two of the more well-known fixation techniques are the GRAVITY Plantar Plate Repair System from Wright Medical Group and the STRoPP System from CrossRoads Extremity Systems [36,37].

1.5.1 Wright Medical Group GRAVITY Plantar Plate Repair System

The GRAVITY Plantar Plate Repair System is considered a conventional approach for plantar plate repair, given its use of sutures and bone tunnels in the proximal phalanx for

tissue fixation [36]. Without an implant, this approach simplifies the overall repair construct for both the surgeon and patient. A dorsal incision over the MTPJ is made to gain access to the joint capsule and injured plantar plate. To gain access to the plantar aspect of the joint, a distal metatarsal head osteotomy and retraction is performed. This step is necessary to provide clearance and access to debride the distal plantar plate and place sutures within the remaining healthy tissue.

Once the residual healthy plantar plate is isolated, size 0 non-absorbable sutures are placed distally in the plantar plate, typically using a single horizontal mattress stitch. Two bone tunnels, approximately 1 mm in diameter, are drilled distal to the proximal head of the proximal phalanx from the dorsal to plantar aspect. A suture passing device is inserted through the bone tunnels to securely shuttle the sutures to the dorsal side of the proximal phalanx. The metatarsal head osteotomy and retraction is reduced and secured with screws in its original, anatomical position. The surgeon adjusts the tension of the repair construct before securing the sutures on the dorsal, cortical bone bridge between the bone tunnels. Multiple surgeon's knots are tied to secure the sutures above the bone bridge. After the repair is complete, the doctor may confirm smooth ROM for toe dorsiflexion and plantarflexion before closing the wound.

The GRAVITY Plantar Plate Repair System provides a simple technique for plantar plate repair secured over a proximal phalanx bone bridge. Without a permanent implant, this approach affords adaptability for anatomical variance, while limiting potential

postoperative complications related to implant rejection. While the GRAVITY surgical technique suggests a dorsal approach is appropriate for the repair, a plantar approach could provide direct access to the plantar plate and eliminate the need for a metatarsal head osteotomy and retraction. This alternative approach could limit additional risks associated with metatarsal osteotomy and its subsequent healing [41, 42]. Ultimately, the GRAVITY technique provides a simple, conventional repair for plantar plate rupture, though some technical considerations leave room for improvement.

1.5.2 CrossRoads Extremity Systems STRoPP System

The Single Tunnel Repair of Plantar Plate (STRoPP) System from CrossRoads Extremity Systems is a surgical technique that employs a single, permanent implant for plantar plate repair [37]. For this approach, a suture button implant is used to mitigate the need for a bone bridge support on the dorsal aspect of the proximal phalanx, as necessary in the GRAVITY repair. The suture button used in the STRoPP System has a recessed platform to support the knotted sutures when the repair is complete. Button placement within the proximal phalanx is achieved with a single tunnel drilled through the proximal phalanx. By displacing the suture knot position from the cortical bone bridge surface to within the suture button, the STRoPP System adds an additional step and implant to enhance the repair construct. The final fixation of the plantar plate repair differs from the GRAVITY approach, though most remaining steps in the procedure are largely unchanged.

A dorsal incision is made above the MTPJ to access the joint with the injured plantar plate. A metatarsal head osteotomy and retraction is performed to expose the plantar side

of the joint from the dorsal aspect. With access to the plantar plate, the distal tissue and surface of the proximal phalanx is debrided, leaving the healthy portion of the plantar plate intact for subsequent reattachment. Size 0 non-absorbable sutures are placed through the healthy remaining plantar plate using a horizontal mattress stitch. A single 2.7-2.8 mm bone tunnel is drilled through the proximal phalanx dorsal to plantar, positioned just distal to the head of the proximal phalanx. The STRoPP System suture button is placed within the tunnel and a suture passing device is inserted through the button from the dorsal to plantar side of the proximal phalanx. The suture passing device shuttles the sutures to the dorsal side of the suture button for fixation. The metatarsal osteotomy and retraction are reduced and the metatarsal head is fixed with screws in its original, anatomical position. Suture-tissue construct is tensioned by the surgeon from the dorsal side, before three surgeon's knots, positioned in the recessed portion of the suture button, are used to complete the repair.

The surgical technique for the STRoPP System is simple, with many similarities to the GRAVITY Plantar Plate Repair System. Much of the repair requires standard surgical instruments, aside from the suture button developed by CrossRoads Extremity Systems. Implementing the use of a suture button further insulates the exposed dorsal cortical bone on the proximal phalanx, potentially amplifying the durability of the repair. While the dorsal approach for the STRoPP System is suggested, a primarily plantar approach with a small, percutaneous incision above the proximal phalanx could provide similar benefits as mentioned for the GRAVITY technique, mainly removing the requirement of a metatarsal osteotomy. In turn, this mitigation could prevent additional risks of avascular

necrosis (AVN) or nonunion at the metatarsal head [41-44]. The STRoPP System from CrossRoads Extremity Systems is a simple technique for plantar plate repair relying on a permanent suture button implant. Aspects of the STRoPP technique provide a basis for enhancing the plantar plate surgical approach and repair construct overall.

1.6 Room for Improvement

Restoring the passive tension of the plantar plate and the MTPJ is a primary consideration when repairing the static stabilizing function lost due to rupture. Both the GRAVITY and STRoPP systems employ a pulley type fixation construct within the proximal phalanx to tension the plantar plate with sutures over a dorsal support [36,37]. Each of these solutions uses a unique fixation support to retain the tension of the plantar plate, either a dorsal, proximal phalanx bone bridge or a dorsal suture button within the proximal phalanx. While each approach seems to restore plantar plate tension and function, both techniques risk adjacent injury through biomechanical aspects of the repair constructs. In either repair, the sutures, carrying passive tensile forces from the remaining healthy plantar plate, come into direct contact with one or more cortical bone surfaces of the proximal phalanx. Biomechanically, the suture-plantar plate construct maintains some tension when in a neutral position, which increases with joint dorsiflexion. In repetitive conditions, such as ambulation or rehabilitative exercises, the suture can cause a shear or frictional force on bony surfaces it is in direct contact with, especially as tensile forces increase in dorsiflexion. During rehabilitation of the plantar plate, toe ROM increases, which can cause concern for higher shear stress concentrations at the sites of direct contact between suture and cortical bone. The shear stresses caused by sutures rubbing on

the cortical bone surfaces are critical to consider when evaluating risk of repair compromise not directly related to remaining tissue integrity.

In the GRAVITY Plantar Plate Repair System, the dorsal bone bridge of the proximal phalanx supports the knotted sutures and tension for the repaired plantar plate [36]. While supporting the initial recovery phase postoperatively seems reasonable for this approach, the durability of the repair hinges on the cortical bone strength, particularly where the suture knot rests. During rehabilitation, the patient aims to restore toe ROM and function through repetitive loading exercises. This causes incremental, cyclic tensioning of the repair construct that wears down the cortical bone where it is in direct contact with the sutures. Specifically, as the joint rotates in dorsiflexion the suture tension increases, contributing to the increase in friction between the sutures and the bone bridge. As the tensile forces cycle between a neutral and dorsiflexed state, the sutures rub along the bone bridge, creating a “suture sawing effect”. Over time the friction between these components of the repair can wear down the cortical bone, which can be especially detrimental for cases of compromised bone quality or osteoporosis. As the bone wears down, risk of fracture and AVN of the proximal phalanx increase [41-44]. The potential for the sutures pulling within the proximal phalanx, reduced suture tension, or suture rupture are additional risks of compromising the plantar plate repair.

The notable difference between the GRAVITY and STRoPP System repairs is the use of a suture button to anchor the sutures for plantar plate repair in the latter. A suture button

within the proximal phalanx serves as the dorsal suture anchoring point and acts as a buffer to insulate the dorsal cortical bone surface. With the knot placed within the recessed region of the suture button, the dorsal side of the proximal phalanx is buffered from direct contact with the tensioned suture. While the suture button extends into the bone tunnel, the plantar portion of the tunnel, where the sutures pass dorsally to be anchored, is not insulated. Thus, contact between the sutures and cortical bone surface is not entirely avoided in the STRoPP System, but displaced to the plantar aspect of the proximal phalanx.

On the plantar side, the sutures rest on the proximal edge of the bone tunnel in the STRoPP System repair. Considering the biomechanics of the repair construct loading during normal ambulation, similar risks of proximal phalanx fracture, AVN, and overall repair compromise exist [43,44]. In dorsiflexion, the passive tension of the plantar plate repair construct increases, which further intensifies the friction force between the sutures and the cortical bone surface on the plantar side of the proximal phalanx. Through repetitive cyclic loading, a similar “suture sawing effect” can wear down the plantar, bony surface of the proximal phalanx. The incidence of repetitive friction between the bony surfaces and sutures that support a plantar plate repair are concerning when justifying the aim to provide a durable repair through patient recovery. Both the GRAVITY and STRoPP System repairs are simple approaches to restore plantar plate function, though considering the underlying biomechanics of the repair constructs leaves room for an improved approach for a durable plantar plate repair.

1.7 A Novel Approach for Plantar Plate Repair

Throughout 2021, our senior design team developed a novel approach for plantar plate repair using a unique, two-piece snap fitting permanent implant (Figure 1.8) [45]. The novel implant was manufactured using a Formlabs Form 3 3D printer in Rigid 4000 resin (Formlabs, Somerville, MA) [46]. This resin was considered similar to polyether ether ketone (PEEK), an approved material for medical device manufacturing and the preferred material for future works with this implant [47,48]. The snap fitting mechanism provides multiple benefits, including a simple fastening system for implantation and variable implant lengths that could accommodate anatomic differences in proximal phalanx size. The dorsally inserted component is considered the female component, and the plantarly inserted component is considered the male component.

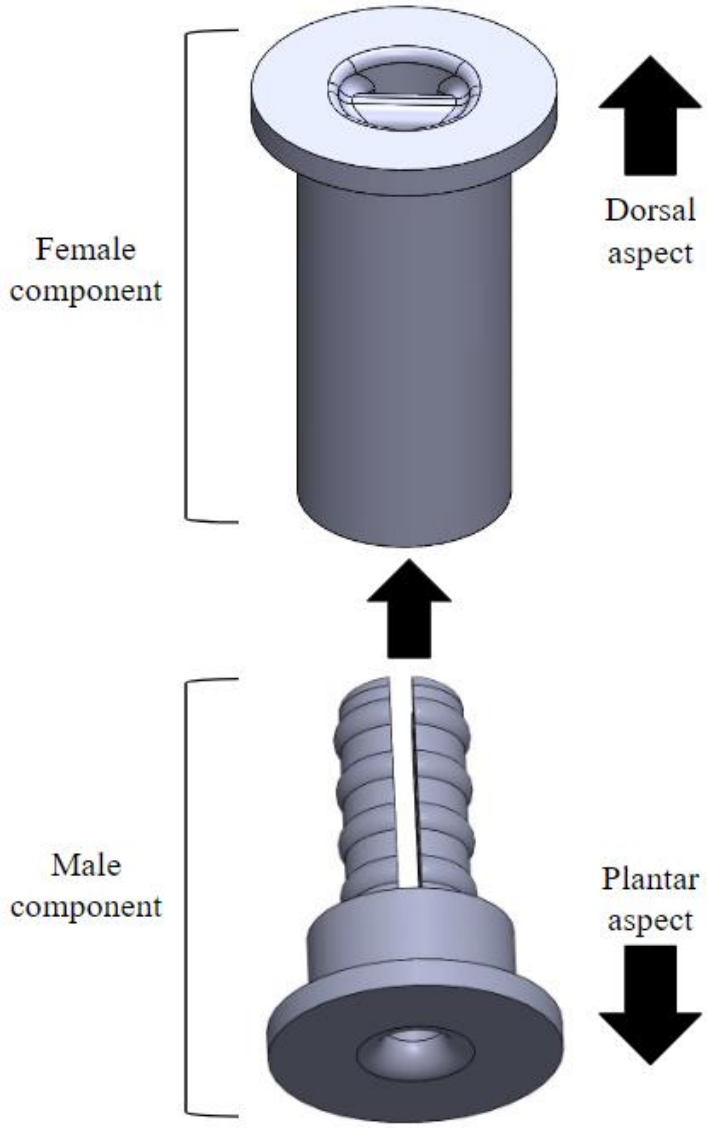

Figure 1.8: Schematic of two-piece snap fitting implant with female and male components.

Within the female component, a crossbar, slightly recessed from the dorsal edge, extends within the hollow portion of the component, and serves as the suture anchor point. The lower portion of the female component has a ridged inner surface to pair with the male component and facilitate the snap fit connection. The wider lip feature above the recessed

crossbar feature allows for approximately flush contact between the lip and the dorsal, cortical bone surface of the phalanx. This allows for the female component to be inserted from the dorsal aspect of the phalanx, within a 3.5 mm diameter hole drilled dorsal to plantar. From the plantar aspect of the phalanx, the male component would be inserted into the hole and snapped within the female component. The male component was designed to insert snugly within the female component, thus possessing two tongues with ridges matching the interface within the female component to allow the implant to snap into an appropriate position. A similar wide lip feature at the base of the male component was included to facilitate implant support of the plantar, cortical bone surface of the phalanx. Both lipped features provide compressive support to the implant placement within the phalanx and insulation of the dorsal and plantar cortical bone surfaces of the phalanx.

With the novel two-piece snap fitting implant design, an adjustment to the existing surgical techniques was proposed to accommodate this device. A notable difference in the approach is that both a dorsal and plantar incision would be required to insert the female and male components on each respective side of the hole within the proximal phalanx. The conventional approaches involved a single, dorsal incision accompanied by a metatarsal head osteotomy for plantar plate access [5,12-14,32,36-39]. Specifically, this surgical approach would directly access the plantar plate from the plantar aspect with a single incision beneath the MTPJ. A smaller, percutaneous incision would be made on the dorsal aspect, over the implant fixation site within the proximal phalanx. The position

and length of both incisions would be governed by the physician's professional opinion on patient anatomy and specifics.

Once the MTPJ is accessed from the plantar aspect, a standard debridement of the torn plantar plate at the distal insertion site in the phalanx would be required. A 3.5 mm diameter hole would be drilled centrally relative to the width of the proximal phalanx, either dorsal-to-plantar or plantar-to-dorsal depending on surgeon preference. The female component, preloaded with a suture-passing device with one suture loop on either side of the crossbar, would be placed from the dorsal aspect within the bone tunnel. From the plantar aspect, the male component would be placed in the bone tunnel, with the suture-passing loops placed through its central opening. With each component positioned appropriately in the bone tunnel, the physician would snap the components together by compressing the outer lip features until the underside of each lip was approximately flush with the cortical bone surfaces on either side of the phalanx.

1.8 Objective

This work aims to provide a successful experimental design, methodology, and preliminary results for the evaluation of a novel approach for plantar plate repair. A non-tissue based experimental design includes a custom test setup to assess isolated implant and suture functionality in uniaxial tension testing. A separate custom setup for a cadaver-based tissue model aims to characterize native plantar plate structural mechanics and compare the novel approach for plantar plate repair to a conventional approach for

plantar plate repair with a uniaxial test protocol. The analyses of isolated implant construct testing, native plantar plate testing, and simulated repair construct comparison testing were considered holistically in the assessment of this novel approach for plantar plate repair.

Chapter 2: Methods

2.1 Novel Implant Design

The novel implant device designed and developed for plantar plate repair was initially created through a Virginia Tech Engineering Science and Mechanics (ESM) Senior Design project. Pilot testing was performed during the Senior Design project phase to assess the end-stage prototype for feasibility and potential proof of concept. This project is a continuation of the Senior Design project that spanned the Spring 2020 to Spring 2021 semesters. Primary design features developed during the previous project were unchanged for the duration of this project, though minor dimensional modifications were adopted for ease of manufacturing and testing. A Formlabs Form 3 3D printer (Formlabs, Somerville, MA) was used to manufacture the components for each novel implant. The Rigid 4000 resin was the material used for each implant and was considered to have similar mechanical properties to polyether ether ketone (PEEK), specifically for tensile modulus [44-46]. PEEK is considered the end goal material for manufacturing this implant prior to clinical use, and it was important to replicate the plastic deformation response in the material of choice.

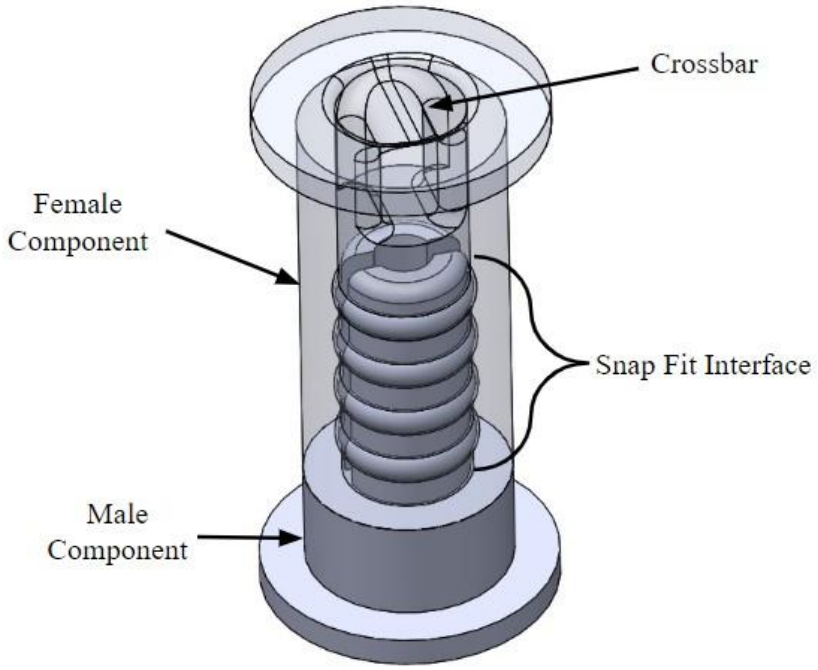

Figure 2.1: Labeled illustration of assembled novel implant construct and interior snap-fit mechanism.

2.1.1 Two-Piece Snap-Fit Connection Features

The novelty of this implant device for plantar plate repair is derived from a two-component design that features a snap-fit connection between the components (Figure 2.1) (Appendix C). The snap-fit connection between the male and female components was designed for multiple implant construct lengths, promoting the accommodation of varying anatomical proximal phalanx depths. The variable size of the implant construct is effective for maintaining an approximately flush contact on either cortical bone surface, dorsally or plantarly. Each component possesses a circular lip feature to rest on either dorsal or plantar cortical bone surface of the proximal phalanx (Figures 2.2 and 2.3). The female component would be inserted dorsally, with the underside of its lip feature resting on the dorsal cortical surface of the proximal phalanx. To ensure appropriate placement, a

dorsal to plantar 3.5 mm diameter hole would be drilled into the proximal phalanx, allowing the female component to fit snugly within it. The male component would be inserted from the plantar aspect, snapping into place within the female component until the male component lip feature rests close to the plantar cortical surface of the proximal phalanx.

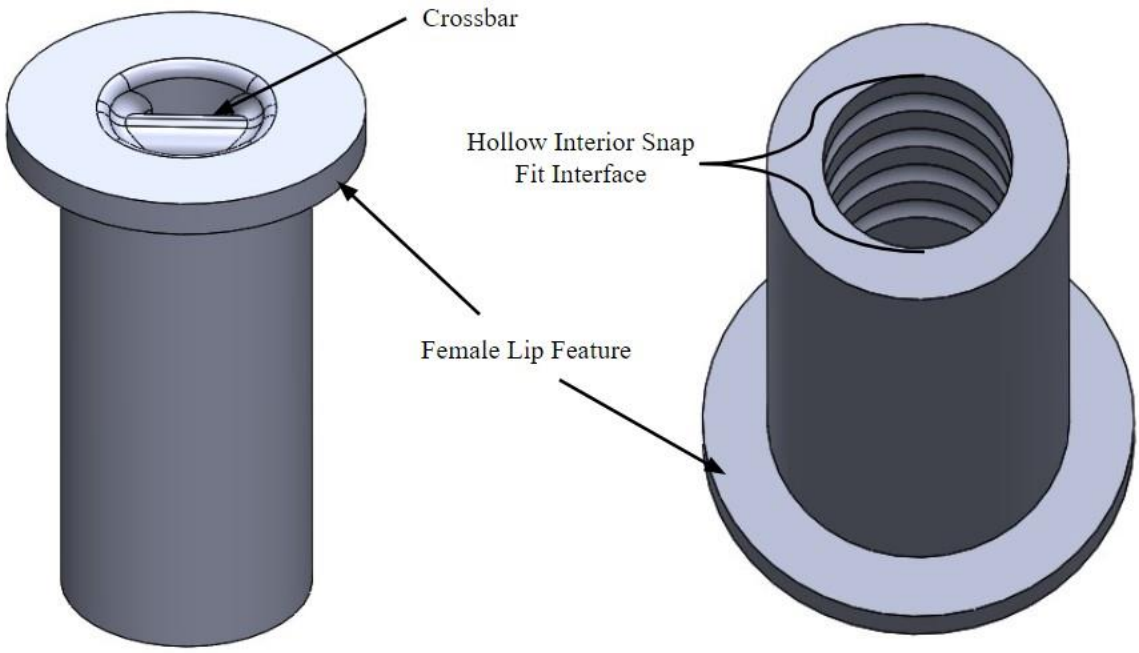

Figure 2.2: Labeled feature illustration of female component.

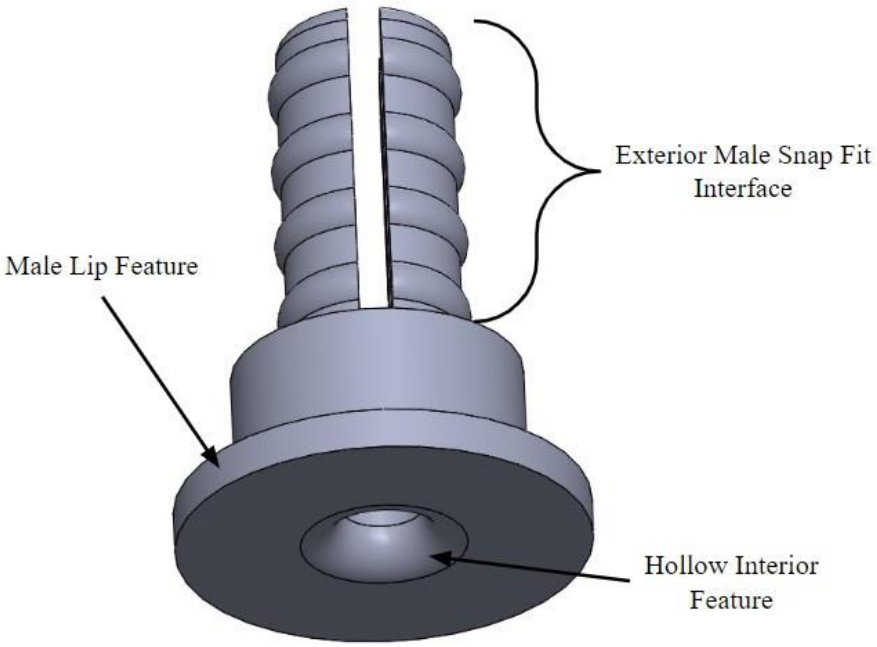

Figure 2.3: Labeled feature illustration of the male component.

2.1.2 Crossbar Feature for Suture Weightbearing and Cortical Bone Insulation

The female component possesses a recessed crossbar designed to insulate suture knot placement and enable mechanical support of suture tensile loads (Figure 2.2). When both components are snapped together in the proximal phalanx, the crossbar feature serves as the suture anchor point on the dorsal aspect. Strength of the crossbar with respect to anticipated tensile loads from the sutures was an important consideration during the development of the novel device. Accessibility and ergonomics for performing the surgical repair were also emphasized in the design phase, resulting in incremental crossbar width adjustments to allow for seamless shuttling of the sutures within the female component. The recess from the top plane of the female component was included to provide ample room to secure an appropriate knot to anchor the repair.

2.1.3 Proposed Surgical Technique Modifications

With the two-piece design of this novel implant, adjustments to existing surgical techniques were necessary to facilitate a plantar plate repair. Notably, both a dorsal and plantar incision would be required to provide access to place the female and male components, respectively. Compared to the recommendations of existing approaches, this approach would replace the need for a metatarsal osteotomy and retraction for plantar access with direct plantar access via incision. The proposed approach involves a plantar incision beneath the MTPJ for direct access to the injured plantar plate. A percutaneous incision would be made dorsally above the proximal phalanx at the site of implant placement, just distal to the head of the proximal phalanx as determined by the physician's expert clinical assessment. By approaching the injured plantar plate directly from the plantar aspect, a metatarsal osteotomy and retraction would be unnecessary to access the injured tissue and perform subsequent repair steps.

With direct access to the injured plantar plate, a standard debridement of the distal, torn plantar plate would be performed. A 3.5 mm diameter hole would be drilled from the dorsal to plantar aspect or from the plantar to dorsal aspect based on physician preference, positioned centrally relative to the width of the proximal phalanx. The female component, preloaded with a suture-passing device, a single suture passing loop on either side of the crossbar, would be placed from the dorsal aspect into the proximal phalanx hole. The male component would be placed from the plantar aspect, with the suture passing loops inserted in the hollow portion and snapped into place within the female

component. Snapping the components in position within the proximal phalanx should result in the lip features of each component to sit approximately flush with the dorsal and plantar cortical bone surfaces.

The surgeon would place size 0, non-absorbable suture through the proximal, healthy plantar plate that remains using a horizontal mattress stitch. The depth of suture placement would be determined at the discretion of the surgeon. Two suture limbs would extend from the dorsal side of the remaining plantar plate and the surgeon would fit a single limb into each of the suture passing loops protruding from the implant. A pull of the suture passing device dorsally would shuttle each limb of the suture to the dorsal aspect of the implant within the proximal phalanx. After tensioning the plantar plate repair, the suture would be secured with three surgeon's knots above the recessed crossbar feature of the female component. Both dorsal and plantar incisions would be closed according to the standard wound closure procedure.

2.2 Implant Mechanical Testing and Validation

2.2.1 Isolated Implant Mechanical Testing Apparatus

The strength and integrity of the novel implant device in isolation was tested under simulated load conditions and suture repair interactions using a custom MTS Insight 10 (MTS Systems Corporation, Eden Prairie, MN) test setup in uniaxial tension. A custom MTS testing apparatus was designed to remain fixed to the base of the MTS, allowing for adjustments to static dorsiflexion angle orientations relevant to the lesser MTPJs, between 0° and 80° dorsiflexion (Figure 2.4) [1,49]. In the custom test rig, an adjustable

centerpiece was designed with a single hole fit to the outer diameter of the novel implant device. The novel implant device would be inserted within the center piece, simulating fixation within the proximal phalanx, for each test sample. A rounded edge was outfitted for the centerpiece, simulating the rounded joint capsule on the plantar side of the MTPJ, allowing the sutures to pass freely into the fixed implant. *In vivo*, the sutures extend distally from the healthy plantar plate and vertically within the fixed implant positioned in the proximal phalanx. Passage along the plantar surface of the joint capsule was replicated using the rounded edge designed for the centerpiece (Figure 2.5). From the center piece, the sutures were suspended vertically from a ring loop fixture attached to the MTS load cell. The ring loop fixture anchor point was representative of the suture attachment to the remaining healthy plantar plate *in vivo*.

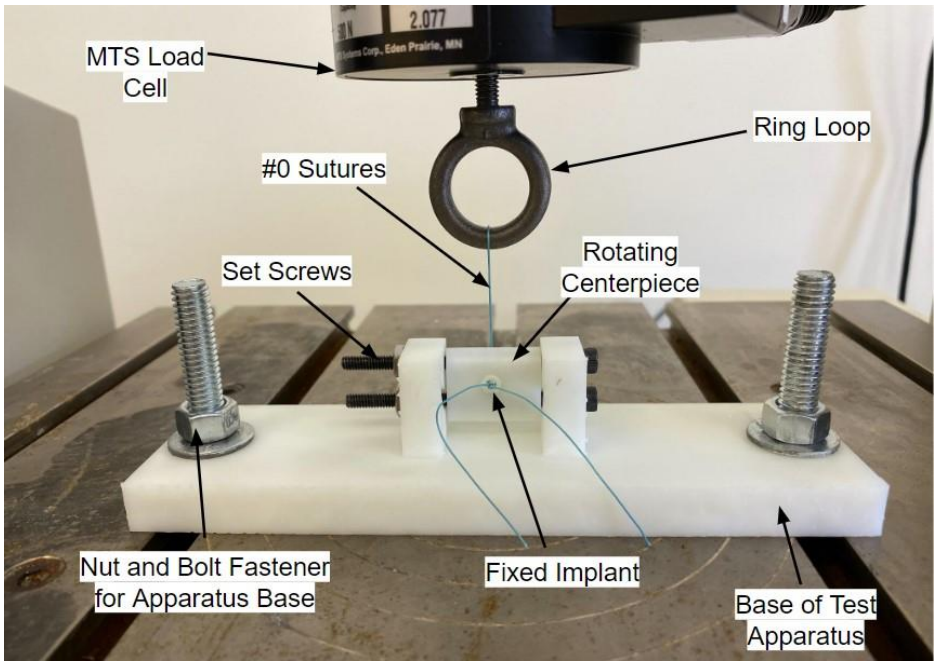

Figure 2.4: Labeled and annotated front perspective of the mechanical testing apparatus for novel implant-suture construct.

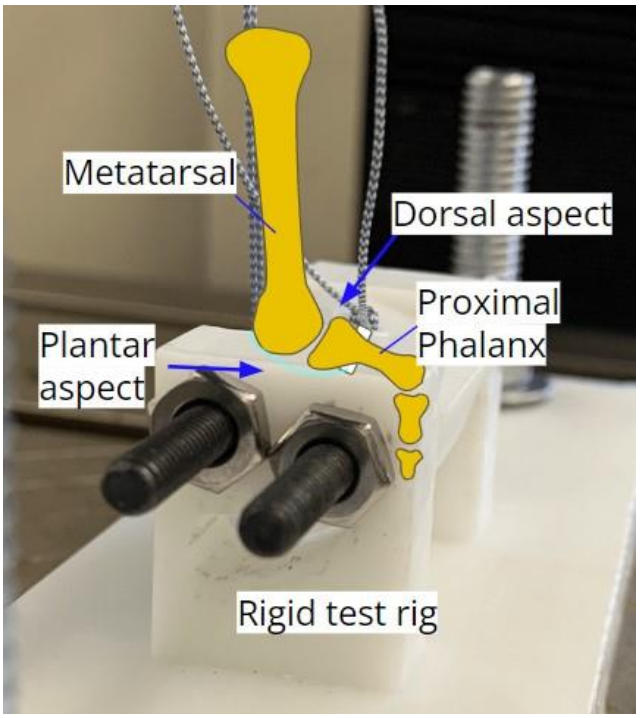

Figure 2.5: Simulated anatomical overlay on testing apparatus in 80° dorsiflexion orientation.

2.2.2 MTS Test Setup

The isolated testing apparatus was fixed to the base of the MTS and used with other replaceable parts to facilitate an anatomically relevant simulated test setup of the novel implant and suture fixation construct. The ring loop or eye bolt part was inserted into the load cell, which was fixed to the MTS crosshead. A single sample setup involved steps to secure the novel implant within the apparatus centerpiece and simulate proper suture fixation within the fixed implant. Before placement of the implant components, each component was examined to remove any excess or residual resin material from the 3D printing process. The female component was preloaded with a suture passing device and placed within the hole in the center piece, until the underside of its lip feature was flush with the flat surface of the centerpiece (Figure 2.6). The male component was placed

within the centerpiece hole from the opposite side, positioning the suture passing device through the hollow portion of the male component before snapping both components together. Both components were snapped together tightly until the underside of each lip feature was approximately flush with each flat side of the centerpiece (Figure 2.7).

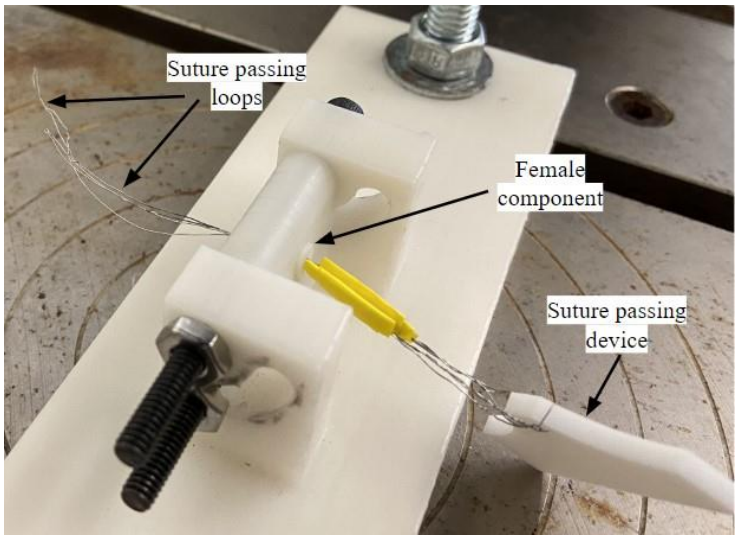

Figure 2.6: Female component preloaded with suture passing device inserted in centerpiece of rigid test apparatus, from simulated dorsal aspect perspective.

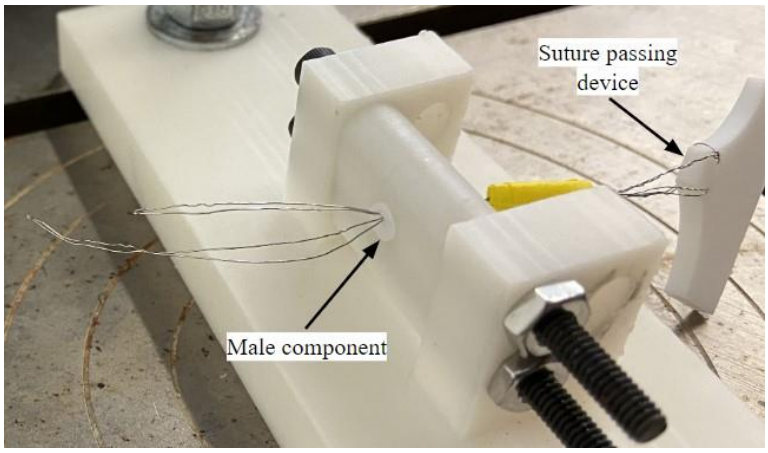

Figure 2.7: Male component snapped within female component in centerpiece of test apparatus, from simulated plantar aspect perspective.

A single, approximately 10 inch size 0, non-absorbable polyester suture was draped to suspend over the ring loop. Each limb of the suspended suture was passed through a single suture passing device loop securely, which extended from the hollow portion of the male component positioned in the centerpiece (Figure 2.8). The MTS crosshead was adjusted vertically as needed to allow the suture limbs to shuttle through the implant smoothly. The suture passing device was pulled through the secured implant, shuttling the sutures from the male component side to the female component side, simulating a pull of the sutures from the plantar to dorsal aspects *in vivo* (Figure 2.9 (a)). Each suture limb was adjusted on either side of the crossbar to maintain approximately equal lengths extending from the implant (Figure 2.9 (b)). The MTS crosshead was adjusted vertically to allow for approximately 5 cm distance between suture contact with the ring loop and suture insertion within the fixed implant (Figure 2.9 (c)). After 5 cm distance was confirmed, the sutures were tensioned manually and knotted over the crossbar with 3 square knots (Figure 2.9 (d)).

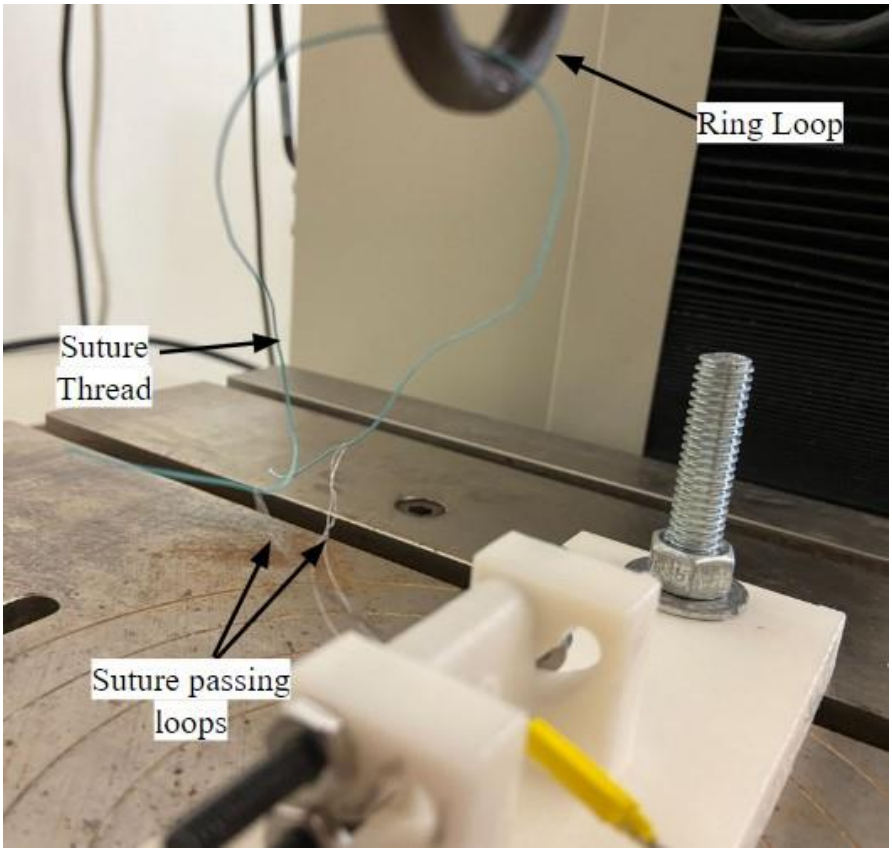

Figure 2.8: Image of suture thread wrapped around ring loop and inserted through suture passing loops for shuttling through implant.

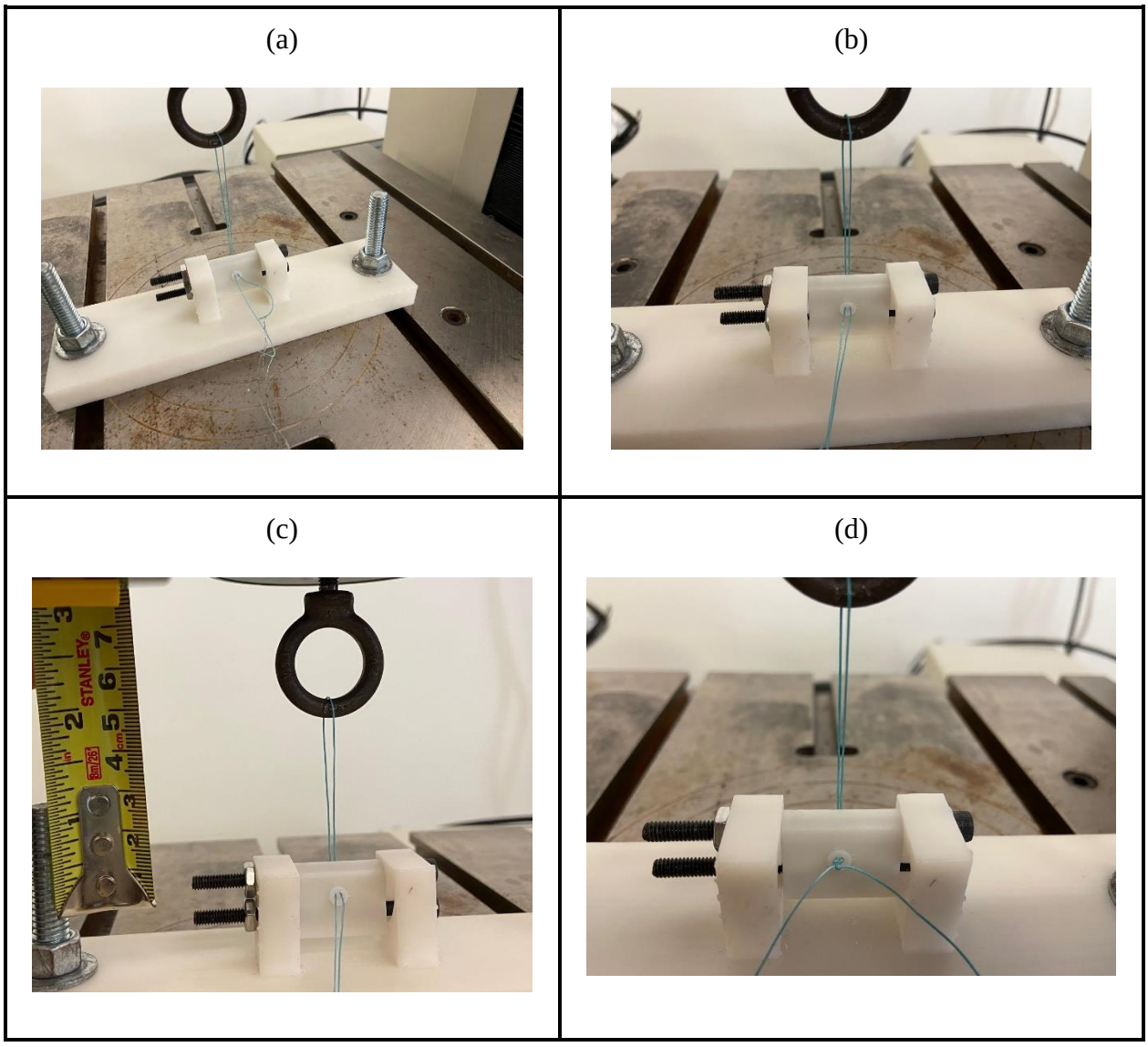

Figure 2.9: Illustration of suture knot fixation. (a) Passage of suture to simulated dorsal aspect, (b) Suture limbs adjacent to crossbar feature, (c) 5 cm suture length measurement, (d) Suture secured over crossbar with three surgeon's knots.

2.2.3 Load to Failure Mechanical Testing

A standardized load to failure test protocol was developed for the rigid apparatus setup to evaluate the mechanical behavior of the novel implant and suture fixation construct. The MTS was fixed with a 500 N load cell, to which the ring loop was secured. For each

sample, a randomly selected combination of one male component, one female component, and one thread of size 0 polyester suture (AD Surgical, Sunnyvale, CA) was setup for uniaxial tension testing. A 0.1 mm/s crosshead speed was prescribed and an upper limit of 450 N was applied within the software for load cell precaution. Before initiating the load to failure method file, the load output signal was zeroed with the sutures in slack. With the signal tared, a manual preload of approximately 10 N was applied to the sample and the method file was run.

During the load to failure test, each sample was monitored closely to note any knot slippage or movement and confirm sample failure before terminating the test. After each test was stopped, maximum load, displacement at maximum load, and the sample mode of failure were recorded in a lab notebook. Recorded signal data was captured at 100 Hz acquisition rate in the MTS TestWorks software and was exported and labeled after test completion for further data analysis. All materials for each sample were carefully removed from the setup and stored in a labeled bag for future reference and documentation.

MTS signal data for load and crosshead displacement were processed for analysis in MATLAB (MathWorks, Natick, MA). Relevant computations were performed to analyze the maximum load, tangent stiffness, and secant stiffness for each sample and recorded for further statistical analysis (Appendix A). Maximum load was determined using the built-in MATLAB “max” function and compared to the TestWorks output of maximum load recorded in the lab notebook. Tangent stiffness was calculated using the built-in

MATLAB “polyfit” function for a 1st order linear regression of the load vs. displacement data. Tangent stiffness was determined as the maximum slope value calculated in a linear regression consisting of a minimum of 40% of the total data points from the first recorded point until maximum load. The tangent stiffness was confirmed to lie outside of the toe region of the load-displacement curve if initial non-linearity was present. The coefficient of correlation or R^2 was calculated for each 40% region analyzed in a linear regression and the relevant value was reported with the tangent stiffness. Secant stiffness was calculated using a straight-line slope calculation between the first data point and the maximum load data point.

Three condition or treatment groups were considered for load to failure testing. Conditions for 0°, 40°, and 80° dorsiflexion were evaluated. These dorsiflexion conditions were determined based on the endpoints for normal MTPJ range of motion and an intermediate value. Dorsiflexion orientations were controlled by adjusting the centerpiece of the rigid test apparatus before sample testing. Each dorsiflexion group was evaluated separately using the load to failure protocol with the centerpiece and rigid test apparatus in the appropriate, static configuration. Physiologically, the MTPJ could rotate freely through the ROM from the neutral position at 0°, to the extreme dorsiflexion case at 80°. The uniaxial tension load to failure test was constrained to a static configuration oriented at a single dorsiflexion angle. Differences in maximum load and stiffness of the implant and suture fixation construct were compared across the dorsiflexion angle conditions. Each condition consisted of 12 samples tested (n = 12) in this load to failure setup, yielding a total of 36 samples overall.

2.2.4 Load to Failure Statistical Analysis

Each variable of interest, maximum load (N), tangent stiffness (N/mm), and secant stiffness (N/mm), was compared using a one-way analysis of variance (ANOVA) in JMP Pro 16 (Cary, NC). A one-way ANOVA was used to assess any differences between the means of a given variable of interest for the three independent dorsiflexion conditions (0°, 40°, and 80°). Prior to a one-way ANOVA, each dataset was confirmed to be normally distributed using both the Shapiro-Wilk and Anderson-Darling Goodness-of-Fit tests of a normal distribution. Assumption of a normally distributed dataset was necessary for a reliable one-way ANOVA. For any statistically significant differences among the dorsiflexion angles in the means of a particular mechanical outcome measure, a post-hoc Tukey's Multiple Comparisons test was used to pinpoint the differences between groups. All statistical analyses were performed with a 95% confidence level and $\alpha = 0.05$.

2.2.5 Cyclic Loading Mechanical Testing

After completing the load to failure test protocol at 0°, 40°, and 80° dorsiflexion, a standardized, load-controlled cyclic protocol followed immediately by a load to failure test was performed. Groups used for the cyclic and load to failure test protocol were changed based on the analysis of the initial load to failure outcomes. The extreme conditions for dorsiflexion, 0° and 80°, were evaluated with the cyclic and load to failure test protocol (Figure 2.10). Omission of the 40° dorsiflexion condition was permitted after a lack of statistically significant differences in the maximum load, tangent stiffness, or secant stiffness outcomes between the 0° or 80° dorsiflexion groups. The test speed for

this cyclic and load to failure protocol was increased by a factor of ten, from 0.1 mm/s to 1 mm/s. The increased crosshead speed was approved due to test length/time concerns for cyclic loading, clinical relevance, and no evidence of non-linearity in the load-displacement curves or significant time dependent, viscoelastic properties. Other studies have employed similar test speeds for braided, polyester suture in both cyclic and load to failure settings. MTS setup employing the rigid test apparatus was unchanged for this test protocol.

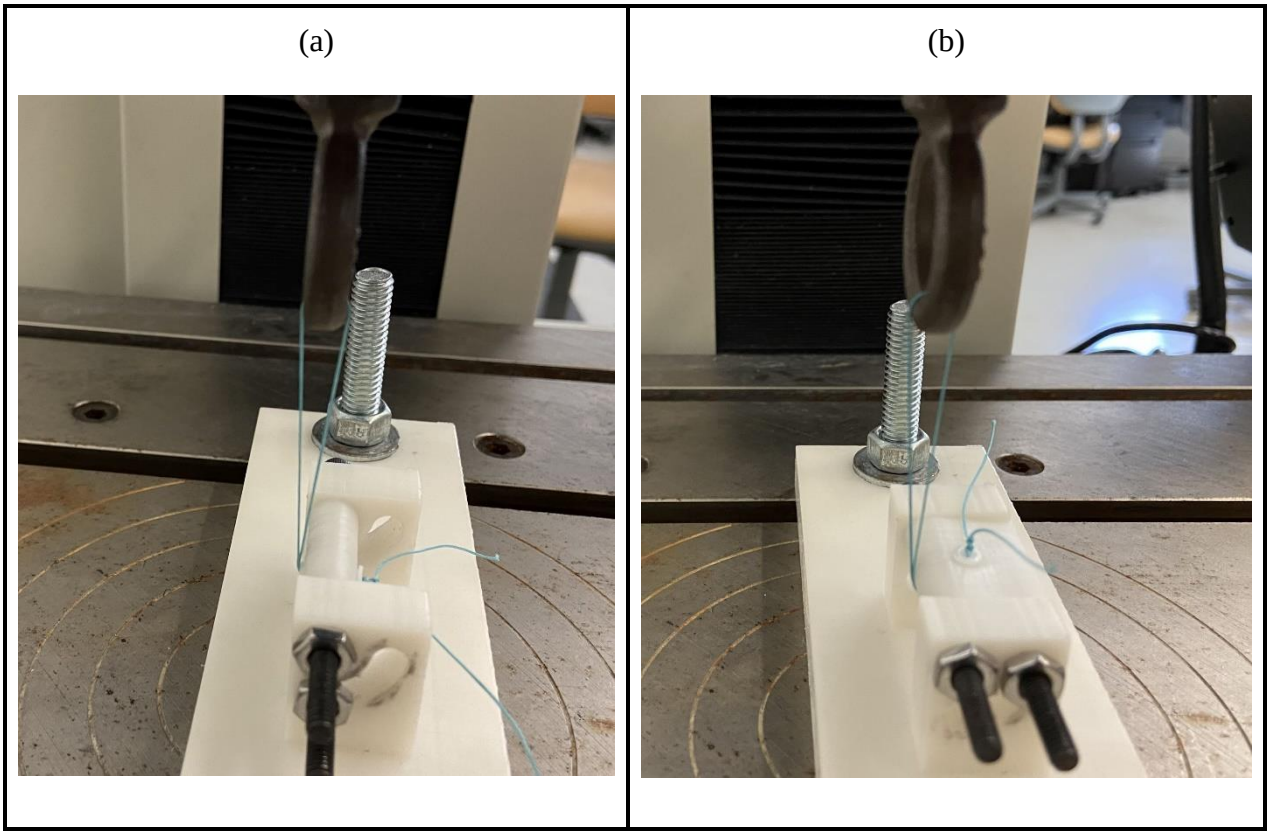

Figure 2.10: Side perspective of centerpiece simulated dorsiflexion orientations: (a) 0° dorsiflexion, (b) 80° dorsiflexion.

Load-controlled endpoints for the cyclic loading portion of this protocol were determined based on assessment of initial maximum load data for 0° and 80° dorsiflexion from the previous load to failure testing. Mean and standard deviation of all maximum load data were calculated. The mean maximum load value was subtracted by 1.5 times the standard deviations to obtain an initial upper load limit that ensured with 90% statistical confidence a given sample would not fail during a single ramp up. After initial pilot test constructs failed after a few cycles with this upper load limit, the upper bound was determined to be too extreme for evaluating many cycles. Subsequently, the previous upper load limit was divided in half, effectively implementing a factor of safety (FOS) of 2 for the implant and suture fixation construct.

Cyclic loading protocol details for the custom MTS method file consisted of a preload to 5 N, where the corresponding crosshead displacement was held constant for 30 seconds, followed by cycling between 10 N and 50 N at 1 mm/s for 100 cycles (Figure 2.11). All samples completed the 100 cycles, thus a load to failure test followed. The MTS crosshead was not moved after cyclic test completion, which allowed for the last cyclic protocol displacement value, corresponding to the displacement for the 10 N endpoint after the 100^{th} cycle, to coincide with the starting displacement in the load to failure test. Before opening the load to failure MTS method file, cyclic test signal data was exported and labeled for future analysis.

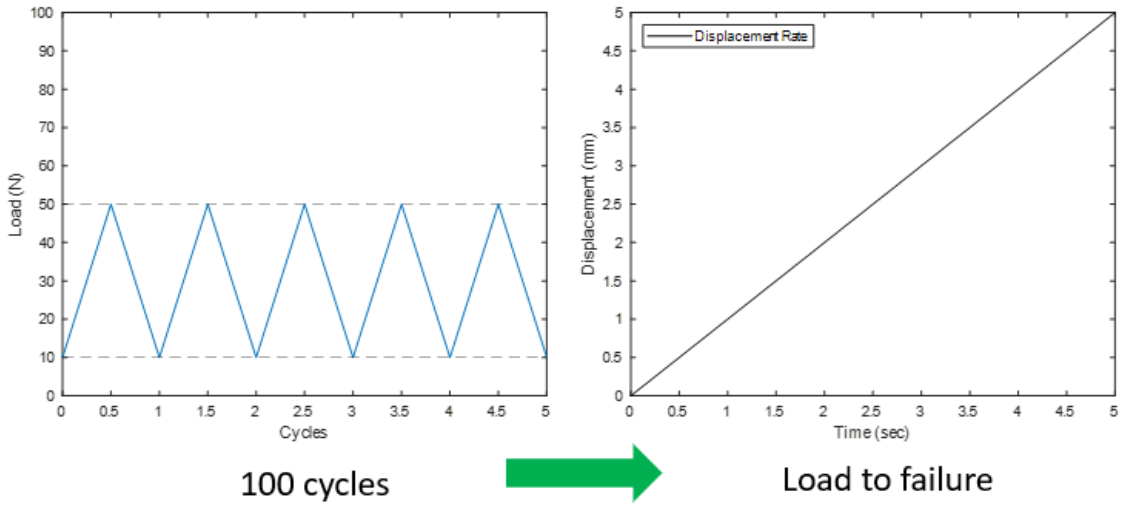

Figure 2.11: Schematic of load controlled cyclic loading immediately followed by load to failure at a constant crosshead speed (1 mm/s)

The load to failure method file was opened to initiate the follow-up test. This method file included a 1 mm/s crosshead speed and precautionary upper load limit of 450 N to protect the 500 N load cell. Once the method file was open, the load to failure test was initialized and run until a break or fracture was confirmed, both audibly and visually, for a given sample. The method file was stopped manually and the maximum load and displacement at maximum load values were recorded in a lab notebook. The sample was carefully disassembled and removed from the rigid test apparatus and stored in a labeled bag. All MTS signal data was exported and labeled for further analysis and the test file was saved as a failsafe. Data from the cyclic loading and load to failure tests were analyzed in MATLAB (Appendix A).

From the cyclic loading test, the elongation amplitude (mm) over the entire cyclic test and mean secant stiffness (N/mm) per cycle were calculated in MATLAB (Appendix A).

The elongation amplitude compared the difference in the mean displacement amplitudes between the last five cycles (cycles 96-100) and first five cycles (cycles 1-5) (Figure 2.12). This value was calculated to indicate the amount of creep that occurred during the cyclic loading test. Mean secant stiffness was evaluated by taking the average of the individual secant stiffness values calculated for each cycle over the entire 100 cycles (Figure 2.13). Evaluation of the secant stiffness was to inform any discrepancies across individual samples tested as well as between group analysis.

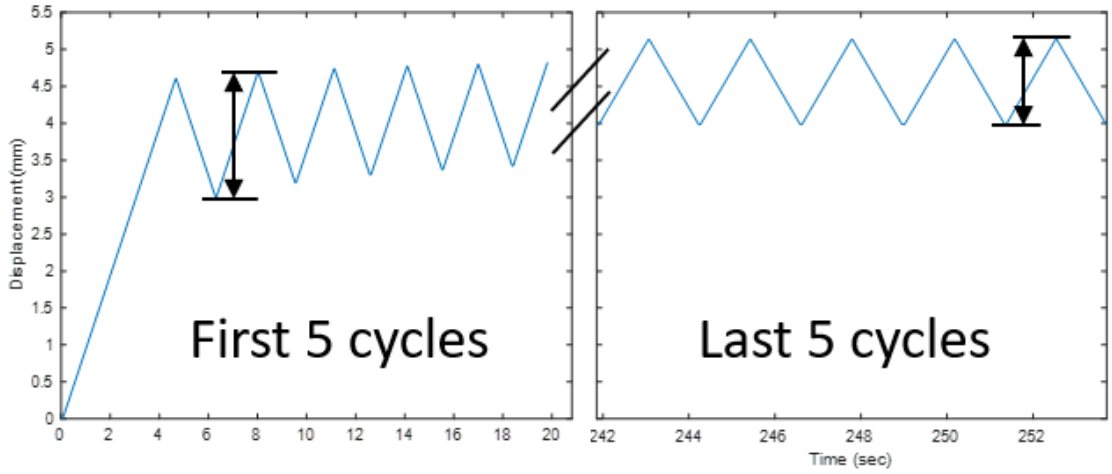

Figure 2.12: Schematic of individual elongation amplitude calculations from first and last cycles.

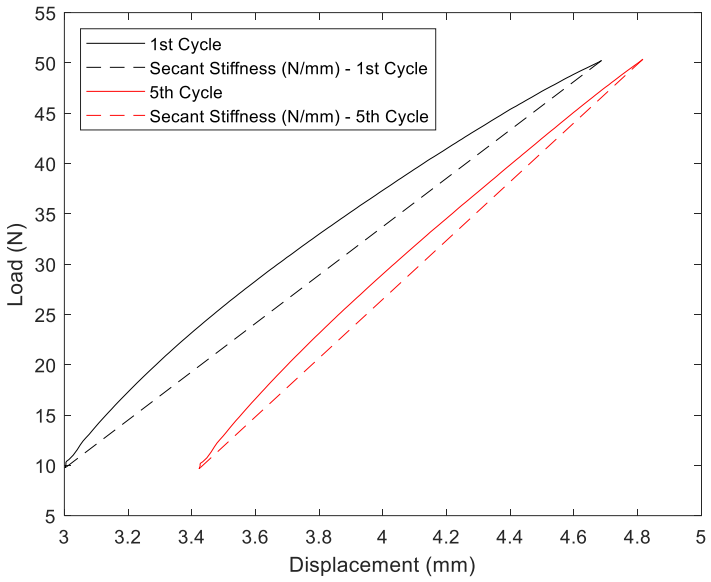

Figure 2.13: Schematic of 1st and 5th cycle secant stiffness calculations.

From the load to failure test, maximum load (N), tangent stiffness (N/mm), and secant stiffness (N/mm) were calculated using MATLAB (Appendix A). Maximum load was determined by the built-in MATLAB "max" function to evaluate the greatest load value achieved during testing. Tangent stiffness was determined as the maximum slope value from a linear regression that consisted of 40% of the data points from the start of the test until the maximum load. An R^2 value or coefficient of determination was calculated for each linear regression modeled and noted for the tangent stiffness value determined. Secant stiffness was calculated as the straight line slope calculation between the maximum load and the start of the test. A total of 24 samples were tested, with 12 samples tested independently for each dorsiflexion condition (n = 12 for 0° and 80° dorsiflexion).

2.2.6 Cyclic Loading Statistical Analysis

Data from the cyclic loading testing was compared with a t-test. Determination of use for either Student's or Welch's t-test was dependent on the results of a preliminary analysis of normality and unequal variances. Both the Shapiro-Wilk and Anderson-Darling Goodness-of-Fit tests were employed for normality assessment using JMP Pro 16. Each of these tests hypothesized that a given dataset follows a normal distribution. The O'Brien, Brown-Forsythe, Levene, Bartlett, and F Test 2-sided tests were employed to assess unequal variances in JMP Pro 16. These unequal variances tests hypothesized that the variances of two datasets, for a single given variable of interest, were equal. Assumption of normality and equal variances were required to conduct a Student's t-test. If the unequal variances tests were not confirmed, Welch's t-test would be conducted. All statistical tests were governed by a 95% confidence interval and $\alpha = 0.05$.

2.2.7 Comparative Load to Failure Analysis

Initial load to failure data analysis was compared to the data analysis of the load to failure tests following cyclic loading. Only data from the 0° and 80° dorsiflexion groups were considered for comparison. The maximum load (N), tangent stiffness (N/mm), and secant stiffness (N/mm) values were compared across the load to failure protocols for a given dorsiflexion condition. Either a Student's or Welch's t-test was used for statistical analysis, depending on the results of the normality and unequal variances assumptions. The Shapiro-Wilk and Anderson-Darling Goodness-of-Fit tests were used to assess normality and the O'Brien, Brown-Forsythe, Levene, Bartlett, and F Test 2-sided tests were used to assess unequal variances. Comparison of the results for each load to failure

protocol were intended to assess the impact of crosshead speed on maximum load and stiffness of the implant-suture fixation construct.

2.3 Cadaver Tissue Sample Harvesting

An *ex vivo*, human cadaver model was chosen to evaluate the native plantar plate structural mechanics and to compare the conventional repair with our novel implant fixation repair. A total of 15 lower ankle and foot limbs were procured from MedCure (Portland, OR). Of the 15 foot specimens, 10 specimens were paired feet (both left and right feet) from the same donor. The remaining five specimens were from five separate donors. In total, 10 donors (63.9 ± 11.7 years old, 6 male donors – 4 paired feet; 4 female donors – 1 paired feet) supplied the 15 foot specimens for our study (Appendix C).

From each specimen, both the 2nd and 3rd lesser MTPJs, including the metatarsal and proximal phalanx, were chosen for use in our study. The original plan of study consisted of 30 total samples, harvested from the 15 specimens (Appendix C). After pilot testing and initial setup validation, a total of 18 samples were used for formal mechanical testing. Of the other 12 samples, two samples were tested with modified preparation that included severing the ACLs, five samples were used in prior pilot testing to confirm the test setup, one sample was compromised during sample preparation, and four samples were excluded due to a lack of saline preservation while refrigerated. For the native plantar plate group, 8 samples (n = 8) were allocated for use. The other 10 samples were designated for the repair groups and divided as four samples for the conventional repair (n = 4) and six samples for the novel implant fixation repair (n = 6). All the samples were

harvested identically using a standard approach for extraction and the repair groups followed a standard, simulated repair fixation for both the conventional group and novel implant group.

2.3.1 Specimen Storage

All specimens were stored in a -20℃ chest freezer at the Virginia Tech Carilion School of Medicine (Roanoke, VA) anatomy lab before sample harvesting. Prior to harvesting, specimens were thawed in the anatomy lab. Two-thirds of the specimens were thawed for 24 hours in a refrigerator and then at room temperature (approximately 63°F) for 24 hours. The remaining one-third of the specimens were thawed for 48 hours in a refrigerator due to lab accessibility delays. All samples extracted from the specimens were harvested within the day for a given, scheduled harvesting session. Once remaining preparation steps were completed, all samples were transported on ice in a cooler to the Orthopedic Mechanobiology Lab at Virginia Tech for storage in a -20℃ stand-up freezer.

2.3.2 Post-Harvest Storage

All 8 samples designated for testing in the native plantar plate group were stored in a refrigerator for 14 days after harvest before transportation to the Virginia Tech campus. During refrigerated storage, the samples were wrapped and preserved with a 0.9% saline soaked gauze. This two week storage period was not intended since these samples were initially designated for use in the repair groups, before the study's sample distribution was altered. Initial pilot testing on the originally designated native plantar plate group

samples was not successful due to test setup, which required reallocation of the remaining samples for use in the native plantar plate group.

Of the 10 samples allocated to the repair groups, one sample (ID: 2203685(L3)) was not stored in the refrigerator between harvesting and simulated repair fixation. After completion of the simulated repair fixation, this sample was transported to the Virginia Tech campus and frozen until testing. The remaining nine samples in the repair groups were stored in the refrigerator for eight days between harvest and simulated repair fixation. Once these samples were prepared with the appropriate simulated repair fixation, all were returned to Virginia Tech and frozen the same day. Periodic storage of these samples in the refrigerator was chosen to maintain a consistent number of freeze and thaw cycles (1) for all samples after harvesting.

2.3.3 Tissue Harvesting

Each specimen was dissected by a podiatry resident to isolate the 2nd and 3rd MTPJs, including the metatarsal and proximal phalanx for each. After dissection and debridement surrounding the bones and MTPJ, the metatarsal, intact MTPJ, and proximal phalanx were extracted (Figure 2.14). A dorsal to plantar cut with either a bone saw or osteotome was made near the proximal base of the metatarsal to preserve the long portion of the bone. The length of both the 2nd and 3rd toes were separated from the adjacent toes manually with a scalpel blade. Distally, the proximal phalanx was cut at the proximal interphalangeal joint with a scalpel blade. With each end of the sample isolated, minor resection of remaining tissue was performed to remove the individual samples from the

specimen (Figure 2.15). Each sample harvested was placed in a labeled bag until further preparation or storage.

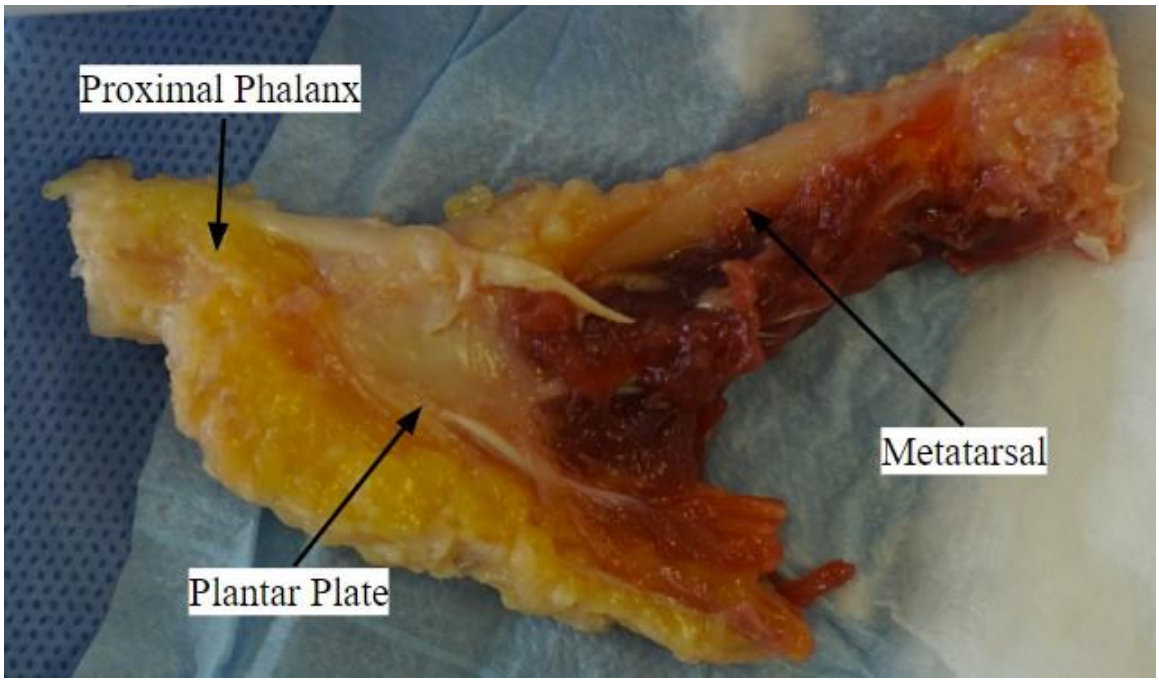

Figure 2.14: Labeled image of dissected sample before resecting surrounding soft tissue.

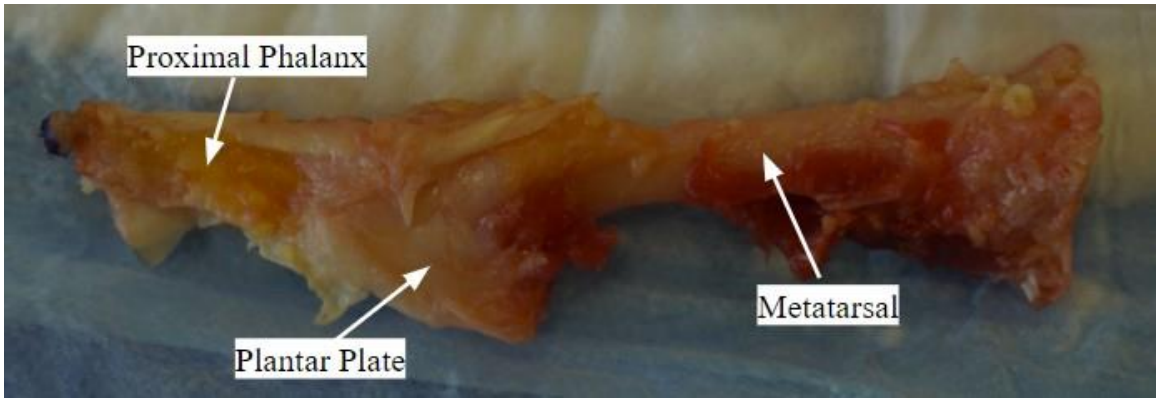

Figure 2.15: Labeled image of dissected sample after resecting surrounding soft tissue.

2.3.4 Simulated Repair Fixations

Each repair group sample was prepared with an identical distal, transverse plantar plate tear by a certified podiatric surgeon using a scalpel blade. The simulated tear location was chosen based on the surgeon's professional experience of the most common site for a plantar plate tear clinically. A size 0, non-absorbable polyester suture was placed in the proximal portion of the plantar plate using a horizontal mattress stitch. The proximal portion of the plantar plate represented the healthy tissue remaining after debridement in a standard, clinical setting.

For the simulated conventional repair technique, the approach was adapted to replicate the GRAVITY Plantar Plate Repair System [36]. Two holes were drilled from the dorsal to plantar aspect just distal to the head of the proximal phalanx using a ~1 mm Kirschner wire (K-wire). These holes were drilled following steps for the GRAVITY approach that would result in a cortical bone bridge between the holes on the dorsal side of the proximal phalanx. A suture passing device was inserted through the holes, with one loop passing separately in each hole, from the dorsal to plantar side of the proximal phalanx. Each limb of suture that was placed in the torn plantar plate was passed through a single suture passing loop. The suture passing device was pulled dorsally to shuttle the suture limbs to the dorsal aspect. On the dorsal side of the proximal phalanx, the suture was tensioned according to the professional opinion of the surgeon before being secured with three surgeon's knots over the proximal phalanx bone bridge.

In the simulated novel implant repair technique, a single 3.5 mm diameter bone tunnel was drilled dorsal to plantar distal to the proximal phalanx head. The female component of the novel implant was preloaded with a suture passing device and inserted into the proximal phalanx bone tunnel. The suture passing loops were inserted through the male component on the plantar aspect of the proximal phalanx and the male component was slid toward the female component in the proximal phalanx bone tunnel. Applying force along the length of the implant construct, the male component was snapped into place within the female component. Each suture limb extending from the torn plantar plate was inserted through a single suture passing loop and the suture passing device was pulled dorsally to shuttle the suture to the dorsal side of the proximal phalanx. The surgeon tensioned the suture according to their expert opinion and secured the suture with three surgeon's knots over the crossbar feature of the implant construct (Figure 2.16).

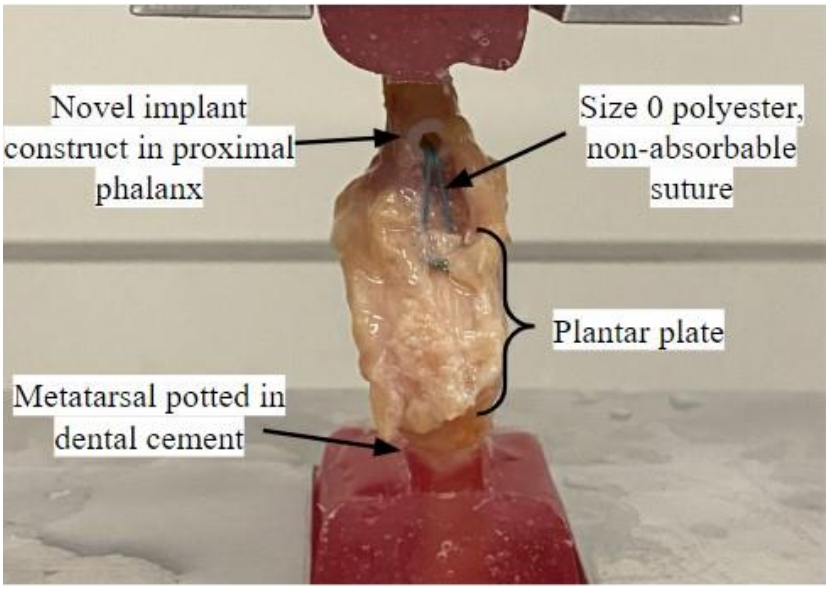

Figure 2.16: Simulated plantar aspect perspective of a novel repair sample fixed for mechanical testing.

After either simulated repair technique was performed on a sample, the sample was wrapped in 0.9% saline soaked gauze for preservation during transport. The wrapped samples were placed in labeled bags and on ice in a cooler before transport to the Virginia Tech campus. After arrival at Virginia Tech, all samples were placed in a -20°C standing freezer in the Orthopedic Mechanobiology lab for long-term storage until subsequent mechanical testing.

2.4 Cadaver Tissue Mechanical Testing Setup

A custom designed wedge grip test setup was fitted for uniaxial tensile testing on a MTS Insight 10 (Figure 2.17). The wedge grip setup was designed to fit a dental cement potted segment on each end. This grip construct allowed for a single sample with both the metatarsal and phalanx potted in dental cement to slide into place within each grip for uniaxial tensile testing [50]. Suspended between the potted bone ends, the MTPJ with the plantar plate of interest would be loaded in tension during testing. The wedge grip and cement mold designs were designed to the MTS dimensions and approximate anatomical dimensions of the 2nd and 3rd metatarsal and proximal phalanx [51,52]. Each wedge grip was manufactured to dimensions with Multipurpose 6061 Aluminum from McMaster-Carr. The proximal phalanx wedge grip was designed to fit in the load cell attached to the MTS crosshead. The metatarsal wedge grip was designed to remain fixed to an attachment plate securely connected to the base of the MTS test frame.

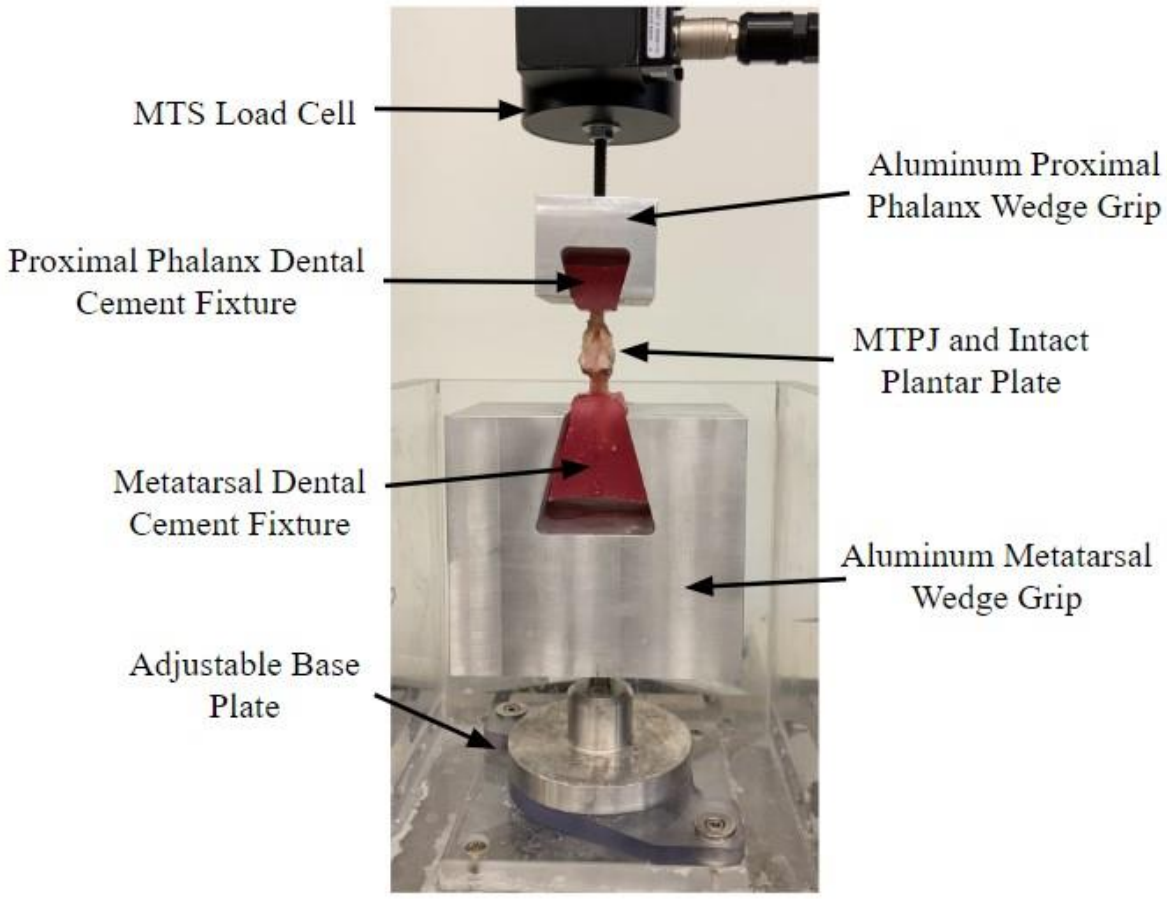

Figure 2.17: Annotated image of cadaver tissue mechanical testing setup.

Prior to mechanical testing, each tissue sample was thawed, surrounding tissue was trimmed, and then fit in custom molds and potted with dental cement (Stoelting Co., Wood Dale, IL), as detailed below. During the preparatory phase, the sample was hydrated with a 0.9% saline solution. While the dental cement cured, the plantar plate and surrounding soft tissues in the MTPJ were kept moist with 0.9% saline soaked gauze. The hardened dental cement fixtures were hand filed to size for precise fitting with the aluminum wedge grips prior to mechanical testing.

2.4.1 Sample Preparation

Each sample, in its storage bag, was removed from the freezer and placed in a water bath for approximately 30 minutes to thaw. Once thawed, the sample was removed from its labeled bag and moved to a preparation area on a cutting board to prepare the sample for fixture dental cement potting. Before resecting any further tissue from the sample, 0.9% saline was applied to rehydrate the sample before scalpel trimming. The sample was then trimmed with a scalpel blade around the long bone portions of both the metatarsal and proximal phalanx. For the metatarsal, scalpel blade resection was performed primarily on the proximal end and toward the distal end, stopping short of the metatarsal neck, specifically near the plantar plate origin at the base of the metatarsal head. Resection of the proximal phalanx was focused on the distal end of the bone, stopping shy of the proximal end, near the plantar plate insertion at the base of the proximal phalanx. Resection of adipose and membranous tissue around the MTPJ soft tissue structures was performed minimally before dental cement potting. Throughout the sample resection, 0.9% saline solution was applied as needed to hydrate the tissues.

After the surrounding tissues were resected from a given sample, two distraction K-wires were placed within the metatarsal and phalanx transverse to the long axis of the sample to better secure the sample in the dental cement. A 0.9 mm, 1.1 mm, or 1.5 mm diameter K-wire was inserted into the metatarsal and phalanx transverse to the bone's long axis and cut down to fit the size of its respective fixture mold. Positioning of the K-wire along the bone length was dependent on the sample size and the bone quality. Ideally, the K-wires were placed as far away from the central MTPJ soft tissue structures as possible. This

placement would allow for a greater size K-wire once placed in either bone to fit within the fixture molds. For samples with lesser bone quality based on observation, K-wire placement was adjusted independently, though usually resulting in the K-wire to be placed closer to the MTPJ and a shorter length wire left within each bone. This positioning was modified to combat the potential of weakening the bone around the location of the K-wire, which would increase the susceptibility of abnormal bone fractures during mechanical testing of the plantar plate.

2.4.2 Dental Cement Potting

The fixture molds were designed to fit the aluminum wedge grips in the MTS setup and were 3D printed using Formlabs Grey Pro resin. After placement of the K-wires in a given sample, the fixture mold pieces were lined with Parafilm on the inner surfaces that would contact the dental cement solution. The fixture mold pieces were then connected with screws and nuts, sealing the inner wedge shape. Two layers of Parafilm were then placed on the base of the fixture molds. The bone ends of the sample were then placed in the slotted gap of the respective fixture mold with the plantar aspect facing upward and away from the base of the molds. The sample was kept in place by guillotine-like pieces, secured with two screws and nuts each. Saline soaked gauze was wrapped around the MTPJ extending between the fixture molds. Fixture molds with the sample in position were then transferred to a fume hood for dental cement mixing and pouring.

The dental cement was created by combining scoops of the cement powder and liquid solution provided in a small cup, mixing with the wood end of a wooden cotton

applicator. Ratio of dental cement powder and liquid was adjusted until the cement had a sticky, gel-like consistency. The dental cement was poured slowly into each of the fixture molds, while the sample was held in its appropriate position. Once the bone ends in the fixture molds were submerged in the dental cement, the sample was left idle for approximately 30 minutes to allow the dental cement to cure and set within the molds. Periodic rehydrating of the saline soaked gauze was performed as needed. After the dental cement was cured, the fixture mold pieces were disassembled and removed carefully. The edges of the wedge-shaped dental cement fixtures were hand filed, smoothing the sides prior to being positioned in the MTS grip system.

2.4.3 Plantar Plate Dissection and Isolation

Two methods were initially used to isolate the plantar plate based on surrounding anatomy and interpretation of the MTPJ biomechanics. Both methods included a dorsal release of the MTPJ capsule, allowing access to the articular surfaces of the metatarsal and proximal phalanx and surrounding collateral ligaments. The first method of preparation was using a complete isolation of the plantar plate as described in the literature by severing the surrounding proper collateral ligaments (PCLs) and accessory collateral ligaments (ACLs) on both the medial and lateral sides of the MTPJ. This technique was to leave the plantar plate as the lone soft tissue structure between the bones, connected at the origin and insertion of the plantar plate. The second method of preparation involved the severing of the PCLs while leaving the ACLs intact with the plantar plate. This technique was justified by the congruence of the ACLs and the plantar plate, whereas the PCLs only directly attach the metatarsal to the proximal phalanx [3].

An initial set of pilot tests were performed to evaluate the suitability of either method of isolating the plantar plate to obtain clinically relevant failure results during mechanical testing. The results from the initial technique comparison indicated that the second method of maintaining ACL integrity in the MTPJ was more effective for providing clinically relevant modes of failure. Severing both the PCLs and ACLs led to a failure mode observed at the plantar plate origin beneath the metatarsal head at much lower loads, whereas with the ACLs intact the failure modes were observed toward the distal plantar plate insertion at a higher load and stiffness. Thus, the second preparation technique, keeping the ACLs intact, was chosen for each repair group sample.

2.5 Cadaver Model Mechanical Testing Protocol

The uniaxial tensile testing protocol to evaluate the cadaver model tissue samples was kept consistent across both the native plantar plate group and each repair fixation group. Using calipers, each sample was measured for width and thickness at three different points along the plantar plate length, proximal to distal. These values were recorded and averaged for reference (Appendix C). The sample was fixed within the top, phalanx grip attached to the MTS and suspended to hang without support at the base, to allow the load signal to be zeroed before testing. After adjusting the crosshead, the sample was placed in each aluminum grip while the soft tissue structures were slack. The base piece of the setup was adjusted horizontally to ensure vertical alignment of the sample during uniaxial tensile testing (Figure 2.18). The MTS crosshead was adjusted manually to ensure appropriate positioning of the dental cement fixtures within the wedge slots of the

aluminum grips. Manual adjustments were monitored closely to prevent excessive loading of the sample before testing. Once the sample was in position, 0.9% saline solution was applied to the plantar plate tissue and fixation construct, for the repair groups.

(a)

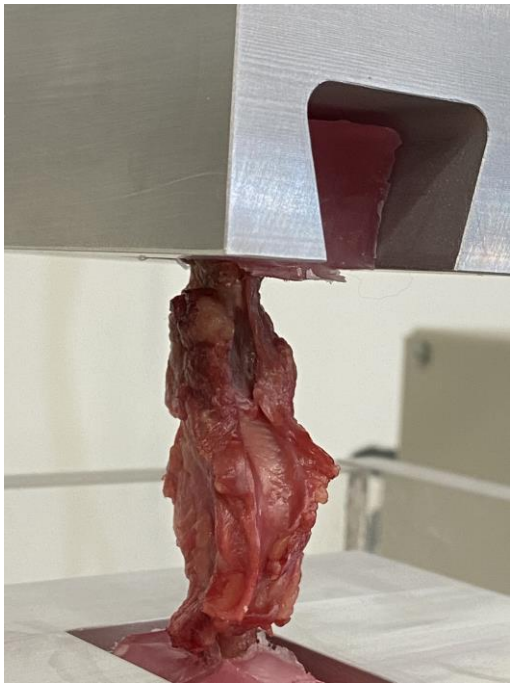

(b)

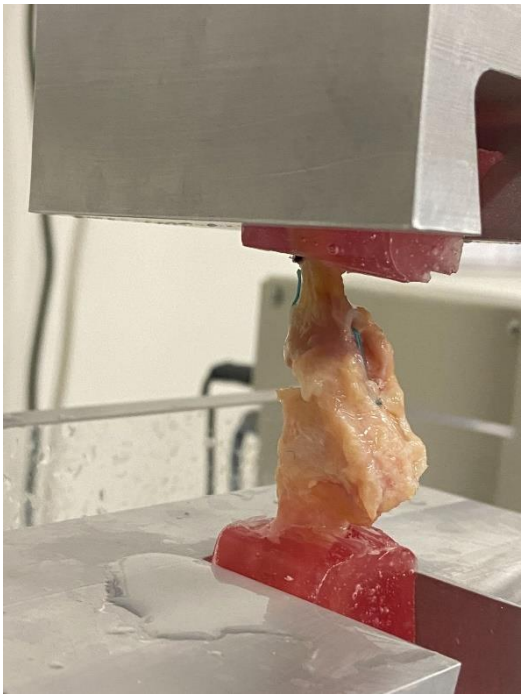

Figure 2.18: Angled perspective of sample vertical alignment for: (a) a native plantar plate tissue sample and (b) a novel implant repair tissue sample.

A custom, preload Testworks Method file was used to initialize the test protocol, applying a 3 N preload to each sample. Once the preload was applied, a timer was set for three minutes before initiating the following preconditioning file. During this time, the length of the plantar plate or plantar plate and repair construct was measured at three

points, the left edge, centrally, and the right edge. These lengths were averaged and provided the initial length of the plantar plate, for which the following test speeds would be based upon. The initial plantar plate length was determined to be the point of 0% strain.

The preconditioning file consisted of cyclic loading between 0% and 5% strain for 20 cycles at a rate of 1% strain per second. These parameters were chosen to provide a consistent strain rate for each sample tested, regardless of relative anatomical size. During the three minute rest period following the preload, the tissue was hydrated with the saline solution. Once the three minute rest period following preload was completed, the preconditioning protocol was initialized and run to completion. After completion of the 20 cycles for preconditioning, another three minute timer was set for rest before initiating the load to failure protocol. Preconditioning signal data was exported and labeled for future analysis. During the rest period, final crosshead displacement was held constant, representing the initial 0% strain point determined after preload.

The load to failure protocol was governed by the same 1% strain per second rate as the preconditioning protocol. Maintaining displacement rate consistency throughout an individual sample tested and normalized across all samples was important for the interpretation of test results. During the rest period following the preconditioning protocol, the plantar plate was hydrated with the saline solution. After completing the rest period following preconditioning, the load to failure file was run until significant failure was observed or a break was detected by the MTS software. The location and mode of

failure was determined and recorded on the sample data sheet after removing the sample from the MTS grips. Signal data was exported and labeled after the load to failure test and a test file was saved as a failsafe mechanism.

2.6 Cadaver Model Data Analysis

Analysis of MTS load and crosshead displacement data, which was acquired at a rate of 100 Hz, was performed using MATLAB. Calculation of maximum load at initial failure, tangent stiffness, and secant stiffness at failure was conducted using a custom MATLAB script (Appendix A). The maximum load at initial failure was corroborated with mode of failure determination during mechanical testing observation. Emphasis was placed on the initial sign of failure rather than the true maximum load achieved throughout testing because of the importance of resisting significant deformation or failure in clinical applications. Tangent stiffness was calculated on the terms of the steepest slope for a linear regression model spanning 40% of the total data points from the start of the test until the initial failure point. This methodology was employed to analyze the linear region between the initial toe region and yield region prior to failure while minimizing the potential to identify the slope from a narrow region of the data that would not represent the linear region of the curve. The coefficient of determination, R^2, was calculated for each linear regression model assessment to ensure tangent stiffness was accurately determined over a linear region. Any coefficient of determination value less than 0.90 for a calculated tangent stiffness resulted in the omission of the tangent stiffness value. Secant stiffness was calculated from the test start point and initial failure point as endpoints in a straight line slope equation. Each of these calculations were evaluated as

structural properties for a given sample from the load and crosshead displacement data reported during the load to failure test.

Statistical analysis and comparison of the cadaver model mechanical testing data focused on assessing differences between the native plantar plate, conventional repair fixation, and novel implant fixation groups. A one-way ANOVA test was performed on each of the maximum initial failure load, tangent stiffness, and secant stiffness calculations using JMP Pro 16. To satisfy the normal distribution assumption of a one-way ANOVA test, a preliminary assessment of normality was performed for each individual group dataset. The Shapiro-Wilk and Anderson-Darling Goodness-of-Fit tests were employed to determine whether the assumption of a normal distribution was appropriate using JMP Pro 16. For any statistically significant difference of means between groups, a post hoc Tukey's Multiple Comparisons test would be performed to identify the group differences. All statistical comparisons were made with a 95% confidence interval and $\alpha = 0.05$.

Chapter 3: Results

3.1 Isolated Implant Construct Analysis

3.1.1 Load to Failure Analysis

A quantitative and qualitative assessment of the isolated implant construct initial load to failure testing was performed. Quantitatively, the maximum failure load (N), tangent stiffness (N/mm), and secant stiffness (N/mm) were calculated in MATLAB and compared across dorsiflexion conditions (Figures 3.1-3.3). Qualitatively, each sample was examined before and during testing to identify any abnormalities or contributing factors to the mode of failure. Discrepancies in the materials or setup during testing were noted in a lab notebook along with each sample mode and location of failure. In total, 36 samples were tested across three dorsiflexion conditions, 0°, 40°, and 80° (n = 12 per group).

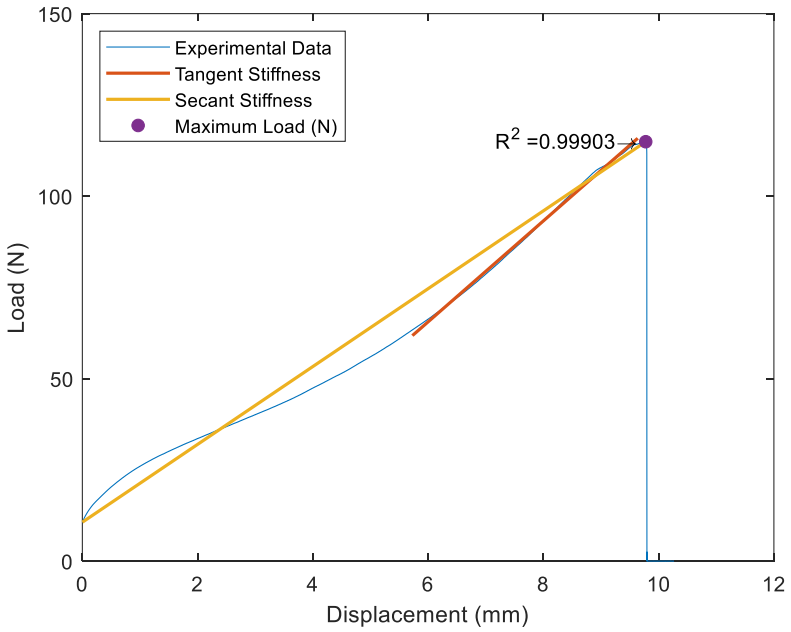

Figure 3.1: Example of 0° dorsiflexion load to failure experimental data and analysis in MATLAB.

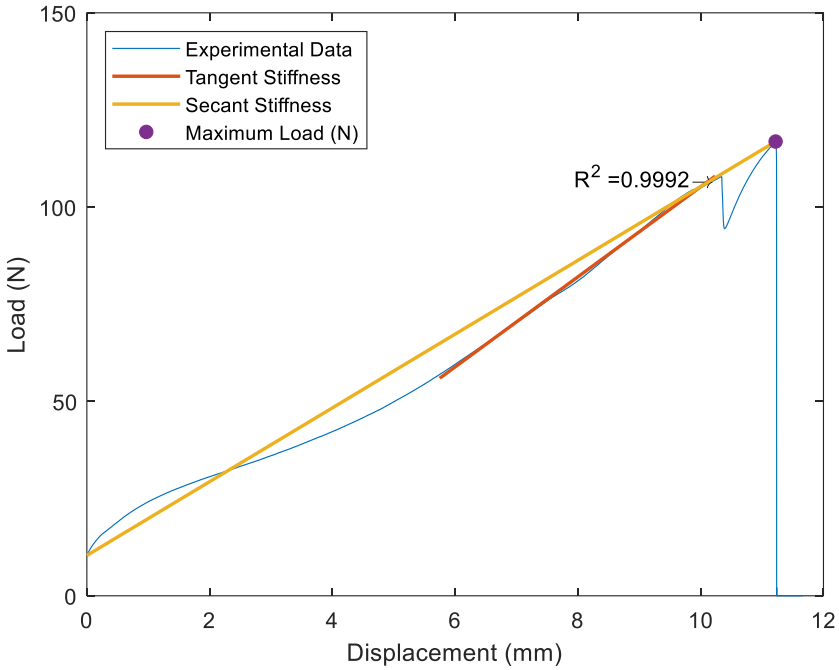

Figure 3.2: Example of 40° dorsiflexion load to failure experimental data and analysis in MATLAB.

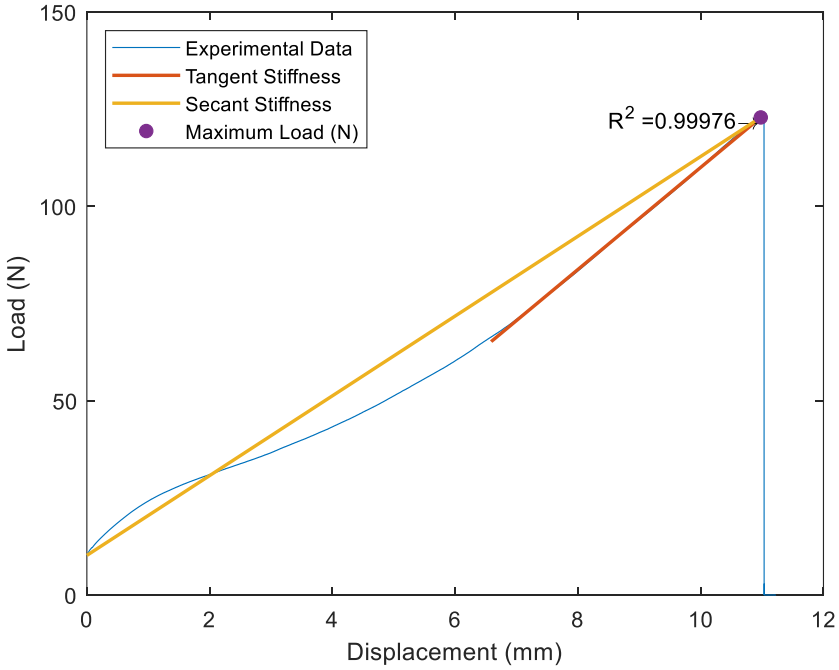

Figure 3.3: Example of 80° dorsiflexion load to failure experimental data and analysis in MATLAB.

The Shapiro-Wilk and Anderson-Darling Goodness-of-Fit tests were performed for each dataset in each dorsiflexion condition. The p-values from the normal distribution Goodness-of-Fit tests are reported in Table 3.1.

Table 3.1: Normal Distribution Goodness-of-Fit Test p-values for Load to Failure Only Testing

Mechanical Testing Data	*Max Load (N)*		*Tangent Stiffness (N/mm)*		*Secant Stiffness (N/mm)*	
Normality Test	*Shapiro-Wilk*	*Anderson-Darling*	*Shapiro-Wilk*	*Anderson-Darling*	*Shapiro-Wilk*	*Anderson-Darling*
Dorsiflexion Condition (Degrees)	*p-values*					
0° (n = 12)	0.3761	0.326	0.7517	0.7324	0.8397	0.8172
40° (n = 12)	0.4535	0.5856	0.4482	0.2864	0.912	0.7208
80° (n = 12)	0.4023	0.2216	0.1046	0.1732	0.6498	0.6588
Total (n = 36)	0.8751	0.8828	0.2529	0.1624	0.8201	0.7824

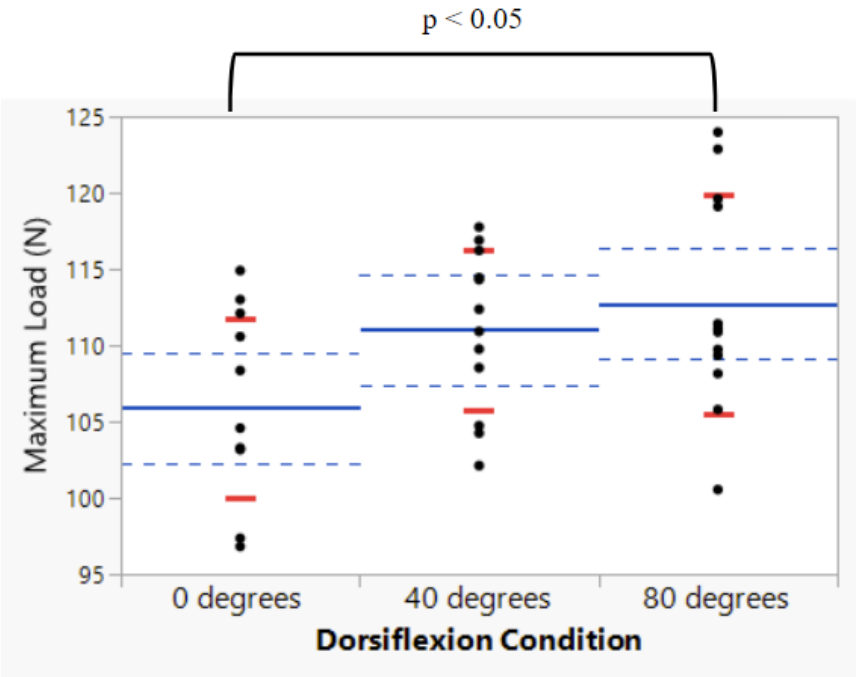

Figure 3.4: Scatterplot of the maximum load (N) data for each dorsiflexion condition. Solid blue line: Mean; Dashed blue line: 95% confidence interval; Red hashes: one standard deviation from mean.

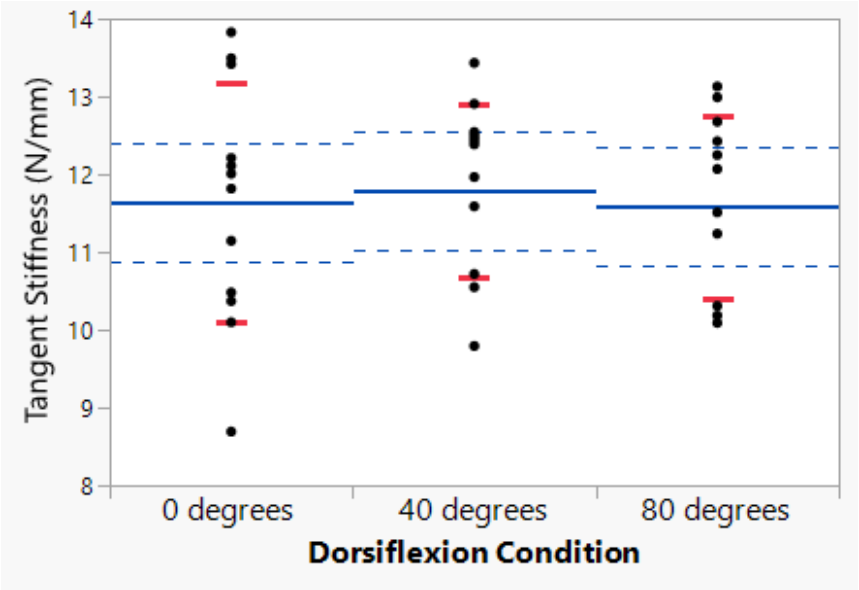

Figure 3.5: Scatterplot of the tangent stiffness (N/mm) data for each dorsiflexion condition. Solid blue line: Mean; Dashed blue line: 95% confidence interval; Red hashes: one standard deviation from mean.

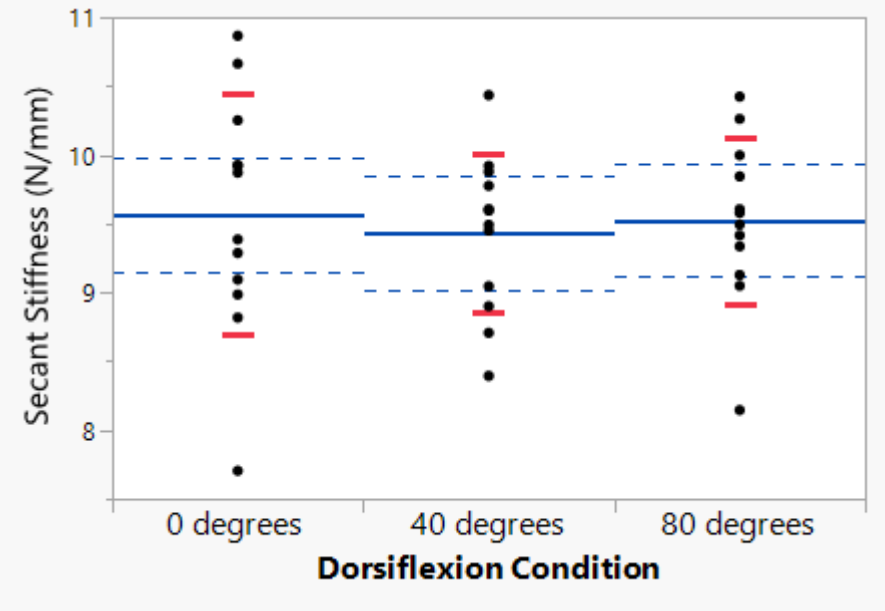

Figure 3.6: Scatterplot of the secant stiffness (N/mm) data for each dorsiflexion condition. Solid blue line: Mean; Dashed blue line: 95% confidence interval; Red hashes: one standard deviation from mean.

We failed to reject the null hypothesis (all $p > 0.05$), assuming that the datasets were normally distributed (Table 3.1). Thus, the assumption that the data followed a normal distribution was satisfied to proceed with a one-way ANOVA test. The p-value for a one-way ANOVA test of the maximum failure load (N) was 0.0278 ($p < 0.05$). We reject the null hypothesis for the maximum failure load that there is no difference in mean maximum failure load across the dorsiflexion conditions. A post hoc Tukey-Kramer Honestly Significant Difference test identified that the 0° and 80° dorsiflexion conditions were significantly different with $p = 0.0275$ (Figure 3.4). This significant difference ($p < 0.05$) was determined to show an increase in the mean maximum failure load with increased dorsiflexion condition, from 0° to 80°. While the maximum failure load showed a significant increase from 0° to 80° dorsiflexion, no significant difference was

observed between either 0° and 40° (p = 0.1175) or 40° and 80° (p = 0.7819). The one-way ANOVA test for both tangent stiffness and secant stiffness revealed no statistically significant difference between the group means, p = 0.9157 and p = 0.8952 respectively (p > 0.05) (Figures 3.5 and 3.6). Since no statistically significant differences were observed between the 40° dorsiflexion condition and either 0° or 80° dorsiflexion conditions across any values determined, the 40° dorsiflexion condition was omitted from further testing in the following cyclic loading protocol.

Table 3.2: Summary Statistics from Load to Failure Only Testing

Dorsiflexion Condition	**Calculated Value (reported as: mean ± standard deviation)**		
	Max Load (N)	*Tangent Stiffness (N/mm)*	*Secant Stiffness (N/mm)*
0° (n = 12)	105.9 ± 5.9	11.6 ± 1.5	9.6 ± 0.9
40° (n = 12)	111.0 ± 5.3	11.8 ± 1.1	9.4 ± 0.6
80° (n = 12)	112.7 ± 7.2	11.6 ± 1.2	9.5 ± 0.6
Total (n = 36)	109.9 ± 6.7	11.7 ± 1.3	9.5 ± 0.7

Qualitatively, a majority of the isolated implant construct initial load to failure tests resulted in a complete suture rupture mode of failure without implant damage. 35 of the 36 total tests (97%) failed by suture rupture during load to failure testing. One of the 0° dorsiflexion condition samples had a noticeable partial implant fracture during the load to failure testing before the suture ruptured. The partial implant fracture occurred at the contact point between the male component of the implant and suture. After the test completed, the partial fracture site showed abnormal surface details missed in the preliminary assessment of implant component integrity before test setup. Evidence of residual 3D printing supports, not a part of the male component design, were noted at the

fracture point. During disassembly of the setup following test completion, six of the 36 total samples (17%) displayed minor fracture to the end of a single tongue feature in the male components. All these cases of minor male component fractures were attributed to the forces applied during disassembly and confirmed with audible cracking while extracting the implant from the test apparatus after test completion.

3.1.2 Cyclic Loading Analysis

The results of cyclic loading testing included assessment of mean secant stiffness (N/mm) and elongation amplitude (mm) throughout cyclic loading. The assumption of a normal distribution of cyclic loading data was satisfied (Table 3.3). Assumption of equal variance between dorsiflexion conditions was satisfied (Table 3.4). A Student's t-test revealed no significant difference across dorsiflexion conditions for the mean secant stiffness and elongation amplitude ($p > 0.05$) (Table 3.5). Further visual confirmation of the Load vs. Displacement plots for each sample confirmed the achievement of an approximate steady-state region at the completion of the 100 cycles (Figure 3.7).

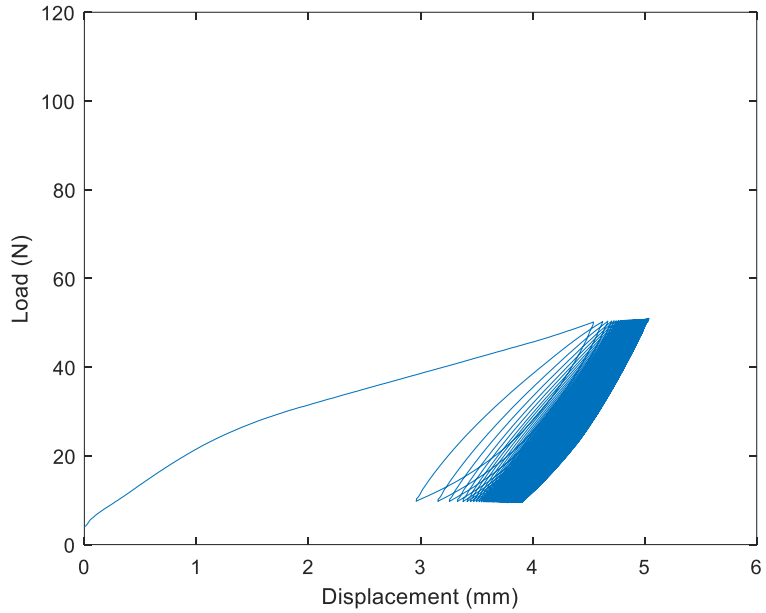

Figure 3.7: Example of cyclic loading experimental data.

Table 3.3: Normal Distribution Goodness-of-Fit Test p-values for Cyclic Loading Data

Mechanical Testing Data→	*Mean Secant Stiffness (N/mm)*		*Elongation Amplitude (mm)*	
Normality Test→	*Shapiro-Wilk*	*Anderson-Darling*	*Shapiro-Wilk*	*Anderson-Darling*
Dorsiflexion Condition (Degrees)↓	*p-values*			
0° (n = 12)	0.0982	0.098	0.0716	0.056
80° (n = 12)	0.995	0.9184	0.3482	0.5132
Total (n = 24)	0.1495	0.2256	0.1484	0.2432

Table 3.4: Unequal Variance Test p-values for Cyclic Loading Data

Unequal Variance Test ↓	**p-value**	
	Mean Secant Stiffness (N/mm)	*Elongation Amplitude (mm)*
O'Brien	0.1334	0.2029
Brown-Forsythe	0.2747	0.183
Levene	0.2489	0.1777
Bartlett	0.0735	0.135
F Test 2-Sided	0.0734	0.135

Table 3.5: Summary Statistics from Cyclic Loading

Dorsiflexion Condition	**Calculated Value (reported as: mean ± standard deviation)**	
	Mean Secant Stiffness (N/mm)	*Elongation Amplitude (mm)*
0° (n = 12)	33.6 ± 0.7	-0.36 ± 0.02
80° (n = 12)	31.7 ± 1.2	-0.42 ± 0.03
Total (n = 24)	32.7 ± 1.4	-0.39 ± 0.04

3.1.3 Follow-up Load to Failure Analysis and Comparison

Given the consistent completion of the cyclic loading phase (100% success rate), assessment of the follow-up load to failure testing was essential. The maximum load (N), tangent stiffness (N/mm), and secant stiffness (N/mm) were calculated for each sample (Figures 3.8 and 3.9). Both assumptions of a normal distribution and equal variance were satisfied. Statistically significant differences in dorsiflexion conditions, 0° and 80°, were found for the maximum failure load, tangent stiffness, and secant stiffness from a Student's t-test ($p < 0.05$). Maximum failure load significantly increased with increased dorsiflexion angle condition (Figure 3.10). Both tangent stiffness and secant stiffness significantly decreased with increased dorsiflexion angle (Figures 3.11 and 3.12). All samples failed due to suture failure during the load to failure test after cyclic loading. Further comparison of the initial load to failure data with the load to failure following cyclic loading data was explored.

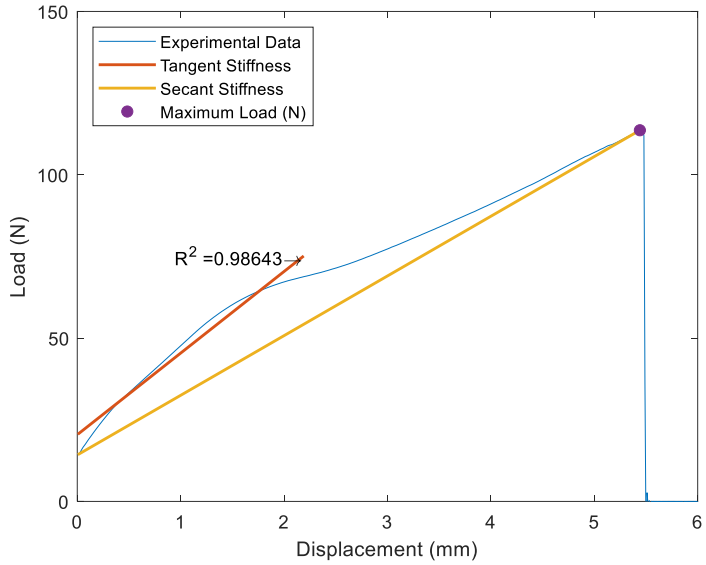

Figure 3.8: Example of 0° dorsiflexion post-cyclic load to failure experimental data and analysis in MATLAB.

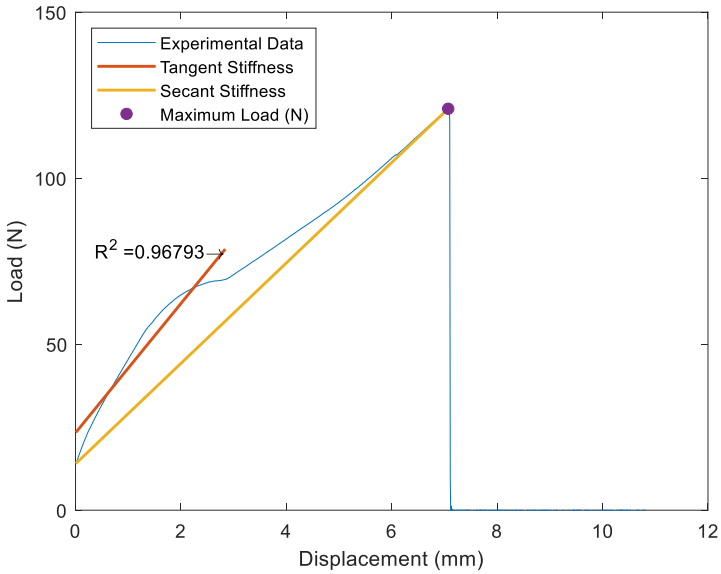

Figure 3.9: Example of 80° dorsiflexion post-cyclic load to failure experimental data and analysis in MATLAB.

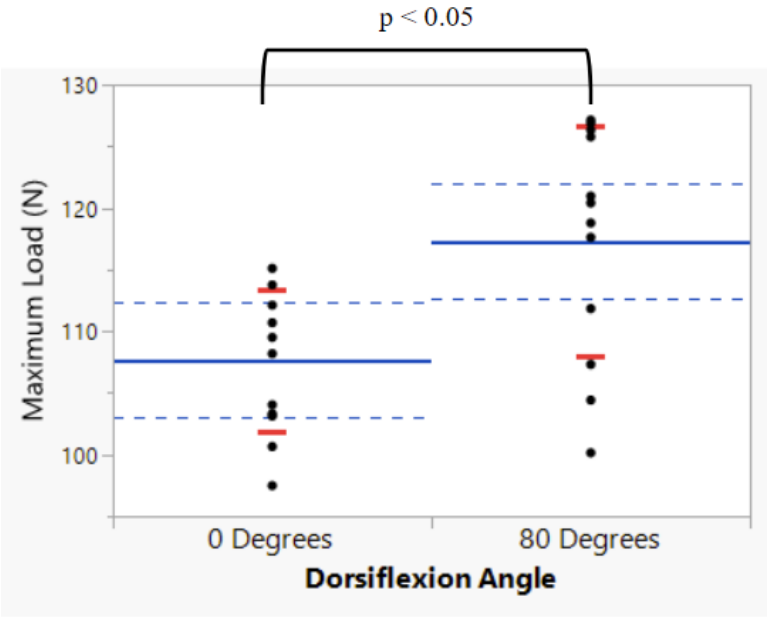

Figure 3.10: Scatterplot of the maximum load (N) data during load to failure testing after cyclic loading.

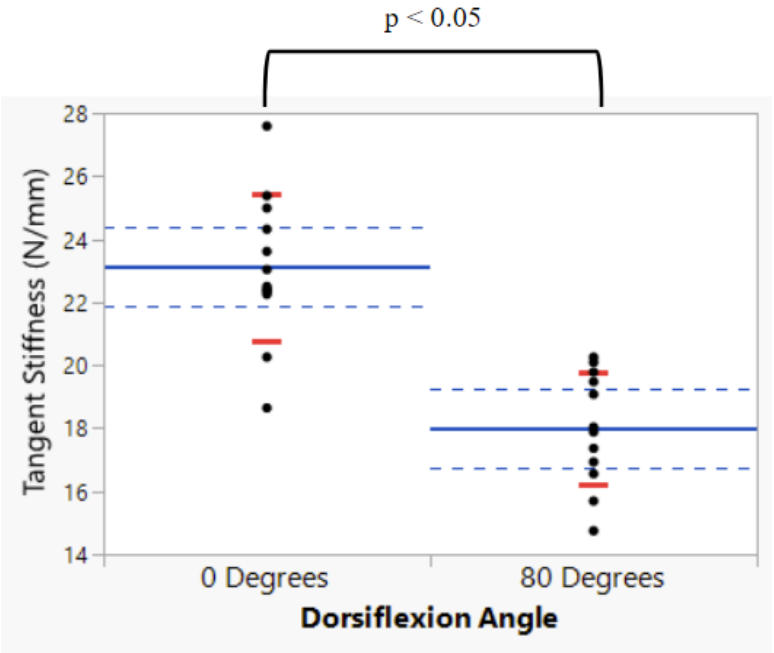

Figure 3.11: Scatterplot of the tangent stiffness (N/mm) data during load to failure testing after cyclic loading.

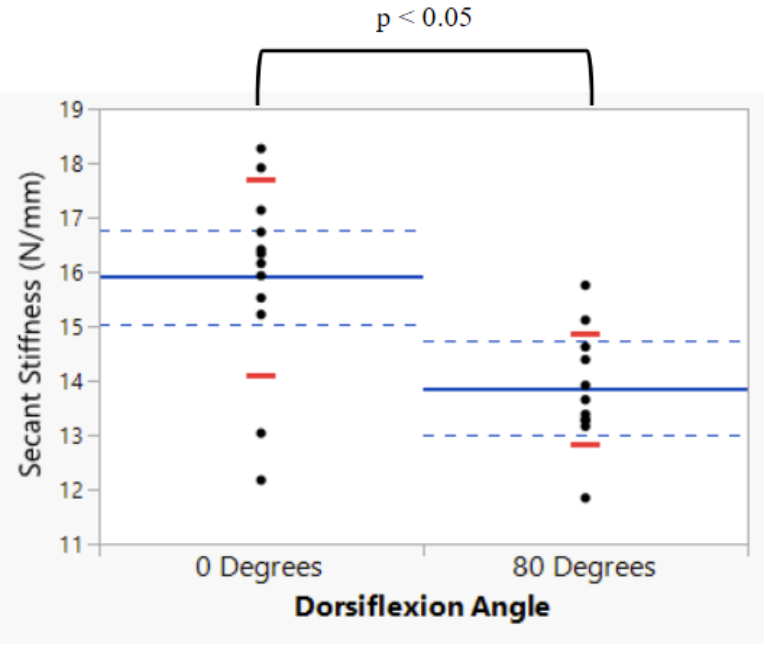

Figure 3.12: Scatterplot of the secant stiffness (N/mm) data during load to failure testing after cyclic loading.

The 0° and 80° dorsiflexion conditions were compared between the load to failure only data and load to failure after cyclic loading data for each of the maximum failure load (N), tangent stiffness (N/mm), and secant stiffness (N/mm). For the 0° dorsiflexion comparison, normal distribution and equal variance assumptions were satisfied for maximum failure load and tangent stiffness. A Student's t-test of the maximum failure load revealed no statistically significant difference between either load to failure protocol ($p > 0.05$) for the 0° dorsiflexion condition (Figure 3.13). The Student's t-test of the tangent stiffness determined that there was a significant difference between the load to failure only protocol and the load to failure after cyclic loading protocol ($p < 0.05$). Tangent stiffness was significantly greater in the load to failure after cyclic loading protocol relative to the load to failure only protocol for the 0° dorsiflexion condition (Figure 3.14). The equal variance assumption for secant stiffness was not met, so Welch's

t-test was performed. The Welch's t-test of the secant stiffness determined there was a statistically significant difference between the load to failure only protocol and the load to failure after cyclic loading protocol ($p < 0.05$). Secant stiffness was significantly greater in the load to failure after cyclic loading protocol relative to the load to failure only protocol for the 0° dorsiflexion condition (Figure 3.15).

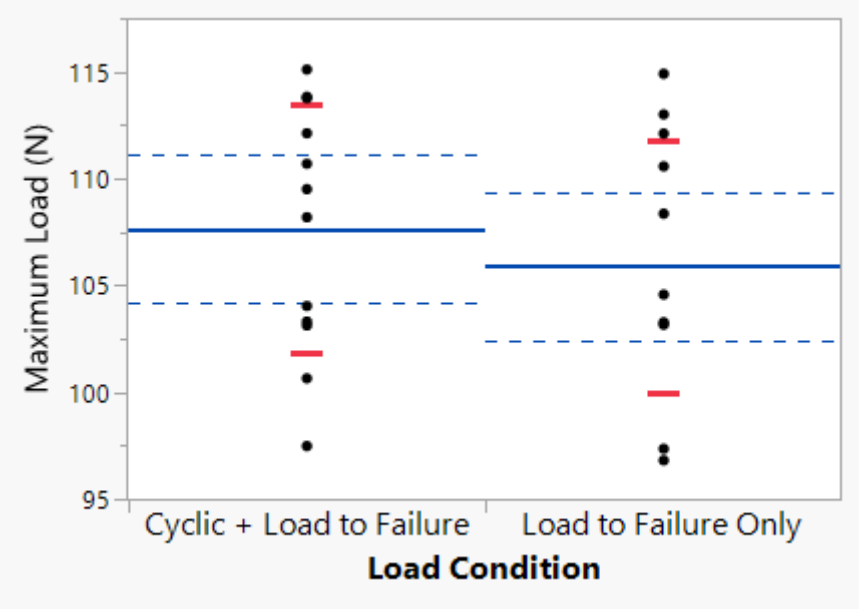

Figure 3.13: Scatterplot data for maximum load (N) comparing the load to failure conditions for 0° dorsiflexion.

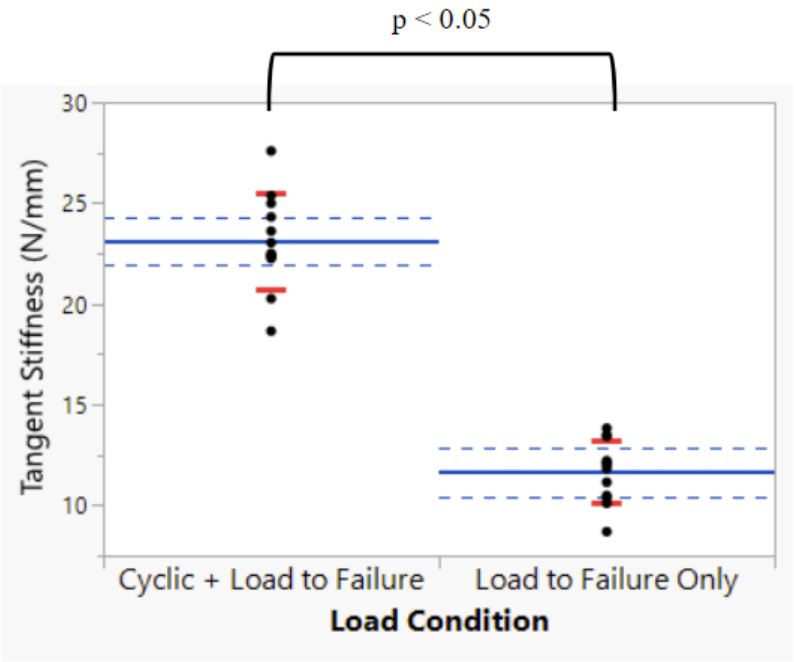

Figure 3.14: Scatterplot data of tangent stiffness (N/mm) comparing the load to failure conditions for 0° dorsiflexion.

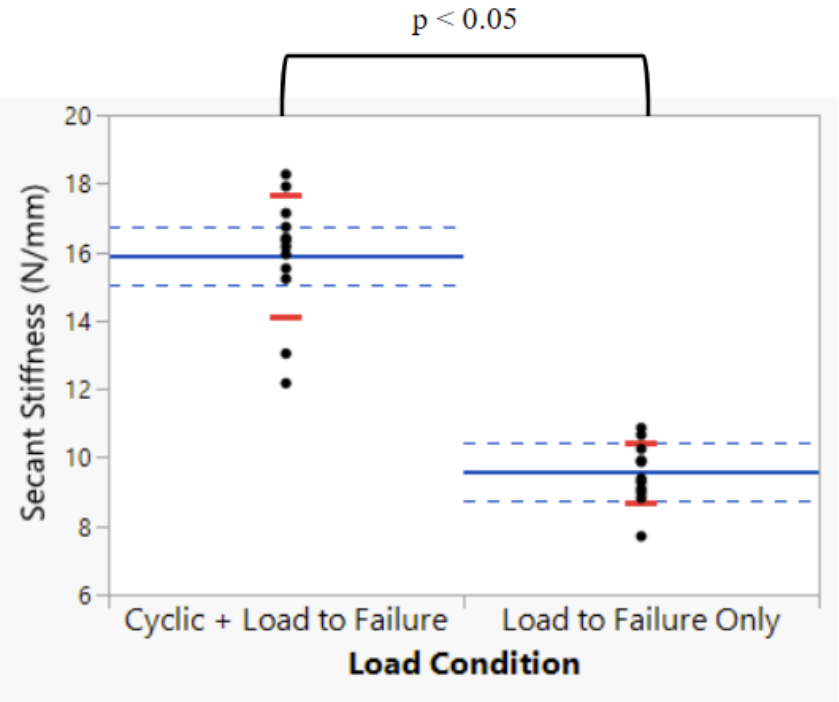

Figure 3.15: Scatterplot data of secant stiffness (N/mm) comparing the load to failure conditions for 0° dorsiflexion.

Normal distribution and equal variance assumptions were met for the comparison of the maximum failure load, tangent stiffness, and secant stiffness between the load to failure only and load to failure after cyclic loading protocols. A Student's t-test of the maximum failure load revealed no statistically significant difference between either the load to failure only or load to failure after cyclic loading protocols ($p > 0.05$) for the 80° dorsiflexion condition (Figure 3.16). The Student's t-test for tangent stiffness determined a significant difference between the load to failure only and load to failure after cyclic loading protocols ($p < 0.05$) for the 80° dorsiflexion condition. Tangent stiffness was significantly greater in the load to failure after cyclic loading protocol relative to the load to failure only protocol for the 80° dorsiflexion condition (Figure 3.17). A Student's t-test of the secant stiffness found a significant difference between the load to failure only and load to failure after cyclic loading protocols ($p < 0.05$). The secant stiffness was significantly greater in the load to failure after cyclic loading protocol relative to the load to failure only protocol for the 80° dorsiflexion condition (Figure 3.18).

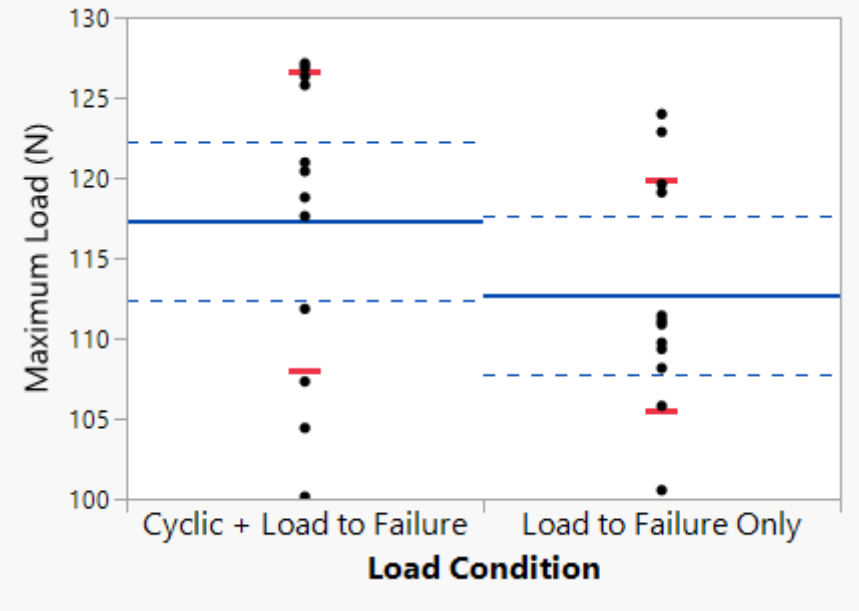

Figure 3.16: Scatterplot data of maximum load (N) comparing the load to failure conditions for 80° dorsiflexion.

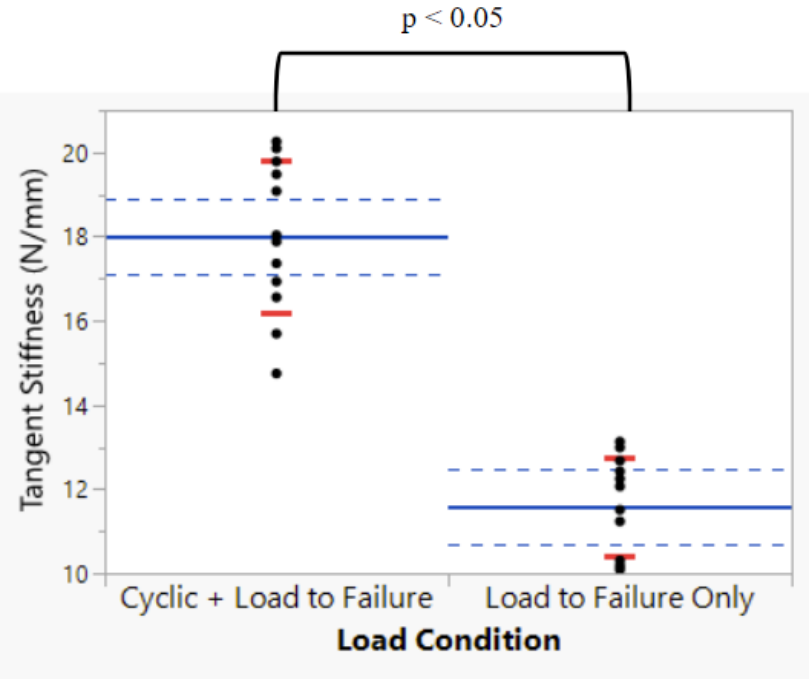

Figure 3.17: Scatterplot data of tangent stiffness (N/mm) comparing load to failure conditions for 80° dorsiflexion.

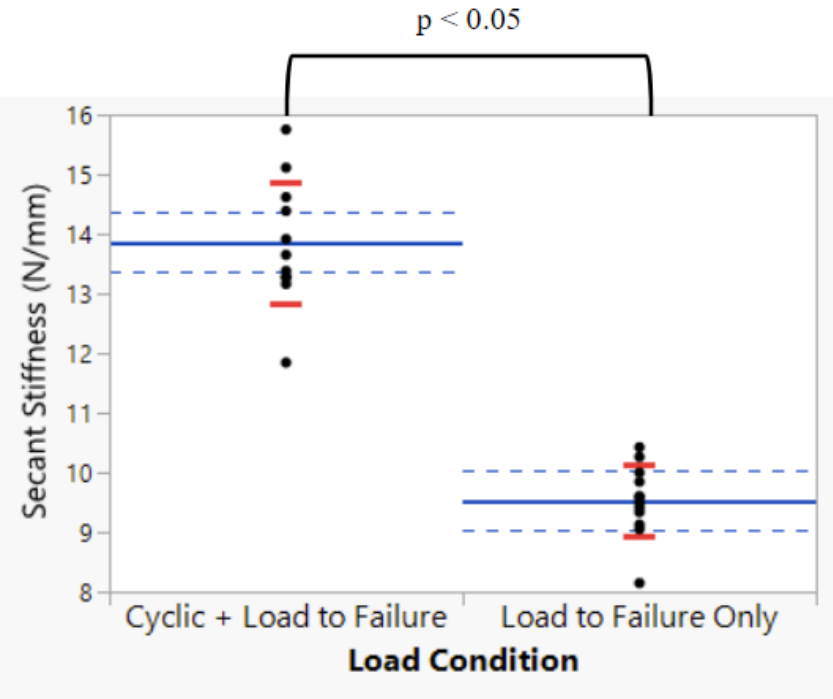

Figure 3.18: Scatterplot data of secant stiffness (N/mm) comparing load to failure conditions for 80° dorsiflexion.

3.2 Cadaver Tissue Model Analysis

Combined quantitative and qualitative analysis was performed for each cadaver tissue sample tested. The quantitative analysis was conducted to compare the results of maximum failure load (N), tangent stiffness (N/mm), and secant stiffness (N/mm) between the native plantar plate (Figure 3.19), conventional repair (Figure 3.20), and novel repair groups (Figure 3.21). During testing, a qualitative assessment of each sample prior, during, and after completion of testing was conducted. The qualitative assessment was paired with the quantitative data collected by the MTS to determine the mode and location of failure. The nature of the mode of failure for multiple samples led to omission from the entire quantitative statistical comparison of all groups.

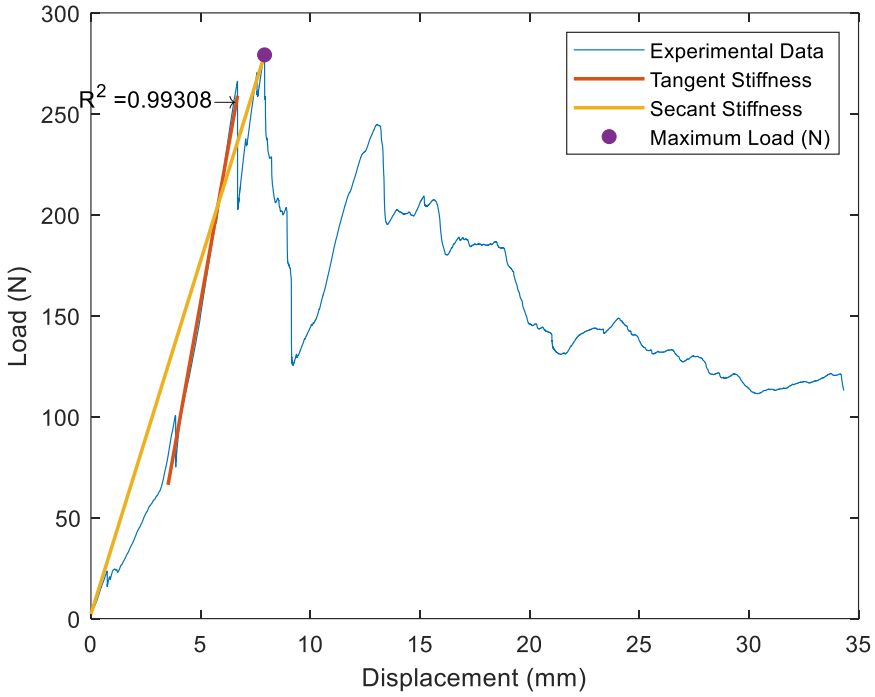

Figure 3.19: Native plantar plate sample experimental data and analysis in MATLAB.

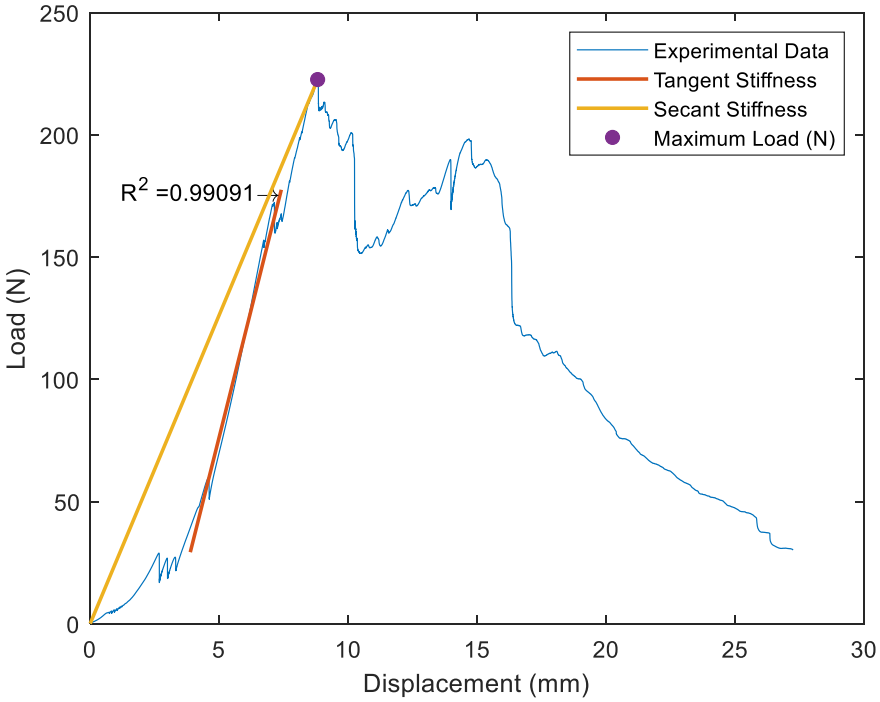

Figure 3.20: Conventional repair sample experimental data and analysis in MATLAB.

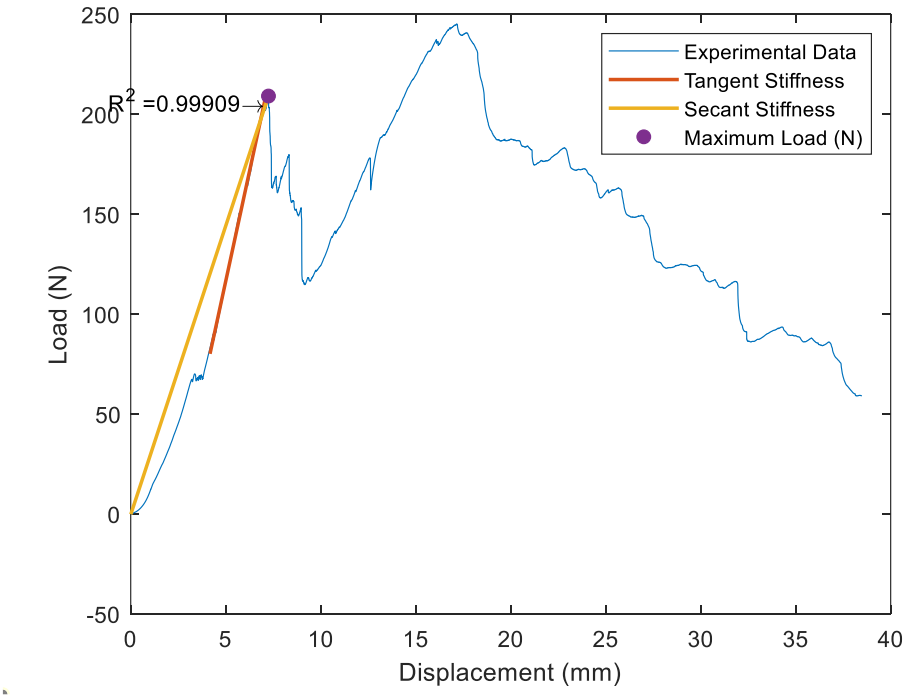

Figure 3.21: Novel repair sample experimental data and analysis in MATLAB.

3.2.1 Sample Exclusion Determination

Five of the 18 total cadaver tissue samples were excluded from the quantitative evaluation of the maximum load (N), tangent stiffness (N/mm), and secant stiffness (N/mm). The basis for this exclusion was that the mode of failure that resulted was not relevant for the assessment and interpretation of the structural integrity of the native or repaired plantar plate tissue construct. A mode of failure defined by the fracture of either the metatarsal or proximal phalanx outside of the bounds of MTPJ and plantar plate region were considered not appropriate for quantitative assessment. All five excluded samples failed based on a fracture in the proximal phalanx, distal to the MTPJ and plantar plate of interest. Two of these samples were from the native plantar plate group, one sample was in the conventional repair group, and two samples were in the novel repair

group. Thus, the number of samples considered in the quantitative analysis of the load to failure testing were six for the native plantar plate group (n = 6), three for the conventional repair group (n = 3), and four for the novel repair group (n = 4).

Table 3.6: Summary Statistics for Cadaver Tissue Mechanical Testing (No significant differences between groups)

Treatment Group	**Calculated Value (reported as: mean ± standard deviation)**		
	Max Load (N)	*Tangent Stiffness (N/mm)*	*Secant Stiffness (N/mm)*
Native (n = 6)	215.5 ± 84.9	45.7 ± 16.7	28.4 ± 11.1
Conventional (n = 3)	150.1 ± 65.5	29.1 ± 12.3	18.8 ± 7.2
Novel (n = 4)	169.0 ± 37.4	35.9 ± 5.6	21.3 ± 5.4

3.2.2 Statistical Analysis

The normal distribution assumption was determined based on the Shapiro-Wilk and Anderson-Darling Goodness-of-Fit tests for each set of maximum failure load, tangent stiffness, and secant stiffness data. Each group and dataset satisfied the normal distribution assumption based on these Goodness-of-Fit tests ($p > 0.05$). A one-way ANOVA test between the three groups was conducted for each of the maximum failure load, tangent stiffness, and secant stiffness values (Table 3.6). The one-way ANOVA p-value for the maximum failure load was $p = 0.3861$ ($p > 0.05$), which informed that there was no statistically significant difference in the maximum failure load between either the native plantar plate, conventional repair, or novel repair groups (Figure 3.22). One-way ANOVA for tangent stiffness resulted in a $p = 0.2334$ ($p > 0.05$), which determined that there was not a statistically significant difference in tangent stiffness between the native

plantar plate, conventional repair, or novel repair groups (Figure 3.23). The p-value for a one-way ANOVA of the secant stiffness was $p = 0.2942$ ($p > 0.05$), concluding that there was not a statistically significant difference in secant stiffness between the native plantar plate, conventional repair, or novel repair groups (Figure 3.24).

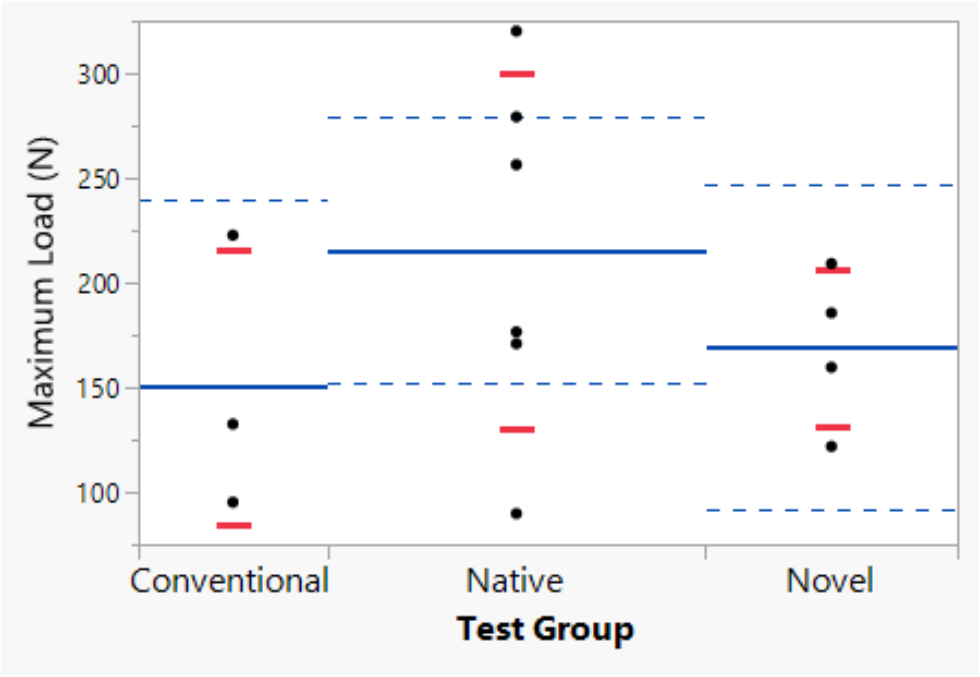

Figure 3.22: Scatterplot data of maximum load (N) for cadaver mechanical testing groups.

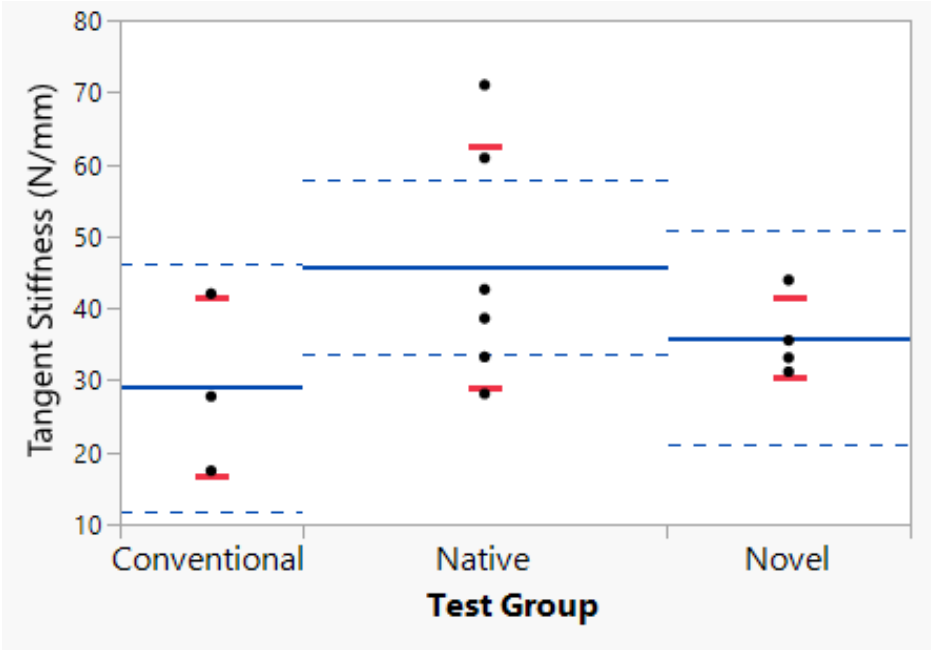

Figure 3.23: Scatterplot data of tangent stiffness (N/mm) for cadaver mechanical testing groups.

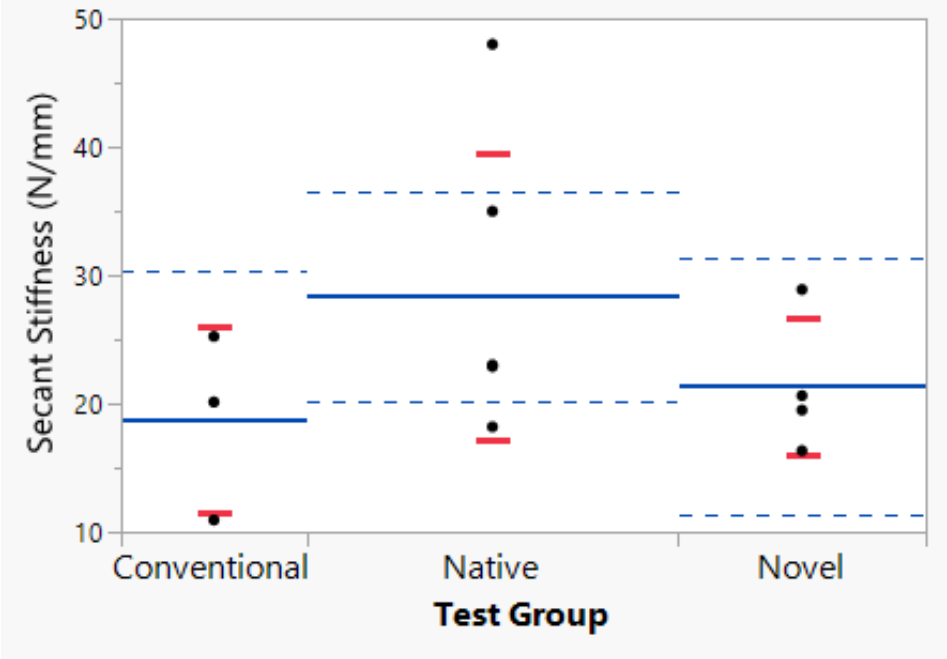

Figure 3.24: Scatterplot data of secant stiffness (N/mm) for cadaver mechanical testing groups.

3.2.3 Failure Modes

For the native plantar plate group, a transverse plantar plate tear was the primary mode of failure for five of the six samples tested. The location of the transverse tears was toward the distal end of the plantar plate for all cases (Figure 3.25). One case showed that the initial transverse tear seemed to cause a longitudinal propagation proximally within the plantar plate. Two samples displayed a follow up shearing of the dorsal plantar plate layer proximally from where the initial transverse tear occurred. One sample primarily failed due to an avulsion tear at the medial insertion site of the plantar plate in the proximal phalanx (Figure 3.26). This sample displayed a secondary transverse tear failure mechanism laterally after the initial avulsion tear.

Figure 3.25: Example of distal, transverse tear of plantar plate in native plantar plate test group sample.

Figure 3.26: Example of avulsion tear at plantar plate insertion in proximal phalanx for native plantar plate test group sample.

In the conventional repair group, a transverse tear of the plantar plate was the primary mode of failure for all three samples. Two of the three samples had a transverse tear occur just proximal to the site of the horizontal mattress suture placement and simulated plantar plate tear, while one sample showed transverse tearing of the plantar plate at the site of the horizontal mattress suture placement (Figure 3.27). One sample that showed transverse tearing proximal to suture placement displayed additional longitudinal propagation of the tear proximally. Evidence of distal, longitudinal suture migration was present for all samples tested. Suture knots over the dorsal aspect of the proximal phalanx remained intact for all samples tested.

Figure 3.27: Example of transverse tear, adjacent to the location of suture placement within plantar plate for conventional repair sample.

For the novel repair group, evidence of fracture in the male component of the implant was shown in all four samples. One sample showed male component fracture as the primary mode of failure during testing, followed by a transverse plantar plate tear propagating longitudinally toward the proximal end of the intact tissue (Figure 3.28). One sample showed male component fracture prior to isolation of the plantar plate and mechanical testing were performed. During mechanical testing, this sample failed due to a transverse tear located proximal to the horizontal mattress suture placement in the plantar plate. Both previous samples showed moderate distal migration of the horizontal mattress suture stitch within the plantar plate. The other two samples primarily failed due to a transverse plantar plate tear before the male component fracture occurred as a secondary failure mechanism. Both samples exhibited significant distal suture migration, with one sample showing complete suture pull through the distal end of the simulated plantar plate tear (Figure 3.28). The other sample also displayed a proximal shearing tear of the dorsal layer of the plantar plate from the initial location and transverse tear.

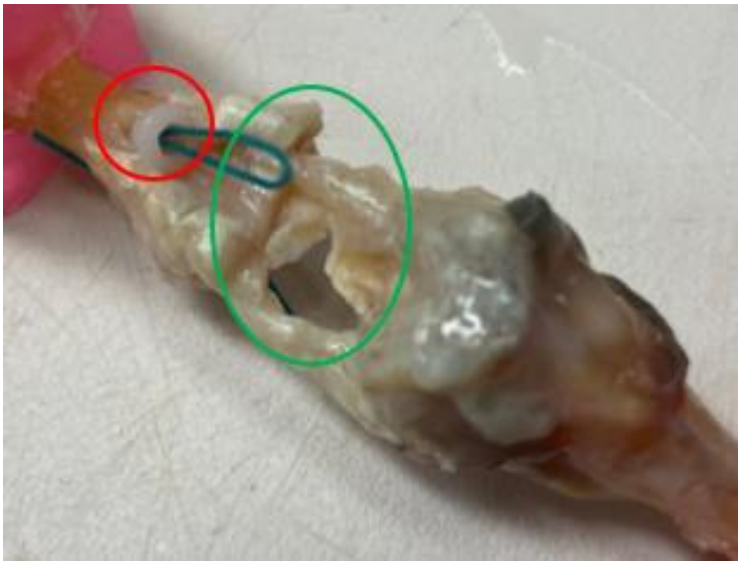

Figure 3.28: Example of male component fracture (red circle) and distal suture pullout (green circle) for a novel repair test group sample.

Chapter 4: Discussion

4.1 Summary and Assessment

This work aimed to provide a methodology for evaluating a novel implant repair for plantar plate tear. An experimental design for isolated implant and suture construct assessment was developed to analyze the independent structural strength and integrity of this novel repair. Uniaxial tensile load mechanical testing was assessed in both a single load to failure and cyclic loading followed by load to failure protocol. These protocols were developed based on the biomechanics and function of the plantar plate [2,4,6,8, 12-14]. A simulated test environment was employed to induce clinically relevant load conditions on this novel implant repair. The outcomes from this isolated implant construct testing were informative for further implant design development and insight into experimental design modifications.

Results from the isolated implant construct testing indicated that with increased dorsiflexion orientation simulated an increase in maximum load was prevalent. For both the load to failure only and load to failure after cyclic loading protocols, a significant increase in maximum failure load was evident. In the load to failure following cyclic loading testing, a significant decrease in both tangent and secant stiffness was observed. These paired outcomes suggest that orientation of the test setup between 0° and 80° dorsiflexion may impact the stiffness response and failure of the implant-suture construct. From observations, the 80° dorsiflexion orientation exhibited greater wrapping of the suture around the centerpiece of the rigid test apparatus relative to the 0° dorsiflexion angle. Increased contact area with the centerpiece in the 80° dorsiflexion orientation may

have contributed to the stiffness decrease during the load to failure after cyclic loading. By increasing the contact area between the suture and centerpiece, the stiffness could have decreased because of the enhanced mechanical support provided to the tension-carrying suture by the rigid centerpiece. Similarly, the increased support from an increased suture and centerpiece contact could have contributed to the increased construct failure load.

Additionally, no differences were observed between either tangent stiffness or secant stiffness for a given load to failure protocol, though comparison of the different load to failure protocols for the 0° and 80° dorsiflexion cases indicated that both tangent stiffness and secant stiffness were significantly greater in the load to failure after cyclic loading protocol. Paired with no significant difference in the maximum failure loads for the load to failure protocol comparison of the 0° and 80° dorsiflexion conditions, these outcomes indicate that protocol differences may account for the increased stiffness of the implant-suture construct. Specifically, the increased crosshead speed, from 0.1 mm/s to 1 mm/s, between the load to failure only protocol and the load to failure following cyclic loading protocol potentially contributed to the increased stiffness noted. Notably, creep during the cyclic loading, as evidenced by the elongation amplitude, may have impacted the stiffness during load to failure testing resulting in greater stiffness magnitudes compared with the load to failure only testing. While the stiffness was greater for the post cyclic load to failure testing, no significant difference in maximum load was found, which could be associated with the prevalence of suture failure during testing. High incidence of suture rupture and minimal deformation of the novel implant during the implant-suture

construct testing seems to indicate that the suture dominated the stiffness and failure characteristics. Minimal viscoelastic effects or behavior has been noted in similar suture mechanical testing and repair studies using braided, polyester suture and was similarly observed in this work [53-57].

The methodology and experimental design developed to evaluate native plantar plate and simulated repair plantar plate structural properties successfully replicated clinically relevant failure modes in all groups. A common mode of failure across all groups included a transverse plantar plate tear toward its distal insertion to the proximal phalanx [6,8]. From observations during sample preparation, the samples that failed due to proximal phalanx fracture and were omitted from quantitative analysis appeared of lesser quality relative to the other samples tested. Subjective assessment of the bone quality aligned with demographic details of these samples, as the specimen donors were of advanced age and frail stature, as determined from BMI provided (Appendix C). For both repair groups, the suture-tissue interface was a notable weak point in each fixation construct. Suture migration was common during load to failure testing and many transverse tears originated directly adjacent or near the site of horizontal mattress suture placement. This outcome is commonly reported in other similar soft, biological tissue repair studies [16,17,55,58].

While the quantitative analysis of the cadaver tissue model mechanical testing revealed no statistically significant differences between the native and repair groups, the trends that resulted coupled with limited sample size suggest further testing is necessary. Based

on the limited data from this mechanical testing, the native plantar plate group logically appears to achieve greater maximum loads. The repair groups seem to perform similarly to each other in maximum load, though trending lower than the previously noted native group. Stiffness across the three groups seems to follow a similar pattern, as the native group appears to provide greater stiffness compared to either repair group. It is important to note that these assessments are not statistically significant, though it is possible that further evaluation with more samples could provide statistically significant conclusions on these noted differences. A post-hoc power analysis indicated preliminarily that approximately 41 samples would provide significant differences between the groups for each of the maximum load, tangent stiffness, and secant stiffness given the same characterization of the data acquired in this work. Further testing and refinement of sample preparation may enhance the power of future studies to obtain statistically significant differences between groups.

Interestingly, the maximum loads achieved in the novel implant repair mechanical testing exceeded that of the implant-suture construct mechanical testing. While the failure modes from the implant-suture construct testing were mainly dominated by suture failure, the novel repair cadaver tissue testing indicated failure due to suture migration and plantar plate soft tissue failure, without any direct suture rupture. These findings suggest that while the novel repair cadaver testing achieved greater maximum loads than the implant-suture construct testing, the loads imposed during the cadaver mechanical testing were primarily focused and distributed through the intact soft tissue structures, mainly the ACLs and the remaining, healthy plantar plate, as opposed to the suture and implant

distally. Thus, the suture within these simulated repairs did not rupture at the higher loads recorded. Of importance, suture migration within the novel repair construct cadaver mechanical testing may pinpoint this suture-plantar plate interface as a site of weakness within the overall repair construct, as similar observations were also apparent in the conventional repair construct testing.

These methodologies developed for cadaver plantar plate mechanical testing as well as the resulting structural property characterization and findings are among the first reported for native plantar plate and simulated plantar plate repairs. The preliminary outcomes of this work suggest that the novel implant device for plantar plate repair performs similarly to a common, existing technique for plantar plate repair. Further study of both the isolated implant construct and the simulated cadaver model mechanical testing should be endorsed and expanded upon as well as the continued development of our novel implant.

4.2 Limitations

A primary limitation for the mechanical testing of the isolated implant construct was the difference in crosshead speed from the initial load to failure testing protocol to the load to failure after cyclic loading protocol. From the outcomes of these protocols, varying degrees of viscoelastic behavior, primarily attributed to the suture, were observed. As such, direct comparison of the data from both load to failure protocols, especially related to the stiffness of the construct, may require further investigation for a robust explanation of these findings. A second important limitation from the mechanical testing of the isolated implant construct was due to the suture length permitted for each test. As per the

protocol described, the vertical distance between anchoring at the ring loop and over the novel implant crossbar in the test setup was measured to be approximately 5 cm. This length was much greater than the distance observed in the simulated plantar plate repair samples, which was visually approximated as less than 1 cm between the horizontal mattress stitch and the proximal phalanx anchor point. This discrepancy in suture length between test setups could have contributed to the difference in stiffness for the isolated implant construct testing compared to the cadaver tissue simulated repair mechanical testing.

Multiple limitations for the cadaver tissue mechanical testing were noted. The difference in sample preparation and storage across the groups was an important limitation in this work. Tissue samples varied between 0 to 14 days spent in the refrigerator between harvesting and final sample preparation followed by freezing for long term storage. Degradation of soft, biological tissue during refrigerated storage as well as reduced mechanical properties as compared to frozen storage have been reported [59]. Additionally, the study design permitted the use of both 2nd and 3rd lesser MTPJs, though size differences between these toes exist naturally. The 2nd MTPJ is commonly larger than the 3rd MTPJ so to withstand the increased forces propagated through the forefoot from the medial, big toe [6,7,13,32]. As such, the plantar plate in the 2nd toe is likely larger and potentially stronger than that in the 3rd toe. By including both 2nd and 3rd toe samples in each group, the variability in structural response is likely greater than if groups were limited to either 2nd or 3rd toe samples. Consideration of tissue donor sex, age, and other characteristics is important when evaluating the impact of this study design

on the variability reported as a result. For this work, donor tissue was procured from both male and female subjects, who varied in size and age among many health characteristics provided. While it is important to assume that tissue quality between donors varied based on their demographics and characteristics, the level for which these details impacted the results is not clear. Ultimately, the limitations to both isolated implant construct and cadaver tissue mechanical testing and interpretation are essential to account for in this work.

4.3 Future Directions

Future studies in furtherance of the findings of this work are abundant from both an implant development and isolated testing phase to further characterization of the plantar plate and existing repair techniques [36-40]. The assessment of suture material properties may provide insight into the increased maximum failure load with increased dorsiflexion orientation. One potential future work could evaluate the size 0 non-absorbable, polyester suture in a modified uniaxial tension setup. This study may provide helpful material properties of these sutures that could be paired with additional details from repeated or modified isolated novel implant studies. For example, a follow-up isolated implant construct load to failure test protocol with a 1 mm/s crosshead speed could provide a robust direct comparison to the load to failure testing after cyclic loading performed in this work. This comparison of load to failure testing protocols with and without prior cyclic loading combined with further suture material properties could better detail the impacts of both the suture and implant portion of the simulated fixation construct.

To enhance the justification for translational comparison between the isolated implant construct and cadaver tissue mechanical testing, modification the suture suspension between anchor points in the isolated implant testing is suggested. Alteration of the vertical distance from 5 cm to 1 cm between the ring loop anchor and the insertion within the novel implant device in the centerpiece would provide a more clinically relevant setup. Further detailed measurements of the distance between the horizontal mattress stitch placed in a torn plantar plate and the proximal phalanx anchor point should provide a more accurate distance to employ in the isolated implant test setup than is suggested here.

Changes to the novel two-piece implant for plantar plate repair are recommended. From this work, the novel implant notably extended plantarly from the proximal phalanx bone tunnel for both 2nd and 3rd toes instead of remaining flush with the plantar cortical bone surface as intended. Excessive implant protrusion from the plantar aspect of the proximal phalanx bone tunnel paired with suture tension along the inner surface of the implant construct contributed to an unaccounted for bending moment imposed on the male component. Specifically, due to the repetitive failure of the male component during simulated repair testing in the cadaver tissue model, alterations to this component for improved mechanical strength and integrity are necessary. Suggested changes include increasing the width of the tongue features on the male component, the base of which was the site for all fractures. This change would directly address the site of a high stress concentration and commonly susceptible to fracture from bending. Decreasing the overall length of the female component to afford increased male component length may improve

the structural integrity of the overall implant construct. This modification would permit the male component to further seat within the proximal phalanx bone tunnel, potentially decreasing the bending moment induced at the base of the male component tongue features seen in this work. Comprehensively, total implant construct dimensional changes may better enable accommodations for varying toe depths.

Future cadaver tissue model plantar plate studies should employ an altered tissue preparation and storage approach. In this work, varying storage conditions contributed to potentially increased variability in cadaver model mechanical testing. An improved approach would include a protocol for freezing samples immediately after harvesting and thawing the samples before administering an assigned treatment followed by refreezing the samples for long term storage before mechanical testing. This approach includes an additional freeze and thaw cycle compared to the approach described in this work, though limited time to degrade in a thawed or refrigerated state is preferred over extended refrigeration [59].

Study designs with a single lesser toe assigned for given groups to compare is suggested. For example, comparison of multiple repair techniques should be considered with the techniques performed in either a 2^{nd} or 3^{rd} MTPJ rather than combination of both in each of these repair groups. Evaluation of the size and structural differences of the plantar plate in the 2^{nd} and 3^{rd} MTPJs is another area of exploration in furtherance of these proposed studies. Limiting the population of the groups based on the demographics of procured tissue in cadaver model based studies could improve the statistical strength of

potential studies. The field of plantar plate tear and repair techniques is abundant with exploratory opportunities for research, many of which would directly pertain to the aims of this work. Ultimately, this work and future directions should follow a meticulous and innovative approach to best equip the podiatry and orthopedic fields with important technical support to advance the administration of medicine and improve future outcomes.

4.4 Conclusion

This work provides a foundation for evaluating this novel approach for plantar plate repair and existing surgical techniques. These methodologies and resulting structural properties for cadaver tissue plantar plate mechanical testing paired with simulated plantar plate repair mechanical testing are among the first reported. Preliminary findings indicate that the novel implant device for plantar plate repair performs comparably to a common plantar plate repair technique. The outcomes from this work encourage the continued development and evaluation of this novel implant device to improve its potential future clinical impact. Future works and methodologies for evaluating plantar plate repair constructs built upon this work will produce a powerful basis to propel continued innovation in podiatric medicine.

References

[1] D. J. G. Stephen, G. W. Choy, and A. G. Fam, "The Ankle and Foot," in *Fam's Musculoskeletal Examination and Joint Injection Techniques,* 2nd ed., G. V. Lawry, H. J. Kreder, G. A. Hawker, and D. Jerome, Eds. 2010, pp. 89-101. doi: 10.1016/C2009-0-31638-4.

[2] R. B. Johnston III, J. Smith, and T. Daniels, "The Plantar Plate of the Lesser Toes: An Anatomical Study in Human Cadavers," *Foot & Ankle International*, vol. 15, no. 5, May, pp. 276-282, 1994. doi: 10.1177/107110079401500508.

[3] J. T. Deland, K. T. Lee, and M. Sobel, "Anatomy of the Plantar Plate and Its Attachments in the Lesser Metatarsal Phalangeal Joint," *Foot & Ankle International*, vol. 16, no. 8, Aug., pp. 480-486, 1995. doi: 10.1177/107110079501600804.

[4] N. M. G. Maas, M. V. D. Grinten, and W. M. Bramer, "Metatarsophalangeal joint stability: a systematic review on the plantar plate of the lesser toes," *Journal of Foot and Ankle Research,* vol. 9, no. 32, Aug., 2016. doi: 10.1186/s13047-016-0165-2.

[5] C. Nery and D. Baumfeld, "Plantar Plate Repair for Subluxed Metatarsophalangeal Joint," in *Operative Techniques: Foot and Ankle Surgery*, 2nd ed., 2017, pp. 128-143. [E-book] Available: Elsevier Health.

[6] K. A. Kirby, "Understanding The Biomechanics Of Plantar Plate Injuries," *hmpgloballearningnetwork.com,* Apr. 2017. [Online]. Available: https://www.hmpgloballearningnetwork.com/site/podiatry/understanding-biomechanics-plantar-plate-injuries. [Accessed Apr. 12, 2023].

[7] F. T. Finney, E. Cata, and J. R. Holmes, "Anatomy and Physiology of the Lesser Metatarsophalangeal Joints," *Foot and Ankle Clinics*, vol. 23, no. 1, Mar., pp. 1-7, 2018, doi: 10.1016/j.fcl.2017.09.002.

[8] J. Gregg, P. Marks, and M. Silberstein, "Histologic anatomy of the lesser metatarsophalangeal joint plantar plate," *Surgical and Radiologic Anatomy*, vol. 29, Feb., pp. 141-147, 2007. doi: 10.1007/s00276-007-0188-2.

[9] S. Standring, "Functional anatomy of the musculoskeletal system," in *Gray's Anatomy,* 42nd ed., 2021, pp. 85-126.

[10] J. Watkins, "Connective Tissues," in *Pocket Podiatry: Functional Anatomy,* I. Mathieson, Eds. 2009, pp. 107-156. doi: 10.1016/B978-0-7020-3032-1.X0001-7.

[11] B. J. Bielajew, J. C. Hu, and K. A. Athanasiou, "Collagen: quantification, biomechanics, and role of minor subtypes in cartilage," *Nature Reviews Materials*, vol. 5, no. 10, Oct., pp. 730-747, 2020. doi: 10.1038/s41578-020-0213-1.

[12] M. J. Coughlin, D. S. Baumfeld, and C. Nery, “Second MTP joint instability: grading of the deformity and description of surgical repair of capsular insufficiency,” *The Physician and Sportsmedicine*, vol. 39, no. 3, Sep., pp. 132-141, 2011. doi: 10.3810/psm.2011.09.1929.

[13] M. Theodoulou, “What Makes The Plantar Plate So Challenging To Treat?,” *hmpgloballearningnetwork.com*, Nov. 2015. [Online]. Available: https://www.hmpgloballearningnetwork.com/site/podiatry/what-makes-plantar-plate-so-challenging-treat. [Accessed Apr. 13, 2023].

[14] J. Doty, M. Coughlin, and J. Jastifer, “Evaluation and Treatment of Lesser Metatarsophalangeal Joint Instability: The Repair of Plantar Plate Insufficiency Through a Dorsal Approach,” *Operative Techniques in Sports Medicine*, vol. 22, no. 4, Dec., pp. 339-347, 2014. doi: 10.1053/j.otsm.2014.09.005.

[15] Y. Krishnan and A. J. Grodzinsky, “Cartilage diseases,” *Matrix Biology*, vol. 71, no. 72, Oct., pp. 51-69, 2018. doi: 10.1016/j.matbio.2018.05.005.

[16] Y. Kocabey, O. Taser, and J. Nyland, “Pullout strength of meniscal repair after cyclic loading: comparison of vertical, horizontal, and oblique suture techniques,” *Knee Surgery, Sports Traumatology, Arthroscopy*, vol. 14, no. 10, Oct., pp. 998-1003, 2006. doi: 10.1007/s00167-006-0079-9.

[17] J. R. Robinson, E. G. Frank, and A. J. Hunter, “The Strength of Transosseous Medial Meniscal Root Repair Using a Simple Suture Technique Is Dependent on Suture Material and Position,” *The American Journal of Sports Medicine*, vol. 46, no. 4, Mar., pp. 924-932, 2018. doi: 10.1177/0363546517749807.

[18] E. A. Makris, P. Hadidi, and K. A. Athanasiou, “The knee meniscus: structure-function, pathophysiology, current repair techniques, and prospects for regeneration,” *Biomaterials*, vol. 32, no. 30, Oct., pp. 7411-7431, 2011. doi: 10.1016/j.biomaterials.2011.06.037.

[19] M. Huber, S. Trattnig, and F. Lintner, “Anatomy, biochemistry, and physiology of articular cartilage,” *Investigative Radiology*, vol. 35, no. 10, Oct., pp. 573-580, 2000. doi: 10.1097/00004424-200010000-00003.

[20] M. J. Mienaltowski and D. E. Birk, “Structure, physiology, and biochemistry of collagens,” *Advances in Experimental Medicine and Biology*, vol. 802, pp. 5-29, 2014. doi: 10.1007/978-94-007-7893-1_2.

[21] P. Mandl, S. Benis, and L. Patonay, “The Normal Joint,” in *Fundamentals of Ultrasound in Rheumatology*, pp. 51-64.

[22] S. Ricard-Blum, “The Collagen Family,” *Cold Spring Harbor Perspectives in Biology*, vol. 3, no. 1, Jan., pp. 1-19, 2011. doi: 10.1101%2Fcshperspect.a004978.

[23] Z. L. Shen, H. Kahn, and R. Ballarini, "Viscoelastic Properties of Isolate Collagen Fibrils," *Biophysical Journal*, vol. 100, no.12, Jun., pp. 3008-3015, 2011. doi: 10.1016/j.bpj.2011.04.052.

[24] S. W. Chang and M. J. Buehler, "Molecular biomechanics of collagen molecules," *Materials Today*, vol. 17, no. 2, Mar., pp. 70-76, 2014. doi: 10.1016/j.mattod.2014.01.019.

[25] J. Bella and D. J. S. Hulmes, "Fibrillar Collagens," in *Fibrous Proteins: Structures and Mechanisms. Subcellular Biochemistry*, vol. 82, D. A. D. Parry and J. M. Squire, Eds. Springer, 2017, pp. 459.

[26] "Tendon Biomechanics," *physio-pedia.com*. [Online]. Available: https://www.physio-pedia.com/Tendon_Biomechanics. [Accessed Apr. 13, 2023].

[27] W. Lowe, "Biomechanics of Tendon and Ligament Tissue," *academyofclinicalmassage.com*, Mar. 29, 2022. [Online]. Available: https://www.academyofclinicalmassage.com/biomechanics-of-tendon-and-ligament-tissue/. [Accessed Apr. 13, 2023].

[28] C. B. Frank, "Ligament, structure, physiology and function," *Journal of Musculoskeletal and Neuronal Interactions*¸ vol. 4, no. 2, Jun., pp.199-201, 2004.

[29] M. G. Patino, M. E. Neiders, and S. Andreana, "Collagen: an overview," *Implant Dentistry*, vol. 11, no. 3, Sep., pp. 280-285, 2002. doi: 10.1097/00008505-200207000-00014.

[30] R. C. Bray, P. T. Salo, and I. K. Lo, "Normal Ligament Structure, Physiology, and Function," *Sports Medicine and Arthroscopy Review*, vol. 13, no. 3, Sep., pp. 127-135, 2005. doi: 10.1097/01.jsa.0000173231.38405.ad.

[31] L. M. Rozmaryn, "The Collateral Ligament of the Digits of the Hand: Anatomy, Physiology, Biomechanics, Injury, and Treatment," *Journal of Hand Surgery*, vol. 42, no. 11, Nov., pp. 904-915, 2017. Doi: 10.1016/j.jhsa.2017.08.024.

[32] L. Weil Jr and E. E. Klein, "Current Concepts in Plantar Plate Repair," *hmpgloballearningnetwork.com*, Apr. 2012. [Online]. Available: https://www.hmpgloballearningnetwork.com/site/podiatry/current-concepts-plantar-plate-repair. [Accessed Apr. 13, 2023].

[33] M. J. Coughlin, S. A. Schutt, and C. B. Hirose, "Metatarsophalangeal joint pathology in crossover second toe deformity: a cadaveric study," *Foot & Ankle International*, vol. 33, no. 2, Feb., pp. 133-140, 2012. Doi: 10.3113/fai.2012.0133.

[34] G. Rubin, “Plantar Plate Tear of the Lesser Toes,” *sportsmedreview.com*. [Online]. Available: https://www.sportsmedreview.com/blog/plantar-plate-tear-of-the-lesser-toes/. [Accessed Apr. 12, 2023].

[35] “Lachman Test,” *physio-pedia.com*. [Online]. Available: https://www.physio-pedia.com/Lachman_Test. [Accessed Apr. 12, 2023].

[36] Wright Medical Group, “GRAVITY Plantar Plate Repair System,” *wright.com*. [Online]. Available: https://www.wright.com/foot_self/gravity-plantar-plate-repair-system. [Accessed Apr. 13, 2023].

[37] CrossRoads Extremity Systems, “STRoPP System (single tunnel repair of plantar plate,” *crextremity.com*. [Online]. Available: https://www.crextremity.com/stropp/. [Accessed Apr. 13, 2023].

[38] T. S. Watson, D. Y. Reid, and T. L. Frerichs, “ Dorsal Approach for Plantar Plate Repair With Weil Osteotomy: Operative Technique,” *Foot & Ankle International*, vol. 35, no. 7, Jul., pp.730-739, 2014. Doi: 10.1177/1071100714536540.

[39] Arthrex, “Complete Plantar Plate Repair System (CPR),” *arthrex.com.* [Online]. Available: https://www.arthrex.com/foot-ankle/complete-plantar-plate-repair-system-cpr. [Accessed Apr. 13, 2023].

[40] M. Asik and N. Sener, “Failure strength of repair devices versus meniscus suturing techniques,” *Knee Surgery, Sports Traumatology, Arthroscopy*, vol. 10, no. 1, Jan., pp. 25-29, 2002. Doi: 10.1007/s001670100247.

[41] M. E. Easley and I. P. Kelly, “Avascular necrosis of the hallux metatarsal head,” *Foot and Ankle Clinics*, vol. 5, no. 3, Sep., pp. 591-608, 2000. [Abstract]. Available: https://pubmed.ncbi.nlm.nih.gov/11232399/. [Accessed Apr. 13, 2023].

[42] D. A. Peterson, J. L. Zilberfarb, and M. A. Greene, “Avascular necrosis of the first metatarsal head: incidence in distal osteotomy combined with lateral soft tissue release,” *Foot & Ankle International*, vol. 15, no. 2, Feb., pp. 59-63, 1994. Doi: 10.1177/107110079401500201.

[43] X. M. Oliva and A. V. Voegeli, “Aseptic (avascular) bone necrosis in the foot and ankle,” *EFORT Open Reviews*, vol. 5, no. 10, Oct., pp. 684-690, 2020. Doi: 10.1302/2058-5241.5.200007.

[44] A. H Matthews, D. D. Davis, and M. J. Fish, *Avascular Necrosis*, StatPearls, Nov. 14, 2022. [E-book] Available: https://www.ncbi.nlm.nih.gov/books/NBK537007/.

[45] S. Carlson, L. Dickinson, and Z. Kozar, “Novel Implant Device for Plantar Plate Repair,” presented at the Midwest Regional Conference for The American Society of Biomechanics, Cleveland, Ohio, 2021.

[46] Formlabs, “Rigid 4000,” FLRGWHO1 datasheet, Oct. 20, 2020.

[47] “Standard Specification for Polyetheretherketone (PEEK) Polymers for Surgical Implant Applications,” ASTM F2026-17, Dec. 13, 2017.

[48] Invibio, “PEEK-OPTIMA Reinforced Mechanical Properties, Physical Properties and Biocompatibility,” INV-MP-PR-0301-A datasheet, Mar. 2014.

[49] S. D. Waldman, “Functional Anatomy of the Ankle and Foot,” in *Physical Diagnosis of Pain*, 4th ed., 2020, pp. 391,392.

[50] N. Verma, M. A. Noerdlinger, and N. Hallab, “Effects of graft rotation on initial biomechanical failure characteristics of bone-patellar-bone constructs,” *The American Journal of Sports Medicine*, vol. 31, no. 5, Sep., pp. 708-713, 2003. Doi: 10.1177/03635465030310051201.

[51] R. Barroco, C. Nery, and G. Favero, “EVALUATION OF METATARSAL RELATIONSHIPS IN THE BIOMECHANICS OF 332 NORMAL FEET USING THE METHOD OF MEASURING RELATIVE LENGTHS,” *Revista Brasileira de Ortopedia*, vol. 46, no. 4, Jul., pp. 431-438, 2011. Doi: 10.1016/S2255-4971(15)30258-5.

[52] S. Patil, G. H. Hanumantharaya, and S. P. Desai, “Radiological Biometric Study of Metatarsals and Phalanges,” *Journal of Clinical & Diagnostic Research*, vol. 11, no. 9, Sep., pp. AC05-AC09, 2017. Doi: 10.7860/JCDR/2017/27887.10589.

[53] D. Acton, A. Perry, and R. Evans, “The effect of two nonresorbable suture types on the mechanical performance over a metal suture anchor eyelet,” *Knee Surgery, Sports Traumatology, Arthroscopy*, vol. 12, no. 2, Mar., pp. 165-168, 2004. Doi: 10.1007/s00167-003-0399-y.

[54] D. Hurwit, G. Fanton, and M. Tella, “Viscoelastic properties of common suture material used for rotator cuff repair and arthroscopic procedures,” *Arthroscopy: The Journal of Arthroscopic and Related Surgery*, vol. 30, no. 11, Nov., pp. 1406-1412, 2014. Doi: 10.1016/j.arthro.2014.05.030.

[55] L. J. Bisson, L. M. Manohar, and R. D. Wilkins, “Influence of suture material on the biomechanical behavior of suture-tendon specimens: a controlled study in bovine rotator cuff,” *The American Journal of Sports Medicine*, vol. 36, no. 5, May, pp. 907-912, 2008. Doi: 10.1177/0363546508314793.

[56] F. Vizesi, C. Jones, and N. Lotz, “Stress relaxation and creep: viscoelastic properties of common suture materials used for flexor tendon repair,” *Journal of Hand Surgery*, vol. 33, no. 2, Feb., pp. 241-246, 2008. Doi: 10.1016/j.jhsa.2007.10.011.

[57] T. Nilsson, “Effect of strain rate on tensile strength and strain of surgical suture materials,” *Scandinavian Journal of Plastic and Reconstructive Surgery*, vol. 16, no. 2, pp. 97-100, 1982. Doi: 10.3109/02844318209006576.

[58] M. J. Feucht, E. Grande, and J. Brunhuber, “Biomechanical evaluation of different suture materials for arthroscopic transtibial pull-out repair of posterior meniscus root tears,” *Knee Surgery, Sports Traumatology, Arthroscopy*, vol. 23, no. 1, Jan., pp. 132-139, 2015. Doi: 10.1007/s00167-013-2656-z.

[59] M. J. Chow and Y. Zhang, “Changes in the mechanical and biochemical properties of aortic tissue due to cold storage,” *Journal of Surgical Research*, vol. 171, no. 2, Dec., pp. 434-442, 2011. Doi: 10.1016/j.jss.2010.04.007.

[60] “Hydrolyzed Collagen: Questions and Answers,” *beta-angel.com*, June 27, 2019. [Online]. Available: https://beta-angel.com/hydrolyzed-collagen-q-a/. [Accessed Apr. 12, 2023].

[61] “Proteoglycans,” *physio-pedia.com*. [Online]. Available: https://www.physio-pedia.com/Proteoglycans. [Accessed Apr. 12, 2023].

[62] K. Robi, N. Jakob, and K. Matevz, “The Physiology of Sports Injuries and Repair Processes,” in *Current Issues in Sports and Exercise Medicine*, M. Hamlin and N. Draper, Eds. 2013, pp. 44-86. doi: 10.5772/54234.

Appendix A: MATLAB Codes

Function: loadDataMTS

```
function [loadVec,dispVec,timeVec] =
loadDataMTS(loadCol,dispCol,timeCol,stressCol,strainCol)
% This function is used to perform simple loading and manipulation of MTS
% .csv file data. The inputs for the function are scalars that represent
% the column organization of the following variables:
%       - Load
%       - Displacement (Crosshead or Extension - chosen by user)
%       - Time
% The function will require user input to locate the data file path of
% interest when used. Following use of the function, outputs will include
% singular column vectors of each of the variables specified in the inputs.

[infile,path] = uigetfile({'*.csv'});

rawdata = readmatrix(strcat(path,infile));

loadVec(:,1) = rawdata(:,loadCol);
dispVec(:,1) = rawdata(:,dispCol);
timeVec(:,1) = rawdata(:,timeCol);

end
```

Function: stiffness

```
function [secantStiff,tangentStiff,Rsquared,yint] = stiffness(load,disp,startPT,endPT)
% This function is used to calculate an both secant and tangent stiffness
% over an interval of load and displacement data. For the tangent stiffness
% calculation, an R-squared value is also determined from the best fit line
% used to determine the tangent stiffness. The input variables are as
% follows:
%
%   load: vector of load values of interest for stiffness calculations;
%   this can be truncated prior to interval of interest or will be indexed
%   by the start and end points passed in
%
%   disp: vector of displacement values corresponding to load data for use
%   in stiffness calculations; can be truncated prior or determined by the
%   start and end points passed in
%
%   startPT: optional variable to be used when determining the start point
%   in the interval of interest within larger span vectors for load and disp
%
%   endPT: optional variable to be used when determining the end point in
%   the interval of interest within larger span vectors for load and disp

if nargin < 3

    start = 1;
    [~,last] = max(load);

    secantStiff = (load(last) - load(start))/(disp(last) - disp(start));

    p = polyfit(disp(start:last),load(start:last),1);
    tangentStiff = p(1);
    yint = p(2);

    R = corrcoef([disp(start:last),load(start:last)]);
    Rsquared = R(1,2);

else
```

```
    secantStiff = (load(endPT) - load(startPT))/(disp(endPT) - disp(startPT));

    p = polyfit(disp(startPT:endPT),load(startPT:endPT),1);
    tangentStiff = p(1);
    yint = p(2);

    R = corrcoef([disp(startPT:endPT),load(startPT:endPT)]);
    Rsquared = R(1,2);
end

end
```

Function: rangefinder

```
function [minToMaxVector,indices,peaks] = rangeFinder(V,xInterestRange)
% This function is designed to extract the range of points between relevant
% minimum and maximum values within the inputted vector, V.
% Used to determine a more precise range of points around a region that may
% not coincide with the overall minimum and maximum range of a dataset.
% Extracts a precise data subset between local minimum and maximum regions
% based on the specified region of interest or vector passed in.
%
% Inputs:
% V = [x,y] - Column organized vector with relevant x and y data, for which
% the y column data is parsed for the minimum and maximum values.
% xInterestRange - Optional input to pass in with vector, V, for which the
% values within this range will further constrain the region of interest to
% search for the minimum and maximum values.
%
% Outputs:
% minToMaxVector - Two column vector organized with the output region for
% both x and y inputs between the relevant minimum and maximum range
% determine by this function.
% indices - Outputs a two value vector of the index values corresponding to
% the original vector, V, input that outlines the start and end points of
% that vector that make up the 'minToMaxVector'
% peaks - A 2x2 vector with the corresponding minimum and maximum values
% for x and y data organized: [xMin yMin; xMax yMax].

x = V(:,1);
y = V(:,2);

count = 1;

for i = 1:length(y)

    if x(i) > xInterestRange(1) && x(i) < xInterestRange(2)

        xRange(count,1) = x(i);
        yRange(count,1) = y(i);

        count = count + 1;
    end
end

[minValY,minidx] = min(yRange);
[maxValY,maxidx] = max(yRange);

minValX = xRange(minidx);
maxValX = xRange(maxidx);

minToMaxVector = [xRange(minidx:maxidx,1), yRange(minidx:maxidx,1)];

indices = [minidx, maxidx];

peaks = [minValX minValY; maxValX maxValY];
end
```

Cyclic Loading Protocol Analysis Script (Cyclic_Load_Analysis.m)

```
%% Clear and Initialize
clear;
clc;
[infile, path] = uigetfile({'*.csv'});

%% Define Parameters
% Initialize cyclic loading protocol parametes for use in analysis
lowerLimit = 10; % N
upperLimit = 50; % N
maxCycles = 100; % Maximum value possible for total cycles run

%% Data Processing
% This section reads and processes the data according to the .csv file type
% and MTS signal data organization
rawdata = readmatrix(strcat(path, infile));
data.crosshead = rawdata(:,2); % Crosshead column
data.load = rawdata(:,4); % Load column
data.time = rawdata(:,5); % Time column
data.ext = rawdata(:,6); % Extension column

% For calculating/iterating (syntactical preference):
loadVec = data.load(:);
timeVec = data.time(:);
dispVec = data.ext(:);

%% Plots
% This plot displays Load vs. Displacement
figure(1);
clf;
plot(dispVec,loadVec);
ylabel('Load (N)');
xlabel('Displacement (mm)');

% This plot displays Load vs. Time
figure(2);
plot(timeVec, loadVec);
xlabel('Time (s)');
ylabel('Load (N)');

% This plot displays Displacement vs. Time
figure(3);
plot(timeVec,dispVec);
xlabel('Time (s)');
ylabel('Displacement (mm)');
hold on;

%% Cycle Number Processing
% This section identifies the relevant indices for each of the 100 cycles
% throughout the cyclic loading protocol. Using iterative evaluation of
% displacement change while comparing loads with the upper and lower
% limits, a peak or minimum is identified for further analysis.
peaks = zeros(200,2);
maxIndicator = 1;
minIndicator = 0;
counter = 1;
diffVec = [diff(loadVec), diff(dispVec)];

for i = 1:length(diffVec) - 1

    if diffVec(i,2) >= 0 && counter == 1 && loadVec(i,1) >= upperLimit
        if diffVec(i+1,2) < 0
            peaks(counter,1) = i;
            peaks(counter,2) = maxIndicator;
            counter = counter + 1;
        end
    elseif diffVec(i,2) >= 0 && counter ~= 1 && loadVec(i,1) >= upperLimit
        if diffVec(i+1,2) < 0 && peaks(counter - 1, 2) == 0
            peaks(counter,1) = i;
```

```
            peaks(counter,2) = maxIndicator;
            counter = counter + 1;
        end
    elseif diffVec(i,2) <= 0 && loadVec(i,1) <= lowerLimit
        if diffVec(i+1,2) > 0 && peaks(counter - 1, 2) == 1
            peaks(counter,1) = i;
            peaks(counter,2) = minIndicator;
            counter = counter + 1;
        elseif i == length(diffVec) -1
            peaks(counter,1) = i + 2;
            peaks(counter,2) = minIndicator;
        end
    elseif diffVec(i,2) <= 0 && i == length(diffVec) - 1
        peaks(counter,1) = i+2;
        peaks(counter,2) = minIndicator;
    else

    end

end

for j = 1:length(peaks)
    plot(timeVec(peaks(j,1)), dispVec(peaks(j,1)), '.r', 'MarkerSize', 5);
end

%% Calculations
% This section iteratively calculates the itermittent stiffness,
% peak-to-peak displacement, load amplitude, and cycle frequency.
dispPeaks = zeros(200,1);
loadPeaks = zeros(200,1);

for n = 1:length(peaks)

    dispPeaks(n) = dispVec(peaks(n,1));
    loadPeaks(n) = loadVec(peaks(n,1));

end

stiffness = zeros(99,1);
dispAmps = zeros(99,1);
loadAmps = zeros(99,1);
frequency = zeros(99,1);

for k = 1:length(peaks) - 1

    if peaks(k,2) == 0

        stiffness(k/2) = (loadVec(peaks(k+1,1)) -
loadVec(peaks(k,1)))/(dispVec(peaks(k+1,1)) - dispVec(peaks(k,1)));
        dispAmps(k/2) = dispVec(peaks(k+1,1)) - dispVec(peaks(k,1));
        loadAmps(k/2) = loadVec(peaks(k+1,1)) - loadVec(peaks(k,1));
        frequency(k/2) = 1/(timeVec(peaks(k+1,1)) - timeVec(peaks(k-1,1)));
    end
end

% Elongation amplitude:
elongationAmplitude = mean(dispAmps(1:5)) - mean(dispAmps(end-4:end)) % mm
% Mean secant stiffness:
meanStiff = mean(stiffness) % N/mm
% Mean cycle frequency:
meanFreq = mean(frequency) % Hz
% Mean load amplitude:
meanLoads = mean(loadAmps) % N
% First to last displacement difference:
firsttolast = dispPeaks(199) - dispPeaks(1)
% Initial secant stiffness:
initialStiffness = (loadVec(peaks(1,1)) - loadVec(1))/(dispVec(peaks(1,1)) - dispVec(1))
% N/mm
% Mean displacement amplitude:
meanDisp = mean(dispAmps) % mm
```

Overall Load to Failure Data Analysis Script (LoadToFailure_Analysis.m)

```
%% Clear and initialize
clear;
clc;
format compact;

%% Load data and plot Load vs. Displacement
% To load data from cadaver tissue testing, uncomment:
%[L,D,t] = loadDataMTS(2,1,3);% PTF

% To load data from implant-suture construct testing, uncomment:
%[L,D,t] = loadDataMTS(1,4,2);% Suture Testing

% Plotting Load vs. Displacement data:
figure(1);
clf;
plot(D,L,'DisplayName','MTS Signal Data');
ylabel('Load (N)');
xlabel('Displacement (mm)');
hold on;

%% Establish parameters for stiffness analysis
% Percentage of data points to max load for consideration
pct = 0.40;

% Calculate maximum load and respective index
[maxLoad, maxidx] = max(L);

% Find displacement at maximum load
dispatmax = D(maxidx);

% From the Load vs. Displacement plot, determine an approximate range of
% data for the given failure point of the sample (initial failure point)
disprange = input('Select displacement range from plot: ');

% If ultimate maximum corresponds to the relevant initial failure point, no
% input is needed for the previous and it is initialized here.
if isempty(disprange)

    disprange = [0,dispatmax];

end

% Using rangeFinder function to organize the relevant data for further
% analysis:
[Vout, idxs, pks] = rangeFinder([D,L], disprange);%

Load = Vout(:,2);
Disp = Vout(:,1);

numpts = round(pct*(length(Load)));

% Initialize an output vector organized: [secant, tangent, R^2]
outputs = zeros(1,3);

% This section iterates through the relevant Load and Displacement data to
% find the maximum tangent stiffness calculated for 40% of the points from
% start to end. The maximum tangent stiffness accounting for 40% of the
% Displacement data range is the outputted value for tangent stiffness.
% R-squared or the coefficient of determination for each linear regression
% determined is reported also to ensure appropriate fit of the line for
% which the tangent stiffness is calculated.
for i = 1:length(Load) - numpts

    [~,tStiff,Rsq,yint] = stiffness(Load(i:i+numpts),Disp(i:i+numpts),1,1+numpts);

    outputs(i,:) = [tStiff,Rsq,yint];

end
```

```
% Calculating the secant stiffness for the appropriate data range:
sStiff = (maxLoad - L(1))/(D(maxidx) - D(1));

% Determining the maximum tangent stiffness value previously calculated to
% designate as the relevant output.
[tangentStiff,stiffidx] = max(outputs(:,1));

% Corresponding R-squared value for the determined tangent stiffness.
Rsquared = outputs(stiffidx,2);

% An equation for the best fit line corresponding to the tangent stiffness
% calculation is used to determine the line to plot on the Load vs.
% Displacement figure for reference.
bestfitline = outputs(stiffidx,3) + (tangentStiff*Disp(stiffidx:stiffidx+numpts));

% Adding both a tangent stiffness and secant stiffness line for their
% respective, corresponding data ranges.
plot(D(stiffidx:stiffidx+numpts),bestfitline,'DisplayName','Tangent
Stiffness','LineWidth',1.5);
plot([Disp(1),Disp(end)],[Load(1),Load(end)],'DisplayName','Secant
Stiffness','LineWidth',1.5)
legend('Location','northwest');
```

Appendix B: Mechanical Testing Protocols

Isolated Implant MTS Load to Failure Only Protocol

1. Properly connect and secure the 500 N load cell to the MTS.
2. Insert and secure ring loop in the MTS load cell such that the ring loop is parallel to the MTS crosshead plane of device loading (Figure 1).
3. Secure custom test apparatus for dorsiflexion range of motion simulation.
    a. Position the rounded edge of the rotating piece directly below the center of the MTS crosshead.
    b. Once in position, secure the base of the apparatus by tightening the nuts on the bolts provided until the base is snugly fit.
    c. Place the rotating piece, in the center of the test apparatus, in the appropriate dorsiflexion position (0°, 40°, and 80° dorsiflexion, depending on the test being performed)
    d. Once the rotating is in position, secure this position by tightening the set screws running horizontally in the apparatus until the rotating piece is snugly fit.

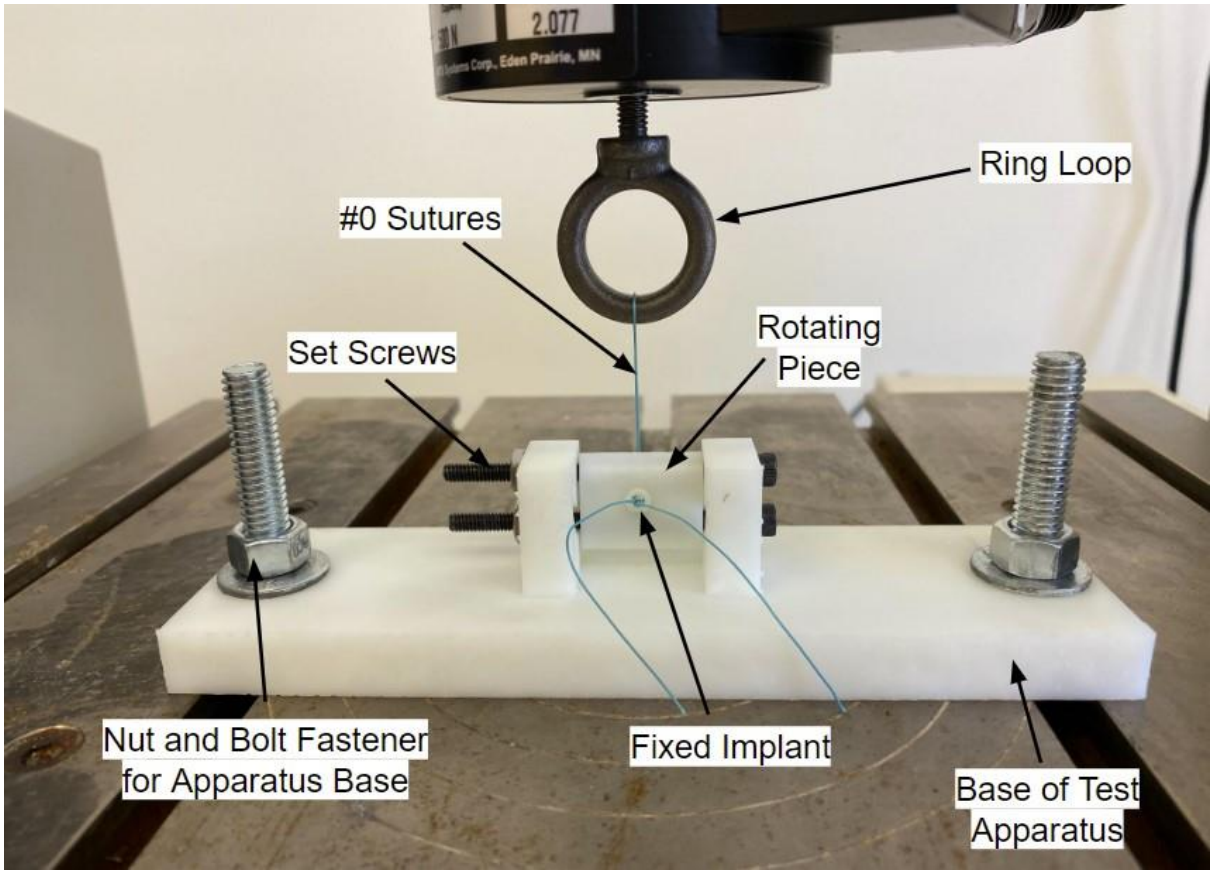

Figure1: The annotated image of simulated dorsiflexion test apparatus in 0° dorsiflexion.

4. Insert the implant for suture fixation.

a. Insert the female component first, with the crossbar portion facing the user.
b. Once the female component is inserted, insert the male component on the side opposing the user's side.
c. Snap the two implant components in place, such that each overhanging lip is as close to flush with the rotating piece as possible.

5. Secure the #0 suture in the test setup, for both the MTS and the fixed implant in the test apparatus.
    a. Pass the suture through the ring loop attached to the load cell, such that two limbs of suture hang down towards the base of the test setup and the MTS platform.
    b. Place the suture passing tool through the fixed implant, from the female (crossbar) component side to the male (open-ended) component side, with one of the suture-passing loops on either side of the crossbar.

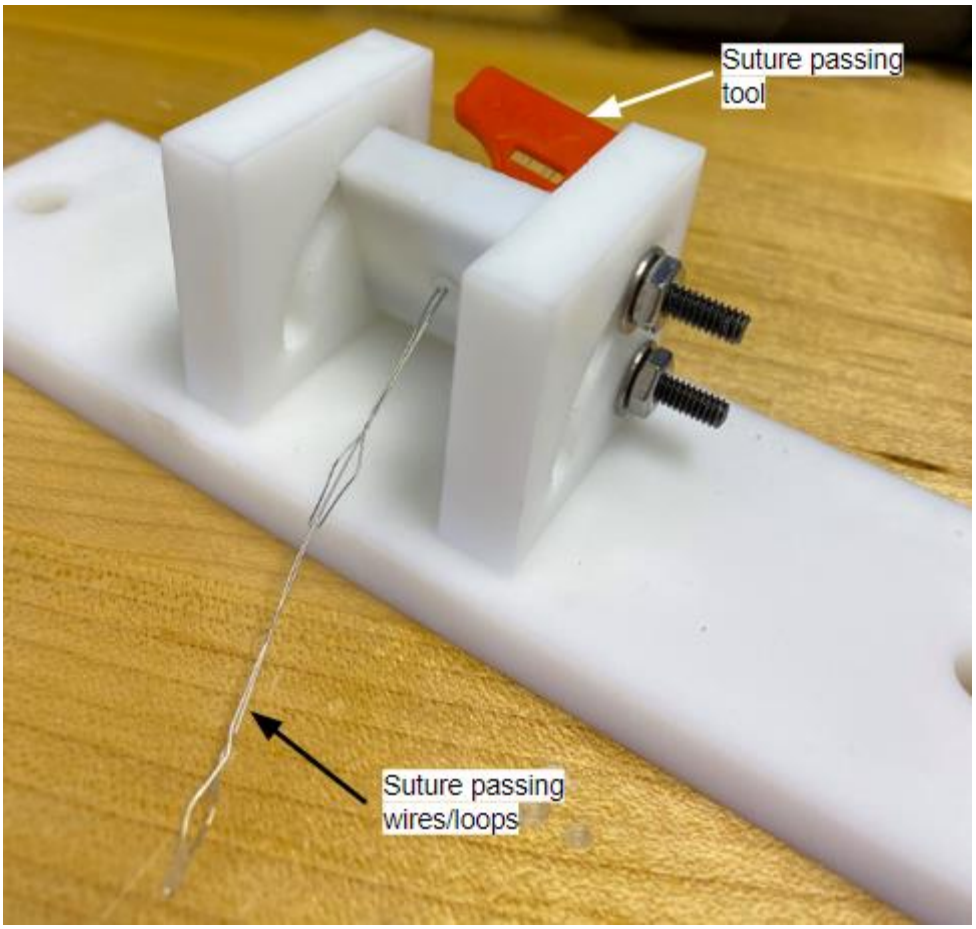

Figure 2: Image of proper initial placement of the suture passing device.

    c. When the two suture passing loops are passed to the male component side (back side of the MTS), take a single limb of the suture hanging from the ring loop and place it inside each of the loops of the suture passing device.

Use enough length of suture (~3-4”) so that there is plenty left on the opposite side after pulling through.

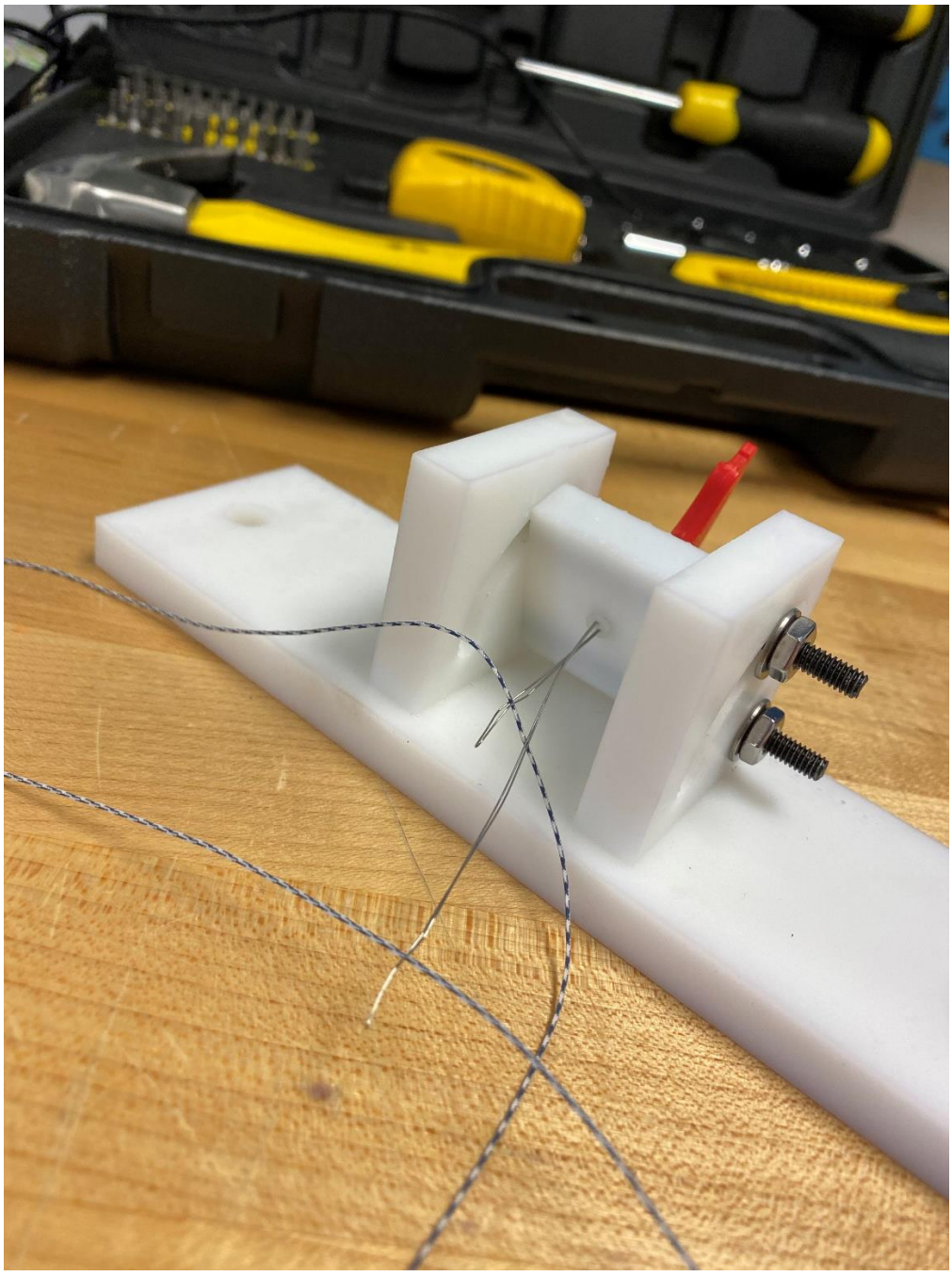

Figure 3: Example of suture properly threaded within the suture passing device before shuttled through the implant.

d. Pull the suture passing device (with a suture limb in each of the loops) through the fixed implant, from the male component side to the female component side. Pull swiftly and until the sutures slide out of the suture

passing device on the female component side (a limb of suture should extend on either side of the crossbar).

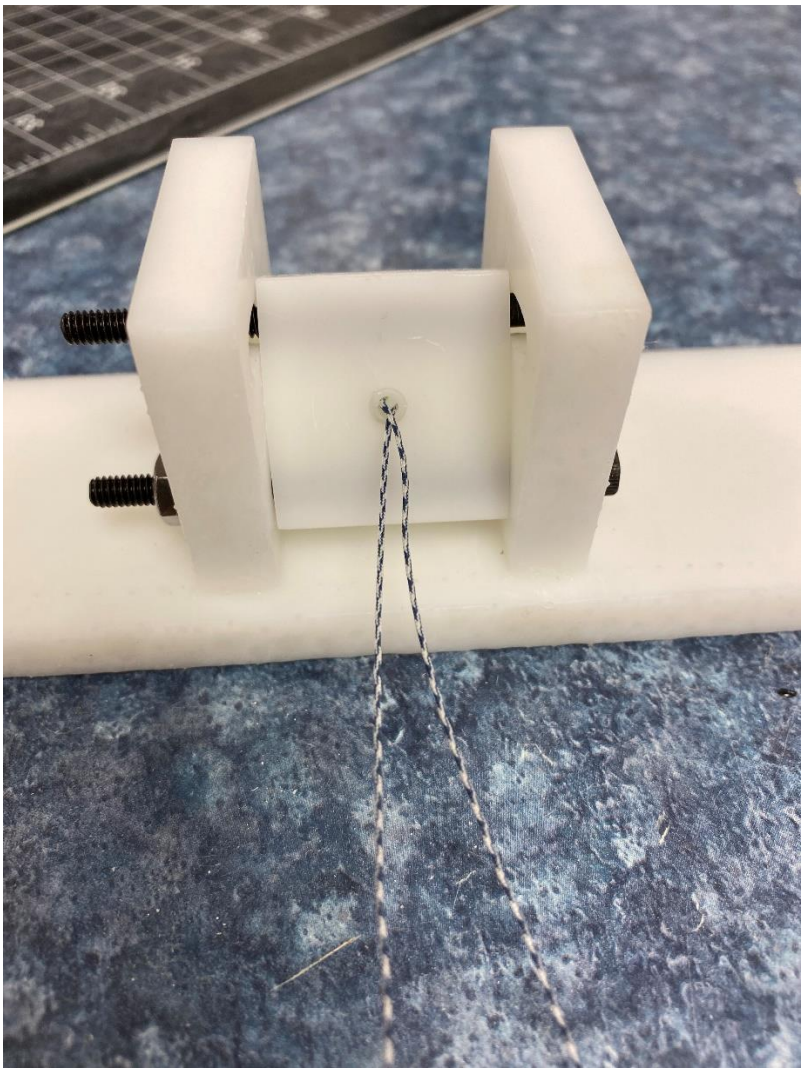

Figure 4: Image of shuttled suture, a limb on either side of the crossbar, on the female side of the implant.

e. Once sutures are on either side of the crossbar, adjust the length of each limb to be approximately the same.
f. Measure the distance from the inner portion of the ring loop (the surface where sutures rest) to the most vertical point on the surface of the rotating piece. Ensure that the distance between these points is approximately 5 cm by measuring with a ruler, caliper, or tape measure. You may need to adjust the MTS crosshead accordingly.
g. Secure the suture by throwing 4 surgeon's knot ties, yielding 3 surgeon's knots, over the crossbar of the fixed implant. Ensure slight tension when tying the suture. Once tied, the suture know should rest on top of the crossbar feature of the implant as displayed in *Figure 1*.

6. Run the load to failure test for the implant device.

a. Open the MTS test file (LD_PTF) with the saved settings for this load to failure test (0.1 mm/s crosshead speed, 450 N upper load cell limit…)
b. Zero (tare) the load cell output.
c. Apply a preload of approximately 10 N to the construct.
d. Start the test file and run until failure.
e. Record the mode of failure for each test. Below are the predicted/common modes of failure:
    i. Suture failure
        1. Complete suture rupture
        2. Partial suture failure (fraying)
        3. Knot slippage (suture will seem thinner where knot originally was)
        4. Suture failure at ring loop (rupture or fraying)
    ii. Implant failure
        1. Crossbar feature fracture (knotted suture pulls through crossbar and into the hollow portion of the implant)
        2. Internal (male component) part fracture
        3. External (female component except for crossbar feature) part fracture
f. Follow the steps to save the raw data from this test as a .csv file and save the test file as a fail-safe.

7. Remove the implant and suture from setup to store in an individual, labeled bag.
    a. Ensure the test has been completed and the MTS crosshead has returned to the initial position or that the suture is in slack (if not ruptured).
    b. If the suture is still intact, cut the suture away from the knot, closer to the ring loop.
    c. Unsnap the fixed implant (carefully, to keep the implant in its original shape/form) and remove each component.
    d. Store the suture and implant components together in a small bag, labeling the sample number and details (including test date).

Isolated Implant MTS Cyclic Loading and Load to Failure Protocol

1. Properly connect and secure 500 N load cell to MTS.
2. Insert and secure the ring loop in the MTS load cell such that the ring loop is parallel to the MTS crosshead plane of device loading (Figure 1).
3. Secure custom test rig/apparatus for dorsiflexion range of motion simulation.
    a. Position the rounded edge of the rotating piece directly below the center of the MTS crosshead.
    b. Once in position, secure the base of the apparatus by tightening the nuts on the bolts provided until the base is snugly fit.
    c. Place the rotating piece, in the center of the test apparatus, in the appropriate dorsiflexion position (0° and 80° dorsiflexion, depending on the test being performed)
    d. Once the rotating piece is in position, secure this position by tightening the set screws running horizontally in the apparatus until the rotating piece is snugly fit.

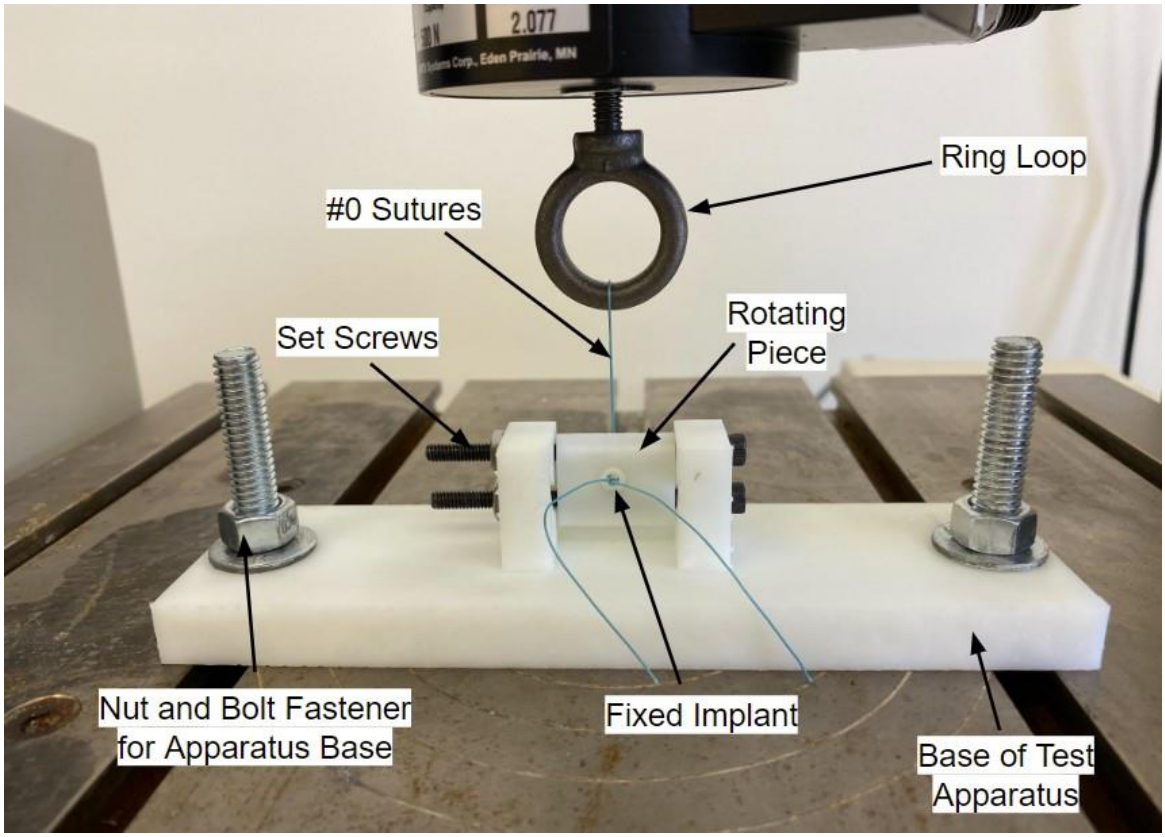

Figure 1: The annotated image of simulated dorsiflexion test apparatus in 0° dorsiflexion.

4. Insert the implant for suture fixation.
    a. Insert the female component first, with the crossbar portion facing the user.

b. Once the female component is inserted, insert the male component on the side opposing the user's side.
c. Snap the two implant components in place, such that each overhanging lip is as close to flush with the rotating piece as possible.

5. Secure the #0 sutures in the test setup, for both the MTS and the fixed implant in the test apparatus.
    a. Pass the suture through the ring loop attached to the MTS, such that two threads of suture hang down toward the base of the test setup and the MTS platform.
    b. Place the suture passing tool through the fixed implant, from the female (crossbar) component side to the male (open-ended) component side, with one of the suture-passing wires (looped) on both sides of the crossbar (the resulting suture passing will provide a single thread on both sides of the crossbar)

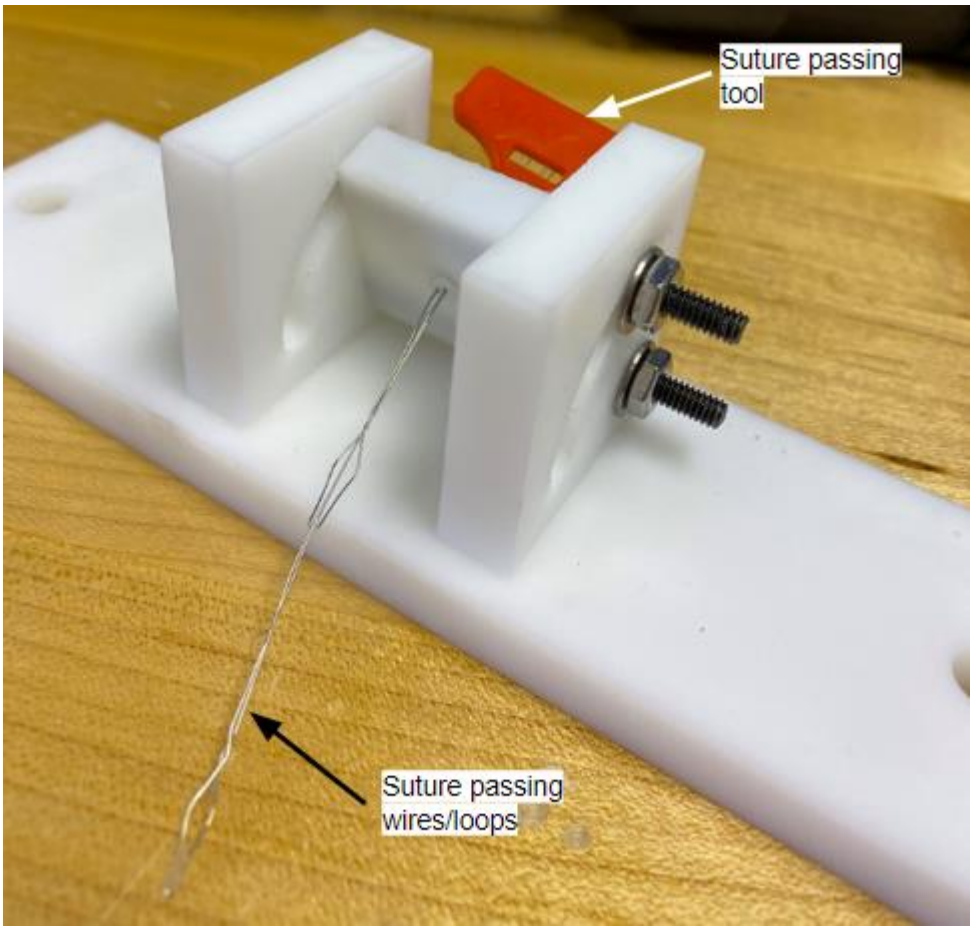

Figure 2: Image of proper initial placement of suture passing device.

    c. When the two suture-passing wires (looped) are passed to the male component side (back side of the MTS), take a single thread of suture that is hanging over the ring loop and place it inside each of the looped wires

for the suture-passing device (use enough length of the suture (3-4”) so that there is plenty left on the opposite side after pulling through).

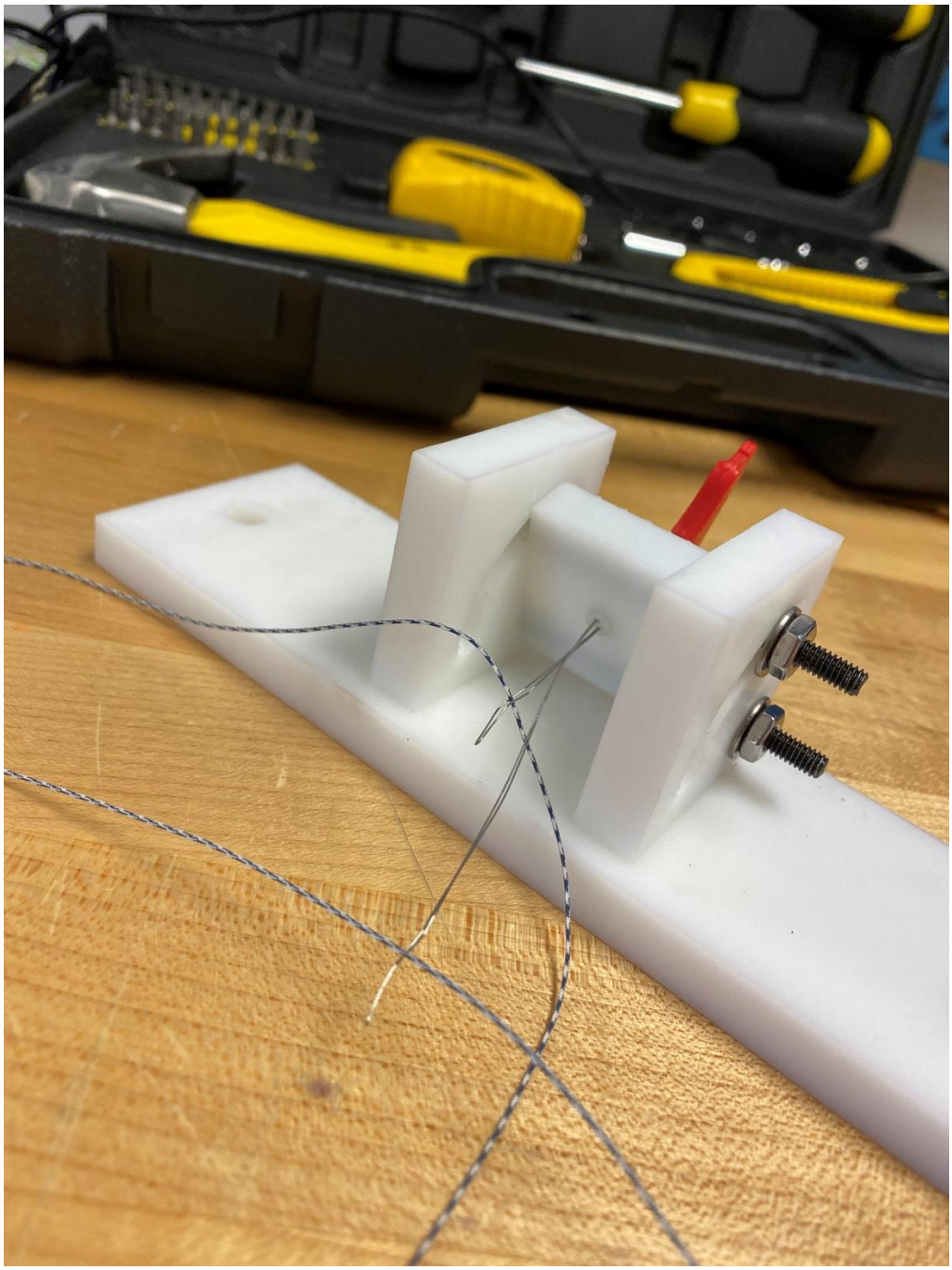

Figure 3: Example of suture properly threaded within the wires of the suture passing tool before passing through the implant.

d. Pull the suture-passing device (with a thread of suture in each of the looped wires) through the fixed implant, from the male component side to the female component side. Pull swiftly and until the sutures slide out of the suture-passing device on the female component side (should hang on either side of the crossbar).

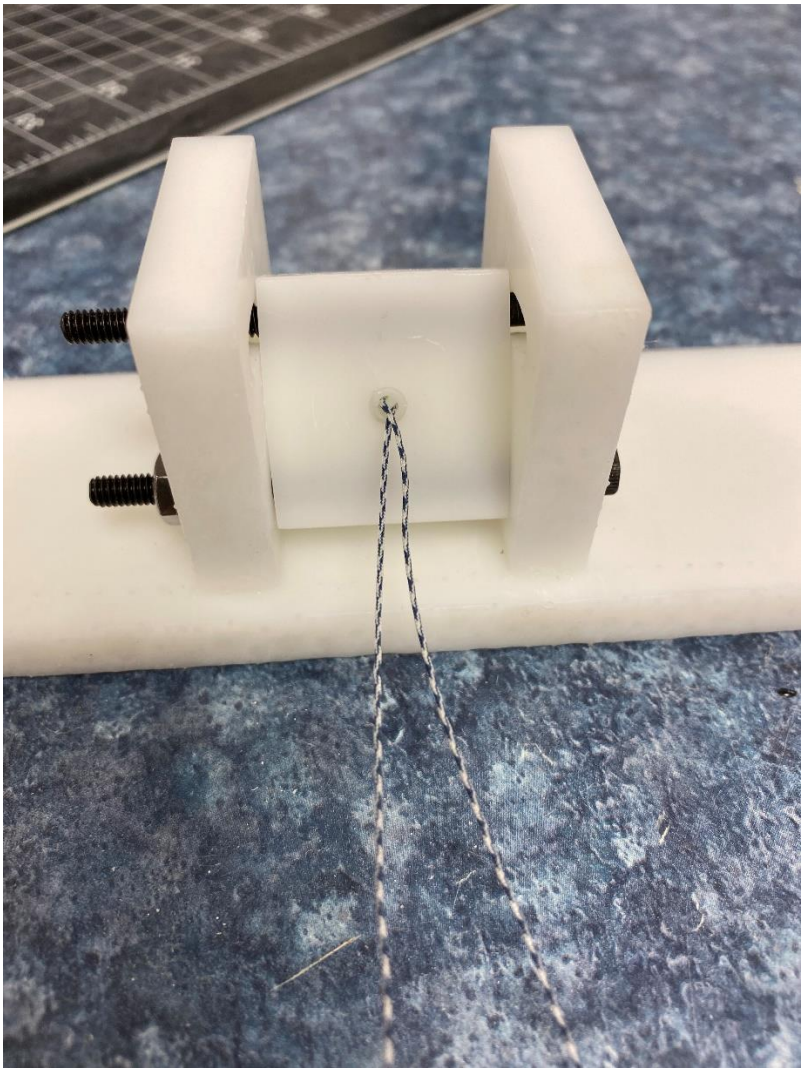

Figure 4: Image of final passed suture, a thread on either side of the crossbar, on the female side of the implant.

e. Once sutures are on either side of the crossbar, adjust the length of each suture limb to be approximately the same.
f. Measure the distance from the inner portion of the ring loop (the surface where sutures rest) to the most vertical point on the surface of the rotating piece. Ensure that the distance between these points is approximately 5 cm by measuring with a ruler, caliper, or tape measure. You may need to adjust the MTS accordingly.
g. Secure the sutures by throwing 4 surgeon's knot loops, yielding 3 surgeon's knots, over the crossbar of the fixed implant. Ensure slight tension when tying the sutures. Once tied, the suture knot should rest on top of the crossbar feature of the implant as displayed in *Figure 1*.

6. Run the cyclic loading protocol test for the implant device.
    a. Open the MTS test file (LD_Cyclic) with the saved settings for this cyclic loading test protocol (1 mm/s crosshead speed, 450 N upper limit, cycling

between 10 and 50 N for 100 cycles following an initial 5 N preload for 30 seconds). The stopping criteria for this file is a breaking condition or drop off in loading, which would be the case in which the test case does not achieve 100 cycles.

b. Zero (tare) the load cell output.
c. Apply a small amount of vertical crosshead displacement manually to ensure that the suture is fixed centrally within the ring loop (load values may fluctuate between 0 and 1 N for this step, which is okay though a load closer to 1 N before starting the test file is preferred). There should be minimal tension on the suture during this adjustment, which is key to keep the suture from maneuvering randomly while in complete slack.
d. Start the test file and run until failure or completion of the 100-cycle maximum.
e. Do not return the crosshead to zero. Record the mode of failure if the entire 100 cycles are not completed. Below are the predicted/common modes of failure:
    i. Suture failure
        1. Complete suture rupture
        2. Partial suture failure (fraying)
        3. Knot slippage (suture will seem thinner near where knot originally was)
        4. Suture failure at ring loop (rupture or fraying of suture)
    ii. Implant failure
        1. Crossbar feature fracture (knotted suture pulls through crossbar and into the hollow portion of the implant)
        2. Internal (male component) part fracture
        3. External (female component except for crossbar feature) part fracture
f. Do not return the crosshead to zero (this will maintain the final displacement and load of the cyclic protocol). Regardless of if the test completes all 100 cycles, follow the steps to export and save the raw data as a .csv file and save the current test as a fail-safe option. If the test fails before all 100 cycles are achieved, be sure to record the number of cycles achieved before the failure and the following load to failure test will not be needed (Step 7).

7. Run the load to failure test protocol to complete the test sample.
    a. Open the MTS test file (LD_PTF) with the saved settings for the load to failure test protocol (1 mm/s crosshead speed, 450 N upper limit)
    b. Do not zero (tare) the load cell output prior to the test. This load output should coincide with the final load value from the cyclic loading protocol (~10 N, though there may be a small amount of relaxation due to the time to save data and switch test files) in the last displacement recorded from the cyclic loading protocol.

c. Start the test file and run until failure.
d. Record the mode of failure. Below are the predicted/common modes of failure:
    i. Suture failure
        1. Complete suture rupture
        2. Partial suture failure (fraying)
        3. Knot slippage (suture will seem thinner near where knot originally was)
        4. Suture failure at ring loop (rupture or fraying of suture)
    ii. Implant failure
        1. Crossbar feature fracture (knotted suture pulls through crossbar and into the hollow portion of the implant)
        2. Internal (male component) part fracture
        3. External (female component except for crossbar feature) part fracture
e. Follow the steps to save the raw data from this test as a .csv file and save the test file as a fail-safe.

8. Remove the implant and sutures to store in an individual, labeled bag.
    a. Ensure the test has been completed and the MTS crosshead has returned to the initial position or that the sutures are in slack (if not ruptured).
    b. If the sutures are still intact, cut the sutures away from the knot, closer to the ring loop.
    c. Unsnap the fixed implant (carefully, to keep the implant in its original shape/form) and remove each component.
    d. Store the sutures and implant components together in a small bag, labeling the sample number and details (including test date).

Cadaver Tissue MTS Load to Failure Protocol

Test Sample Prep

1. Thaw out the sample (keep in the bag from the freezer and place in a container of water for 30 minutes).
2. Measure both the thickness centrally and the width of the plantar plate using calipers at 3 different points along the tissue length (proximal, central, and distal).
3. Record the width and thickness values for the sample.
4. Once all measurements are complete, securely wrap the plantar plate and joint capsule between the metatarsal and phalanx in saline soaked gauze (0.9% saline solution).

Dental Cement Potting

1. Apply parafilm to all inner surfaces of the multi-piece wedge molds for both the metatarsal and phalanx. **Make sure to stretch the parafilm tightly around the edges of the molds.**
2. Secure the outer pieces of the wedge molds using screws and nuts to fasten tightly.
3. Place a final piece of parafilm to the bottom face of each mold, around the edges resting on the lab bench.
4. Resect any excess soft tissue away from the metatarsophalangeal joint and plantar plate, mainly on either the metatarsal or proximal phalanx. This is necessary to provide a rigid surface for the cement to adhere to.
5. Place a (~1 – 1.5 mm diameter) Kirschner wire (K-wire) transversely into each of the metatarsal and proximal phalanx. K-wire placement should be as far removed as possible from the metatarsophalangeal joint, without being inserted into compromised bone, if possible. Once the K-wires are through either the metatarsal or proximal phalanx, cut the K-wire down to size using wire cutters to fit within the respective molds.
6. With the narrow ends of each mold facing each other at a short distance (~2 inches), place the sample into the slotted portions of each mold, exposing the saline soaked portion of soft tissue between the molds. **Ensure that the plantar aspect of the sample is facing upward for ease of visualization during testing.**
7. Secure the respective "guillotine" fastener to each mold. Tighten each screw slowly to keep the sample as horizontally inline as possible for subsequent potting.
8. Without impeding the joint capsule or soft tissue (allowing adequate space from either plantar plate origin or insertion site), adjust the sample such that the maximum amount of the metatarsal and phalanx is within each respective mold.
9. For potting 1 sample, use about 4 scoops (2.5-3 for metatarsal, 1-1.5 for phalanx) of the cement powder and pipet or pour the solution together in a disposable cup (solo or Dixie cup) incrementally. Continue mixing and adjusting ratios until the consistency is a sticky gel like substance.
10. Slowly pour or pipet the cement into each mold, careful to fully cover each bone.

11. Let the cement set and cure for about 30-45 minutes. Use a toothpick or small disposable device to check that the cement is fully cured.
12. Throughout the curing process, check that the saline soaked gauze on the soft tissue remains moist. If it has dried out, replace with another gauze.
13. To remove the molded sample, unscrew and detach each "guillotine" fastener individually before unscrewing the wider wedge mold pieces.
14. Once unscrewed, the thinner end of the wedge mold should detach easily. The wider end of the mold may require some peeling of the parafilm away from the inner portion of the mold and loosening vertically to dislodge the cemented sample.

MTS Test Bench and Software Setup

1. Secure the 500 N load cell to the MTS crosshead.
2. Secure the wedge grip system such that the larger (metatarsal) grip is on the adjustable tank base and the smaller (phalanx) grip is connected to the crosshead.
3. Align each grip with the wedge slot facing you and parallel to the vertical plane of the test frame.
4. Adjust the tightness of each grip using the appropriate nut for either bolt fastener (M6 for phalanx grip and ¼" for metatarsal grip).
5. Adjust the crosshead height before placing the cemented sample into the grips to ensure the sample is slack during placement of the potted bones.
6. Remove the saline soaked gauze from the soft tissue region of the sample before inserting into the grips.
7. Slide the cemented bony ends into the grips fixed to the MTS, with the flat face of the cement facing away toward the flat end of the grips, exposing the plantar aspect of the sample.
8. The tank base can be adjusted horizontally forward or backward on the MTS base, which may be necessary to adjust the sample's vertical alignment within the grips.

MTS Preconditioning Protocol

1. Tare (zero) the load with the sample in slack.
2. Manually adjust the crosshead to apply light tension (~1 N) to the sample and let rest for 1 minute.
3. Load and run the MTS Method file for the 3 N preload (*LD_PP_Preload.TWTemplate*).
4. Measure and record the initial plantar plate length (L_0). The initial plantar plate length should be measured at three distinct points: left edge, center, and right edge of the tissue as aligned within the MTS grips. The average of these three lengths will represent the value of 0% strain.
5. Let the sample rest for 3 minutes at the preload extension value to allow for creep to a steady-state load.
6. Load the MTS Method file for the preconditioning protocol (*LD_PP_Preconditioning.TWTemplate*).

7. Input the initial plantar plate length (L_0) to initialize the test sample crosshead speed (1% strain rate or 0.01*L_0) and upper strain limit (5% strain or 0.05*L_0). You may need to calculate and input these values numerically.
8. Start the preconditioning protocol after the 3 minutes of preload are complete.
9. After preconditioning, the sample should be at the preload extension position or 0% strain and the load value should be less than the initial preload of 3 N (due to stress relaxation).

MTS Mechanical Testing Steps

1. Let the sample rest for 3 minutes. Load the pull-to-failure MTS Method file during this period (*LD_PP_PTF.TWTemplate*).
2. Input the initial plantar plate length (L_0) to initialize crosshead speed (1% strain rate).
3. After the rest time has finished, start the pull-to-failure protocol.
4. Once the test has finished, if the MTS has not halted crosshead displacement, manually stop the test by clicking the red square button. **Do not return the crosshead to the initial position to prevent damaging the sample.**
5. Record the maximum load and strain or displacement at the maximum load from the graph and data provided in the MTS TestWorks software in a separate lab notebook.
6. Record the location and mode of failure of the sample in a lab notebook.
7. Take a picture of the sample, with a focus on the site and mode of failure.

Data/File Saving

1. Export the test data in the form of a .csv file, following the instructions provided near the MTS computer.
2. Make sure to export this file into the appropriate folder location and label accordingly.
3. As a failsafe, save the test file to the same folder path as the exported data and label appropriately.
4. Following the steps above, rename the folder(s) and file(s) precisely to best identify each test case.

Post-Test Cleanup and Storage

1. Once all testing steps and data recording is complete, remove the wedge sample from the MTS grips.
2. Place the sample within a Ziploc bag and label the bag with the appropriate test ID.
3. Put the sample into the freezer space, appropriately sorted with other completed test samples.

Miscellaneous Notes

1. To keep the plantar plate tissue hydrated, periodically apply 0.9% saline solution to the tissue, unless otherwise wrapped in a saline soaked gauze (i.e., during dental cement potting) or in the process of testing with the MTS.

Appendix C: Supplemental Materials

Mechanical Drawings of Two-Piece Snap Fitting Implant Components

Female Component

Top View (Dorsal aspect/crossbar perspective)

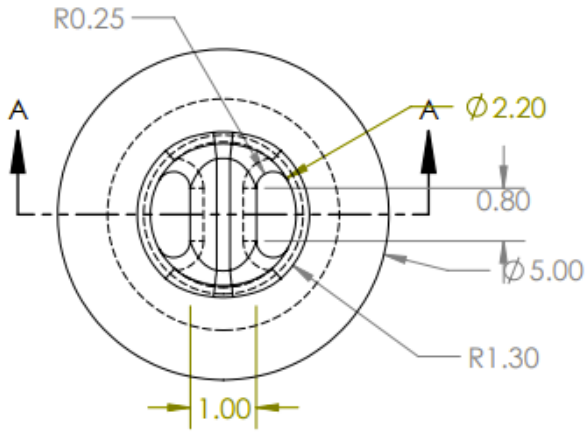

Section A-A from Top View

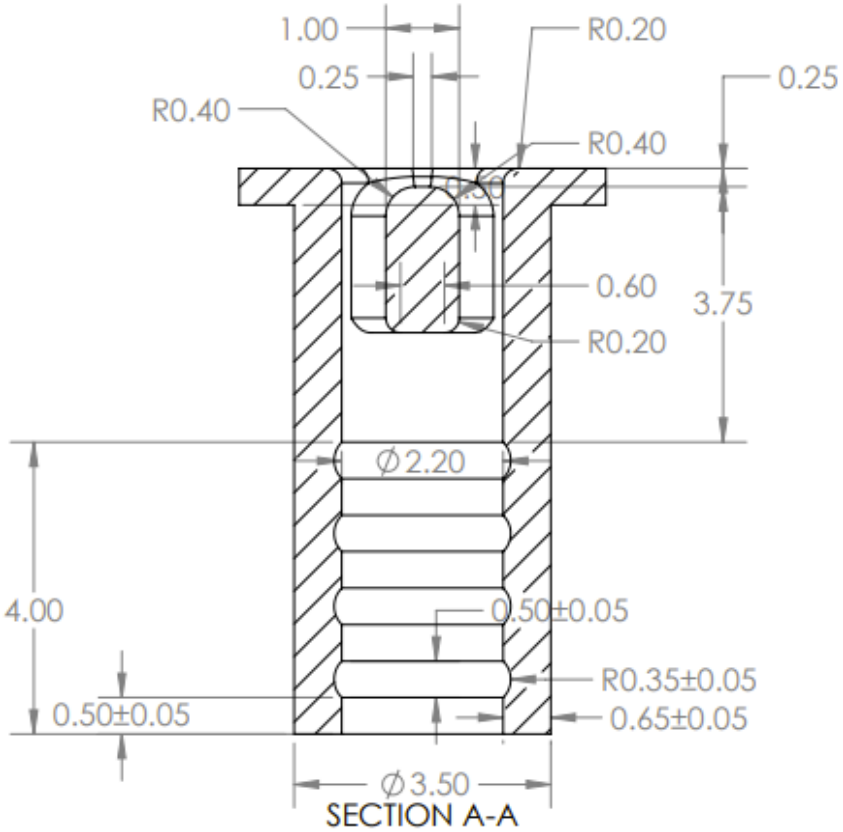

Side View

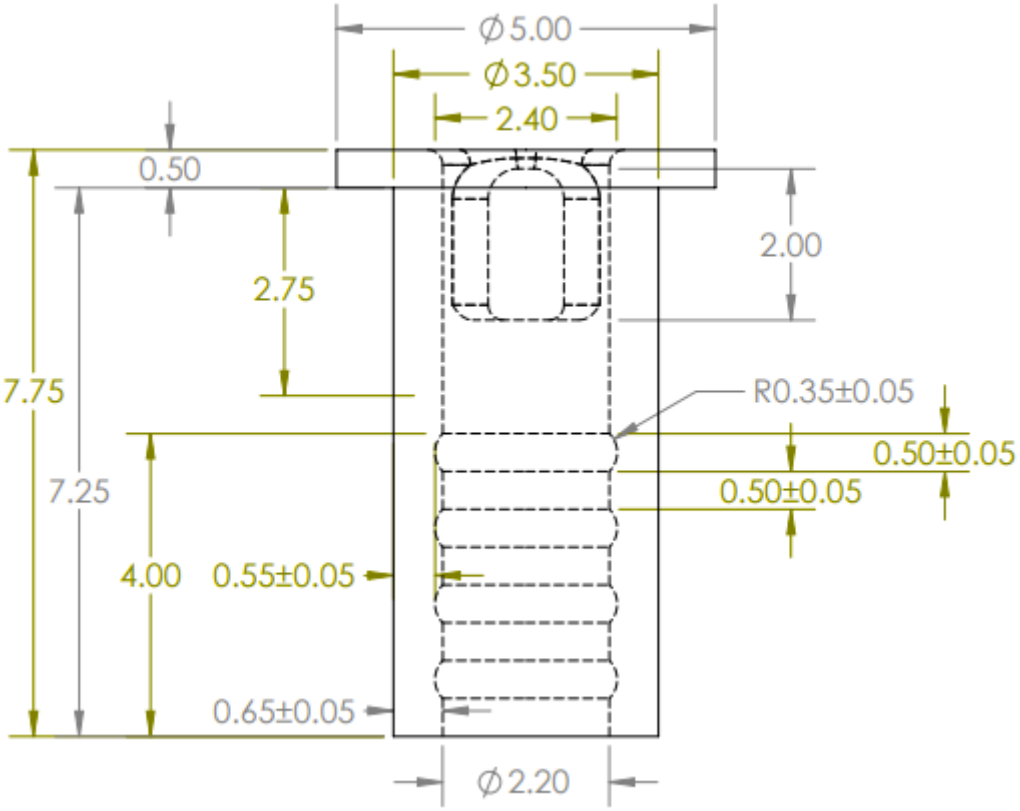

Bottom View (Plantar aspect)

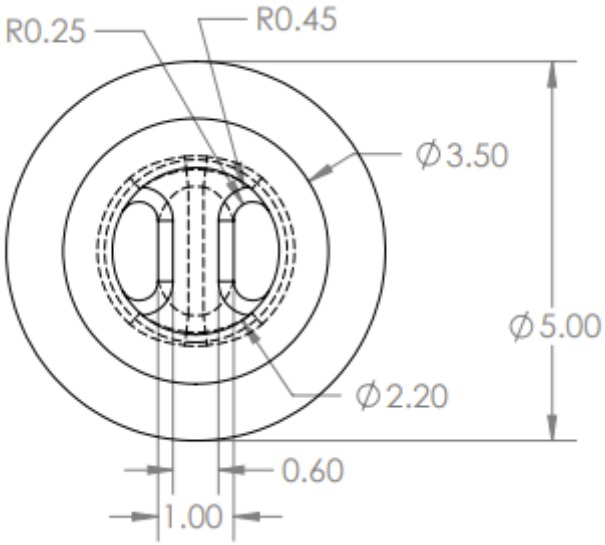

Isometric View

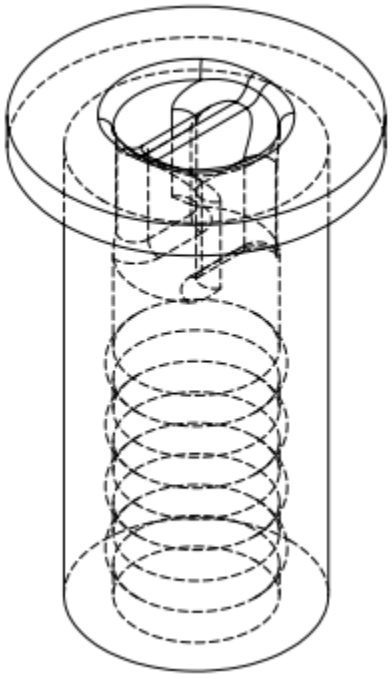

Male Component

Top View (Plantar aspect/male lip feature side)

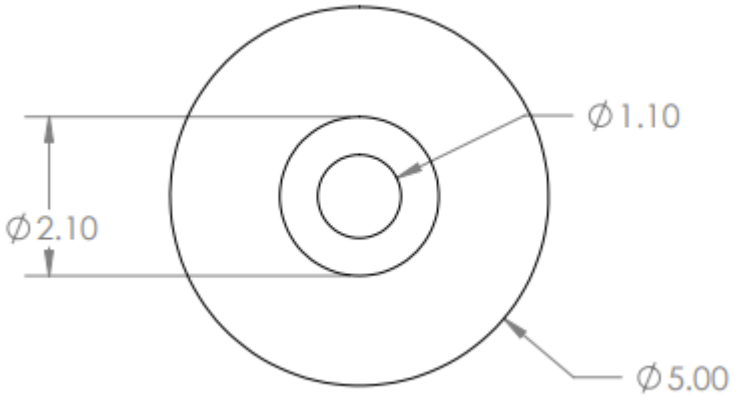

Side View

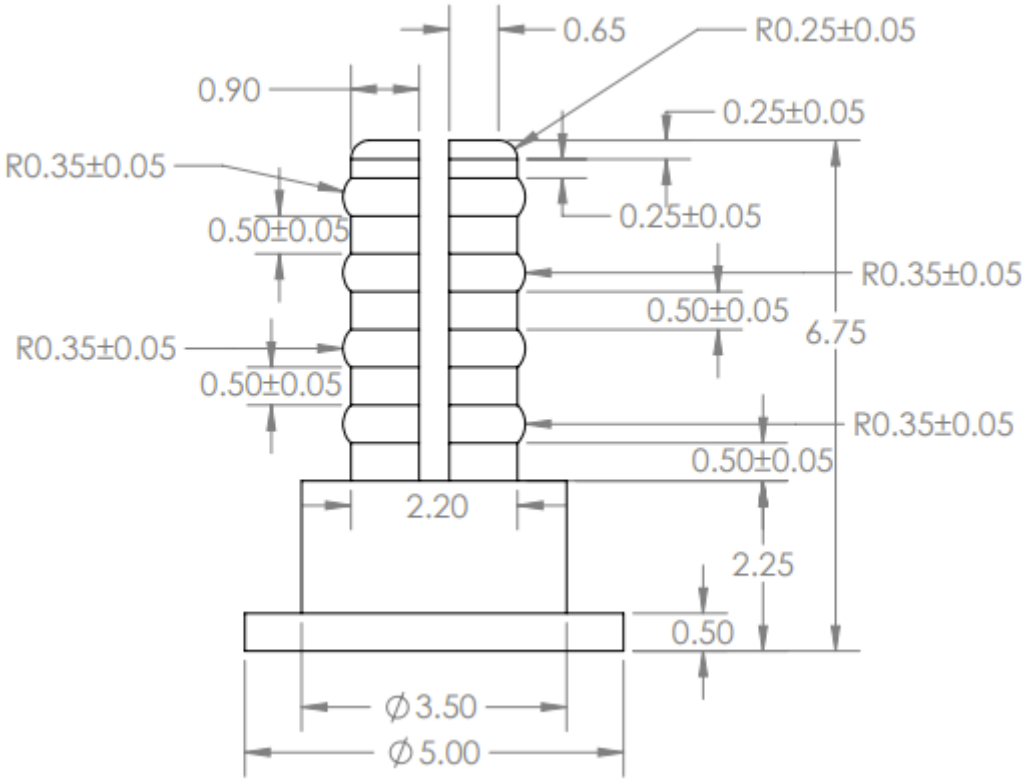

Bottom View (Dorsal aspect/snap fitting tongue side)

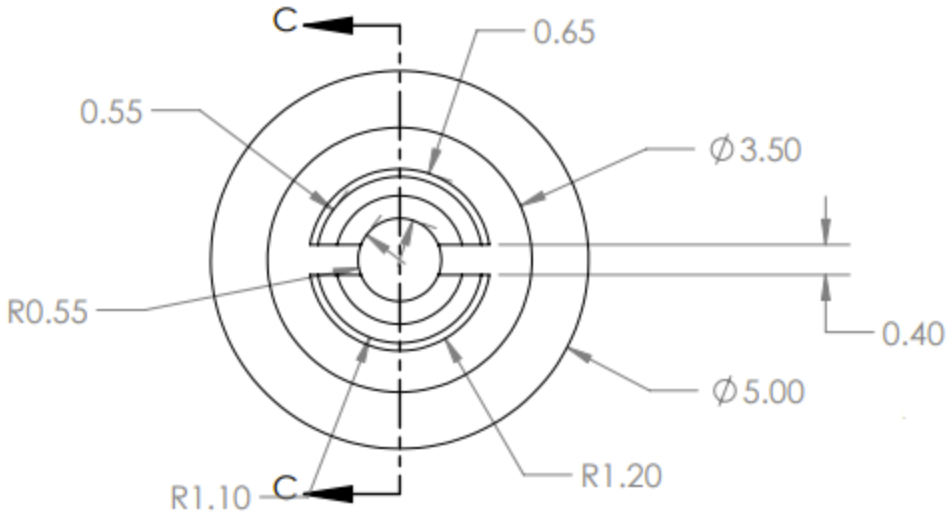

Section C-C from Bottom View

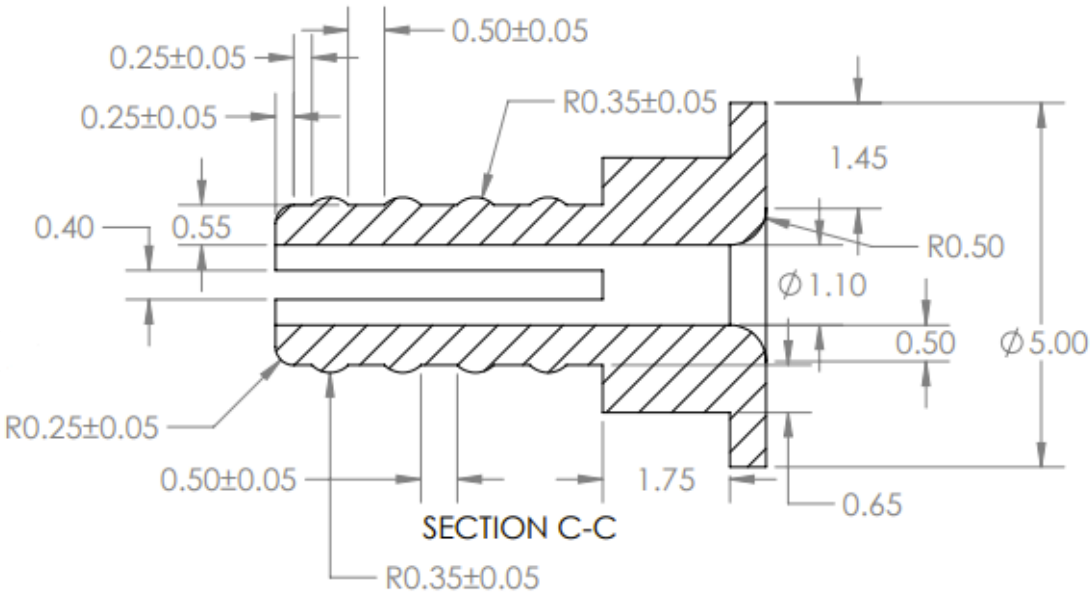

Isometric View

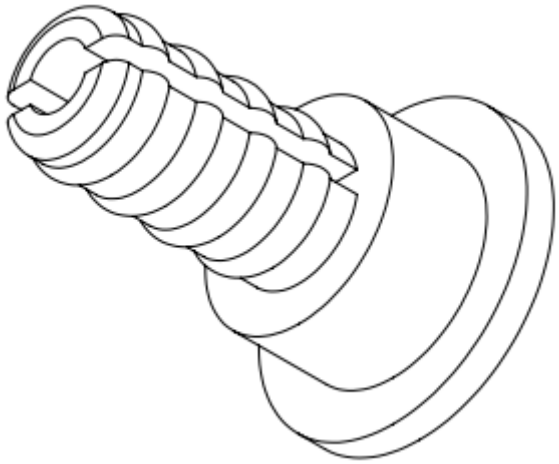

Cadaver Tissue Sample IDs and Assignments

Cadaver Mechanical Testing Tissue Samples and Group Order

Native Plantar Plate		
Order Number	**Study ID**	**Outcome**
1	2204760(L2)	Tested and excluded
2	2204760(L3)	Tested and excluded
3	2203677(L2)	Successful test
4	2204756(R2)	Successful test
5	2201297(R3)	Successful test
6	2203677(L3)	Successful test
7	2201297(R2)	Successful test
8	2204756(R3)	Successful test
Conventional Repair		
Order Number	**Study ID**	**Outcome**
1	2203685(L2)	Tested and excluded
2	2204754(L2)	Successful test
3	2203685(L3)	Successful test
4	2204754(L3)	Successful test
Novel Repair		
Order Number	**Study ID**	**Outcome**
1	2203685(R3)	Tested and excluded
2	2204754(R3)	Successful test
3	2204756(L3)	Successful test
4	2203685(R2)	Tested and excluded
5	2204754(R2)	Successful test
6	2204756(L2)	Successful test

Cadaver Tissue Samples for Pilot Testing – ACLs Severed

Pilot Samples - ACLs Severed		
Order Number	**Study ID**	**Outcome**
1	2204760(R2)	Failed at plantar plate origin
2	2204760(R3)	Failed at plantar plate origin

Excluded Cadaver Tissue Samples

Excluded Samples	
Study ID	**Outcome**
2204732(R2)	Pilot test; successful test without K-wire fixation
2202473(L2)	Pilot test; successful test without K-wire fixation
2204761(R2)	1st pilot test unsuccessful - phalanx pulled out of mold; 2nd pilot test with K-wire fixation - plantar plate origin failure
2204761(R3)	1st pilot test unsuccessful - phalanx pulled out of mold; 2nd pilot test with K-wire fixation - plantar plate origin failure
2204732(R3)	1st pilot test unsuccessful - phalanx pulled out of mold; 2nd pilot test with K-wire fixation - plantar plate origin failure
2202473(L3)	Failed dissection; ruptured plantar plate
2204734(R2)	Torn plantar plate before harvesting; not preserved with saline during refrigeration
2202473(R2)	Not preserved with saline during refrigeration
2202473(R3)	Not preserved with saline during refrigeration
2204734(R3)	Not preserved with saline during refrigeration

Cadaver Mechanical Testing Group Demographics

Native Plantar Plate Group Demographics

Native Plantar Plate		
Before Exclusion (n = 8)	*Age (Years)*	64 ± 14.89
	Height (in)	66 ± 4.21
	Weight (lbs)	118 ± 33.62
	BMI	19.19 ± 5.57
After Exclusion (n = 6)	*Age (Years)*	61.33 ± 16.62
	Height (in)	66 ± 4.98
	Weight (lbs)	129.67 ± 30.48
	BMI	21.12 ± 5.06

Conventional Repair Group Demographics

Conventional Repair		
Before Exclusion (n = 4)	*Age (Years)*	65 ± 9.24
	Height (in)	68 ± 0
	Weight (lbs)	164 ± 62.35
	BMI	24.93 ± 9.48
After Exclusion (n = 3)	*Age (Years)*	62.33 ± 9.24
	Height (in)	68 ± 0
	Weight (lbs)	182 ± 54
	BMI	27.67 ± 8.21

Novel Repair Group Demographics

Novel Repair		
Before Exclusion (n = 6)	*Age (Years)*	56.67 ± 14.76
	Height (in)	67.67 ± 0.52
	Weight (lbs)	165.67 ± 48.37
	BMI	25.44 ± 7.39
After Exclusion (n = 4)	*Age (Years)*	48.5 ± 9.81
	Height (in)	67.5 ± 0.58
	Weight (lbs)	193.5 ± 28.29
	BMI	29.81 ± 3.85

Total Demographics

Total Samples		
Before Exclusion (n = 18)	*Age (Years)*	61.78 ± 13.58
	Height (in)	67 ± 2.87
	Weight (lbs)	144.11 ± 49.17
	BMI	22.55 ± 7.37
After Exclusion (n = 13)	*Age (Years)*	57.62 ± 13.91
	Height (in)	66.92 ± 3.35
	Weight (lbs)	161.38 ± 46.78
	BMI	25.3 ± 6.8

Cadaver Mechanical Testing Group Sample BMIs

Native Plantar Plate Group (red: excluded samples)

Native Plantar Plate		
Order Number	Study ID	BMI
1	2204760(L2)	13.4
2	2204760(L3)	13.4
3	2203677(L2)	15.2
4	2204756(R2)	26.47
5	2201297(R3)	21.68
6	2203677(L3)	15.2
7	2201297(R2)	21.68
8	2204756(R3)	26.47

Conventional Repair Group (red: excluded sample)

Conventional Repair		
Order Number	Study ID	BMI
1	2203685(L2)	16.72
2	2204754(L2)	33.14
3	2203685(L3)	16.72
4	2204754(L3)	33.14

Novel Repair Group (red: excluded samples)

Novel Repair		
Order Number	**Study ID**	**BMI**
1	2203685(R3)	16.72
2	2204754(R3)	33.14
3	2204756(L3)	26.47
4	2203685(R2)	16.72
5	2204754(R2)	33.14
6	2204756(L2)	26.47

Cadaver Mechanical Testing Sample Measurements and Cross-Sectional Area

Native plantar plate group measurements (red: excluded samples)

	Order Number	1	2	3	4	5	6	7	8
Native Plantar Plate	**Study ID**	2204760(L2)	2204760(L3)	2203677(L2)	2204756(R2)	2201297(R3)	2203677(L3)	2201297(R2)	2204756(R3)
	Proximal	7.4	7.16	10.62	9.76	8.43	8.52	8.44	6.88
	Central	9.03	7.75	9.53	9.11	8.05	8.31	8.61	7.09
	Distal	7.9	6.62	8.35	9.08	7.94	8.02	8.22	6.9
Width (mm)	Mean	8.11	7.18	9.5	9.32	8.14	8.28	8.42	6.96
	Proximal	2.36	3.03	3.96	4.05	3.06	3.68	3.03	3.37
	Central	4.11	2.5	3.86	3.41	2.97	3.88	3.33	3.64
	Distal	1.47	2.96	4.12	3.66	2.84	4.23	3.07	2.83
Thickness (mm)	Mean	2.65	2.83	3.98	3.71	2.96	3.93	3.14	3.28
	Medial	16.1	15.61	19.93	17.81	16.87	19.54	18.4	17.52
	Central	15.21	14.66	18.48	15.89	16.78	19.15	17.95	16.71
	Lateral	18.07	13.69	20.83	17.01	16.43	20.19	18.43	17.16
Length (mm)	Mean	16.46	14.65	19.75	16.9	16.69	19.63	18.26	17.13
Cross-Sectional Area (mm^2)		21.49	20.32	37.81	34.58	24.09	32.54	26.44	22.83

Conventional repair group sample measurements (red: excluded sample)

	Order Number	1	2	3	4
Conventional Repair	**Study ID**	2203685(L2)	2204754(L2)	2203685(L3)	2204754(L3)
	Proximal	7.85	8.52	8.36	8.03
	Central	8.38	7.9	7.65	7.24
	Distal	8.03	7.98	7.26	7.76
Width (mm)	Mean	8.09	8.13	7.76	7.68
	Proximal	3.41	4.32	2.76	3.32
	Central	2.74	3.71	3.46	3.89
	Distal	2.67	3.81	2.8	2.7
Thickness (mm)	Mean	2.94	3.95	3.01	3.3
	Medial	20.83	22.82	20.74	22.14
	Central	22.29	22.12	22.35	22.48
	Lateral	23.24	21.63	21.26	23.88
Length (mm)	Mean	22.12	22.19	21.45	22.83
Cross-Sectional Area (mm^2)		23.78	32.11	23.36	25.34

Novel repair group sample measurements (red: excluded samples)

	Order Number	1	2	3	4	5	6
Novel Repair	**Study ID**	2203685(R3)	2204754(R3)	2204756(L3)	2203685(R2)	2204754(R2)	2204756(L2)
	Proximal	8.54	6.63	7.95	8.23	7.81	7.91
	Central	8.65	7.96	7.04	8.55	8.29	7.85
	Distal	7.79	7.38	6.92	8.04	7.6	7.07
Width (mm)	Mean	8.33	7.32	7.3	8.27	7.9	7.61
	Proximal	2.06	3.35	2.72	3.29	3.27	3.21
	Central	2.94	4.28	2.66	3.01	4.18	3.81
	Distal	2.63	3.89	2.02	3.35	3.7	3.25
Thickness (mm)	Mean	2.54	3.84	2.47	3.22	3.72	3.42
	Medial	23.37	22.39	19.73	23.34	22.74	21.44
	Central	24.02	22.03	20.78	23.39	23.16	21.62
	Lateral	22.33	21.73	20.06	21.32	23.2	21.33
Length (mm)	Mean	23.24	22.05	20.19	22.68	23.03	21.46
Cross-Sectional Area (mm^2)		21.16	28.11	18.03	26.63	29.39	26.03

Bivariate Statistics for Cadaver Mechanical Testing

Linear fit of maximum load (N) with cross-sectional area (mm^2): Statistically significant correlation ($p < 0.05$) between maximum load and cross-sectional area for all cadaver mechanical testing data except samples excluded from analysis (n = 13) (native plantar plate, conventional repair, and novel repair groups).

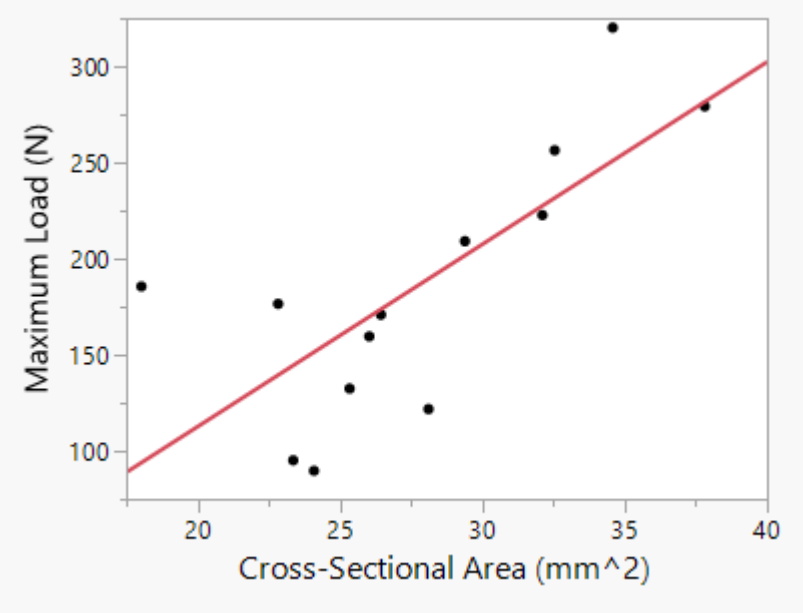

Linear fit of tangent stiffness (N/mm) with cross-sectional area (mm^2): Statistically significant correlation ($p < 0.05$) between tangent stiffness and cross-sectional area for all cadaver mechanical testing data except samples excluded from analysis (n = 13) (native plantar plate, conventional repair, and novel repair groups).

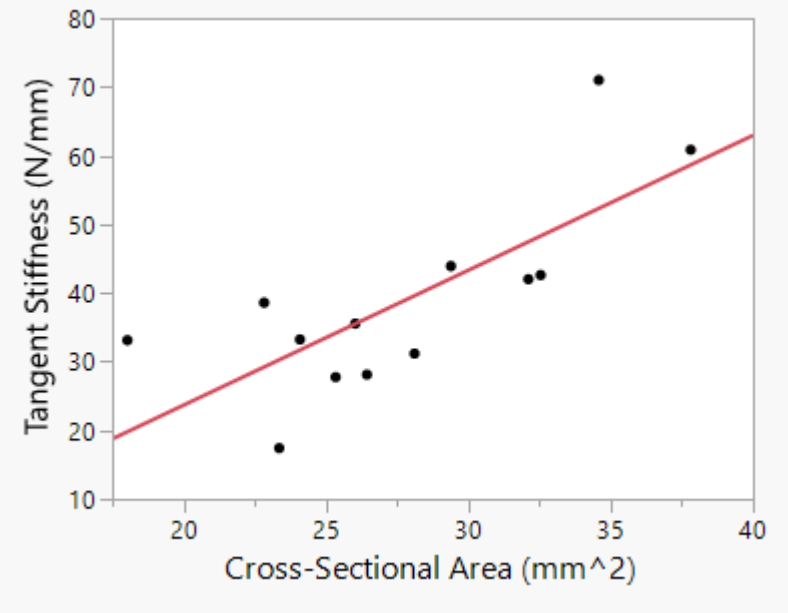
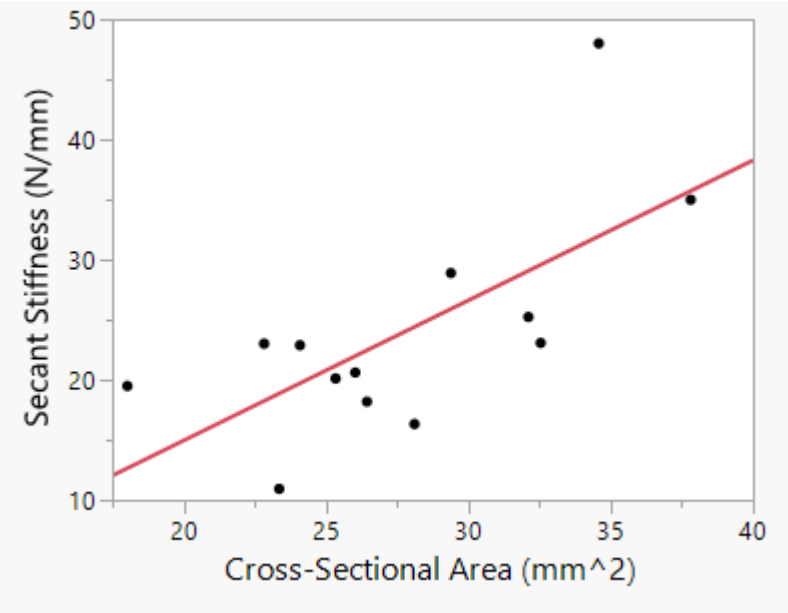
Linear fit of secant stiffness with cross-sectional area (mm^2): Statistically significant correlation ($p < 0.05$) between secant stiffness and cross-sectional area for all cadaver mechanical testing data except excluded samples (n = 13).